ORGANISATION EUROPEENNE POUR LA RECHERCHE NUCLEAIRE
CERN EUROPEAN ORGANIZATION FOR NUCLEAR RESEARCH

CERN/INTC/2000-004
11 February 2000
SW 200009

Neutron TOF Facility (PS 213)

Technical Design Report

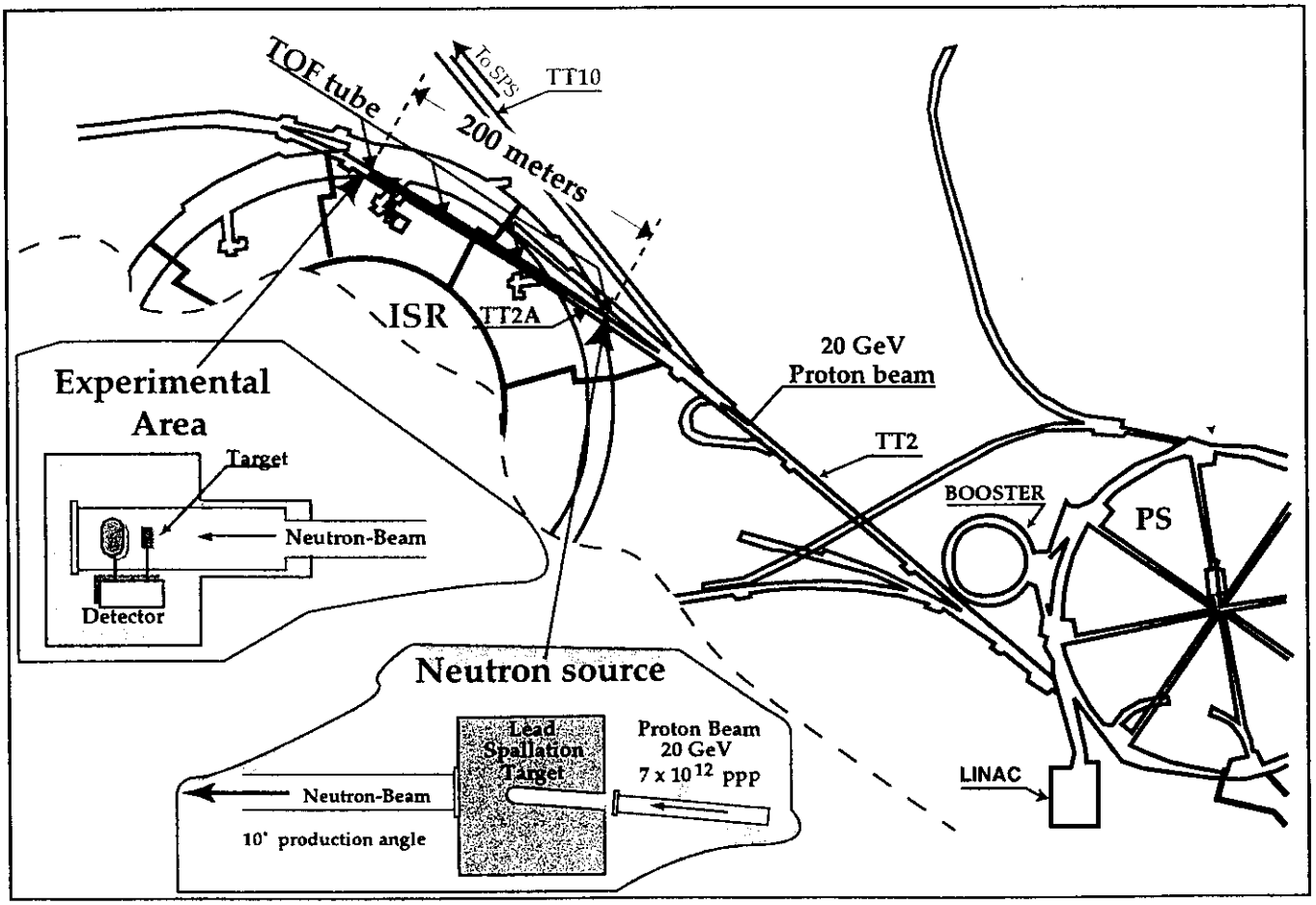

Neutron TOF Facility (PS 213)

Technical Design Report

S. Andriamonje[4], J. P. Bertuzzi[5], D. Blanc[5], R. Bonzano[5], C. Borcea[5], P. Bourquin[5], J. Buttkus[5], D. Cano-Ott[8], R. Cappi[5], J. C. Carlier[5], E. Cennini[5], P. Cennini[5], D. Chapuis[5], V. Chohan[5], C. Coceva[3], N, Colonna[1], J. P. Come[5], G. Daems[5], S. Diez[8], T. Dobers[5], L. Durieu[5], C. Eleftheriadis[9], M. Embid[8], A. Ferrari[5], C. Flament[5], M. Gaidon[5], J. Gascon[5], D. Gasser[5], M. Giovannozzi[5], E. M. Gonzales-Romero[8], I. Goulas[5], M. Heil[6], Y. Kadi[5], F. Kaeppeler[6], G. Kowalik[5], J. Kuhnl-Kinel[5], V. Lacoste[5], J. M. Lacroix[5], A. Magnani[3], R. Magnin[5], E. Mahner[5], P. F. Mastinu[7], A. Mengoni[3], R. Messerli[5], G. Metral[5], P. Milazzo[10], J. Monteiro[5], B. Nicquevert[5], T. Papaevangelou[9], P. Pavlopoulos[2], M. Poehler[5], E. Radermacher[5], U.Raich[5], R. Reifarth[6], J. P. Riunaud[5], G. Rollinger[5], F. Saldana[5], M. Silari[5], G.Tagliente[1], A. Tzima[9], W. Van Baaren[5], V. Vlachoudis[5], M. Zanolli[5]

[1] Università di Bari e Sezione dell'INFN, Bari, Italy
[2] Department of Physics and Astronomy, University of Basel, Basel, Switzerland
[3] ENEA, Bologna, Italy
[4] CEN, Bordeaux-Gradignan, France
[5] CERN, Geneva, Switzerland
[6] Institut für Kernphysik III, FZK Karlsruhe, Germany
[7] INFN, Legnaro, Italy
[8] CIEMAT, Madrid, Spain
[9] University of Thessaloniki, Thessaloniki, Greece
[10] Università di Trieste e Sezione dell'INFN, Trieste, Italy

Editor:
E. Radermacher
Ernst.Radermacher@cern.ch

TABLE OF CONTENTS

1. INTRODUCTION

The experimental determination of neutron cross sections, elastic and inelastic, across the whole Mendeleiev Table has always been of primary importance in nuclear physics. Many of the salient features of nuclear levels can be determined from the resonant structure of such cross sections and of their decay schemes. These cross sections have many different channels and exhibit a complex phenomenology with very many resonances over a very wide energy spectrum, extending from a fraction of eV to many MeV of neutron kinetic energy.

In addition to such primary interests, recent developments at CERN and elsewhere have raised the practical need for better known cross sections aimed specifically at the design and understanding of the behaviour of Accelerator-Driven Systems (ADS). In such devices, a charged particle beam is used to produce intense neutron fluxes.

These practical studies make massive use of Montecarlo techniques in order to predict ADS behaviour in a variety of possible configurations and running conditions. A fundamental pre-requisite of any computing method is the availability of reliable cross section data for many channels and at the appropriate energies. Unfortunately, the available Compilation Databases [1] — in general based on a mixture of experimental measurements and of theoretical prejudices — present many 'holes' and substantial differences amongst them, most likely due to the different fitting procedures used and the reliance on different theoretical models. These cross sections cannot be considered today as a totally reliable basis for the design of innovative ADS for the incineration of nuclear waste [2], energy production (EA) [3] and radio-isotope activation [4] for medical applications as well as many other subjects in nuclear physics. Indeed, while the thorium and uranium related cross sections are relatively well known, there are sometimes gigantic differences between Databases [1] when it comes to americium and curium, or more generally to higher actinides.

For the transmutation of several long-lived fission fragments into stable species, the information is even more lacunary and in many important cases, like for instance ^{90}Sr, there are orders of magnitude discrepancies in the experimental data [5], mostly confined to the region of thermal or epi-thermal neutrons. Instead, the most promising of transmutation methods, the TARC [6] requires precise information on the resonances and specifically on their widths.

Existing data comes from compilations of many different experiments, often not in perfect agreement and generally, each dedicated to specific energy domains and elements. They are currently mostly performed in association with a time of flight (TOF) measurement of the incoming neutron. This technique has been generally limited by the strength of the primary neutron source used, which conditions the length of the flight-path and therefore the energy resolution vs. counting rate.

As a result of the studies reported in a first paper [7] and an addendum [8], we proposed [9] a time of flight facility (TOF) at the CERN PS — delivering a maximum intensity of $\approx 3 \times 10^{13}$ protons per cycle at a momentum of 24 GeV/c — which allows one to study, systematically and with excellent resolution, neutron cross sections of almost any element using targets of very modest mass (even a few milligrams), necessary for unstable or otherwise expensive materials, for instance transuranics, in the interval from 1 eV to 250 MeV.

In this facility, we make use of the spallation mechanism as a strong source for neutrons by using a lead target and a flight path of 200 m.

The spallation mechanism [7, 8] is a remarkably powerful source of neutrons: in a lead spallation target, one 24 GeV/c proton may produce as many as 760 neutrons. Furthermore, lead has a high transparency for neutrons of energy ≤ 1 MeV. As mentioned above the CERN PS accelerator is capable of accelerating $\approx 3 \times$€ 10^{13} protons per cycle, resulting in as many as 2×10^{16} neutrons at each cycle. This extraordinarily prolific source can be concentrated in short time pulses, which are typically of the order of about 7 ns r.m.s. long, offering the added feature of a tremendous potential accuracy in the time of flight (TOF) determination of the neutron energy.

The neutrons produced by spallation are canalized to an experimental area located 200 m downstream through a vacuum pipe, making use of the existing TT2A tunnel about 7 m below the ISR tunnel (see Fig. 1.1).

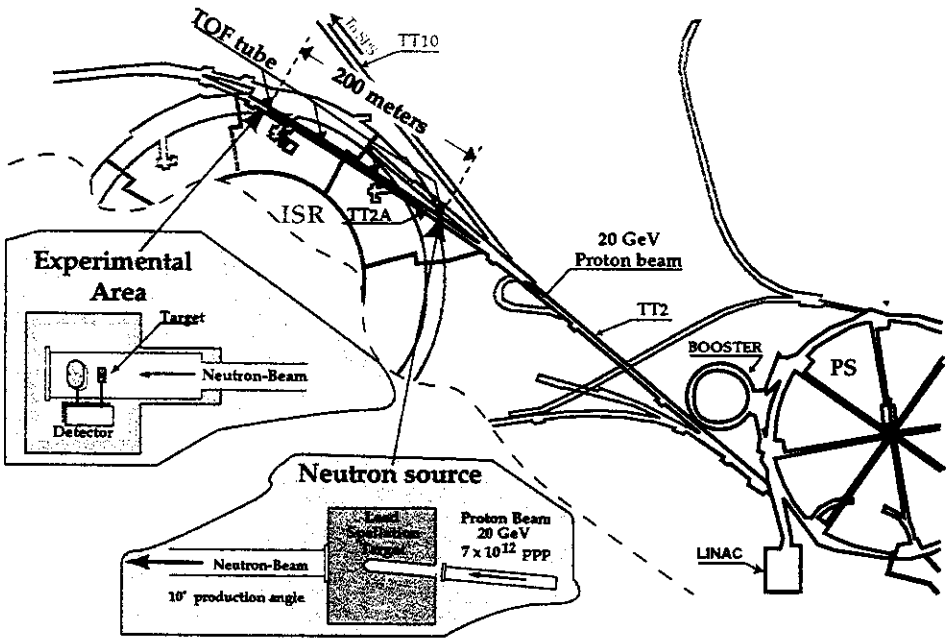

Figure 1.1: General layout of the experiment. The proton beam is extracted via the TT2 transfer line and hits the lead target. At the end of the TOF tunnel (TT2A), neutrons are detected about 200 m from the primary target.

We only report here the initial phase of the project, the so-called '1st year test phase' which differs from the 'final phase' essentially in the proton beam intensity requirements. In the '1st year test phase' only one bunch of 0.7×10^{13} protons will be extracted at 20 GeV/c. In the 'final phase' four bunches with a total intensity of $\approx 3 \times 10^{13}$ protons will be extracted, one every 50 ms, at 24 GeV/c. More details about this phase can be found in [10]. The initial phase does not require any modification in the PS machine itself, while the final phase requires important modifications in the power supplies of the fast extraction elements (septum magnet, bumps, etc.) as well as a more refined cooling system for the lead target.

2. THE PS BEAM

2.1 GENERAL CONSIDERATIONS

The PS proton beam requirements are the following:

- Momentum: 20 GeV/c, which is the maximum attainable for a 1.2 s repetition rate of the PS magnetic cycle. A 24 GeV/c momentum could be obtained using a 2.4 s magnetic cycle.
- A single proton bunch of $N_b < 7 \times 10^{12}$ particles/pulse with a r.m.s. length of < 7 ns.
- The number of cycles per supercycle of 14.4 s will vary from 1 to 4 depending on that shared with other PS users. The maximum number 4 is related to the maximum amount of beam losses which can be accepted into the PS machine, on the maximum power dissipation on the lead target and on the radiation level in the target area.

The beam will be fast extracted onto the lead target using the present Fast Extraction FE16 with no modifications in the PS ring. Recent preliminary tests have allowed the above beam characteristics to be achieved, which can be considered as a record for the PS machine in terms of peak intensity, using the procedures briefly described below (Fig. 1.1).

A single bunch in a single Booster ring is accelerated and injected into the PS at 1.4 GeV/c. This higher injection energy (recently modified for the LHC beam requirements) allows the self-field space charge tune shift to be kept to a reasonable value of < 0.3 on the 20 ms injection flat bottom. The bunch is injected and then accelerated with the RF frequency at harmonic number h = 8. The horizontal and vertical working points are precisely adjusted during the acceleration to avoid, as much as possible, resonance crossings. Head-tail transverse instabilities at low energy are cured using linear coupling with skew quadruples. The horizontal and vertical chromaticities are set to ~ –1 before transition and to +0.1 after transition, to avoid head-tail instabilities at high energy. The RF voltage is adjusted during the acceleration to decrease the longitudinal acceptance and to improve Landau damping and minimise longitudinal instabilities. Preventing beam break-up instabilities at transition, destroying 50% of the beam, requires increasing the longitudinal emittance from 2 to 2.5 eVs, using the standard longitudinal blow-up and a 200 MHz cavity on the injection flat bottom.

Once on the 20 GeV/c flat top, a phase jump RF gymnastic squeezes the bunch length, just before extraction, from 13 to 6 ns (r.m.s.). The normalised r.m.s. transverse emittances are 40 and 30×10^{-6} m in the horizontal and vertical plane respectively. The total transmission efficiency is better than 90%.

Two modes of operation are foreseen: the 'dedicated mode' and the 'parasitic mode'.

In the 'dedicated mode' one or more 20 GeV/c – 1.2 s cycles are dedicated to the TOF experiment. This mode achieves the best performance in beam quality, namely the highest bunch intensity.

In the 'parasitic mode', the TOF bunch is accelerated together with a much lower intensity bunch which is slow-extracted at 24 GeV/c to the East Hall experimental area. The high intensity TOF bunch is fast-extracted onto an intermediate flat top at 20 GeV/c. The small bunch goes through a bunch compression as well, and has to be decompressed, with a reverse RF gymnastic to recover its normal shape well-suited for the slow extraction.

Recent experiments have shown that in the 'dedicated mode' an intensity of $N_b = 0.7 \times 10^{13}$ particles/bunch and a r.m.s. bunch length of 6 ns can be achieved (see Fig. 2.1). In 'parasitic mode' the bunch length will be the same but the maximum intensity will be ~ 0.4×10^{13} particles/bunch. The advantages of running in 'parasitic

mode' are in an easier TOF scheduling (e.g. setting up's) as the slow extraction cycles are present almost all of the time (see Figs. 2.2 a, b).

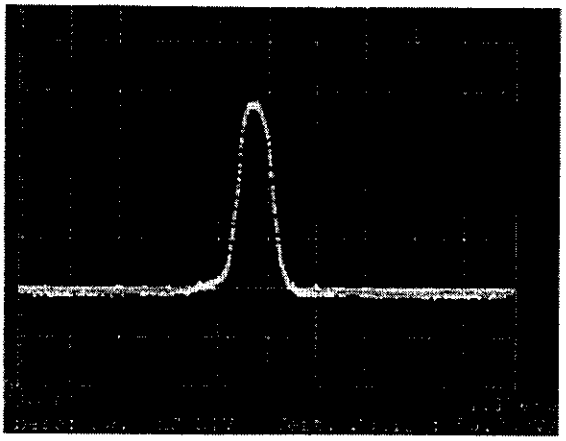

Figure 2.1: TOF proton bunch before and after compression. $N_b = 0.7 \times 10^{13}$particles/bunch, r.m.s. bunch length ~6 ns. Time scale 20 ns/div.

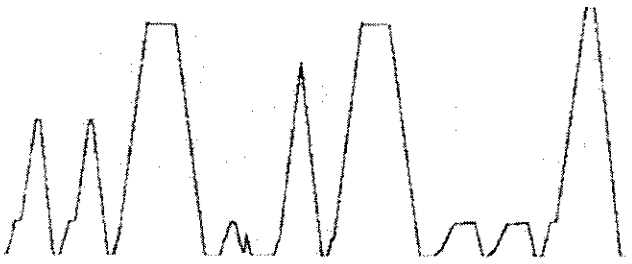

Figure 2.2 a: Example of a typical PS supercycle showing a TOF 20 GeV/c-1.2s cycle among other users in 'dedicated mode'. Total duration = 14.4 s.

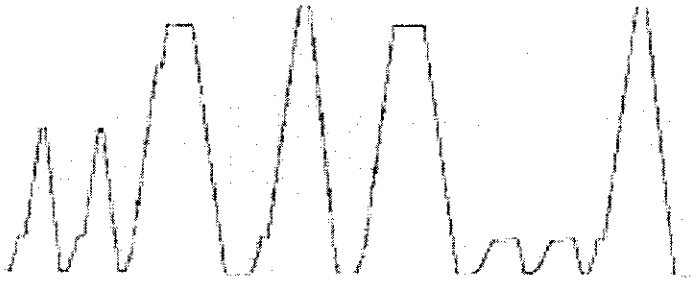

Figure 2.2 b: Example of a typical PS supercycle showing a TOF 20 GeV/c-2.4s cycle among other users in 'parasitic mode'. Total duration = 14.4 s.

2.2 BEAM LINE LAYOUT

The geometry of the new layout of the FTN transfer line can be summarised as follows [11]:

a) Three bending magnets (of type MCA) are used to deflect the beam to the left-hand side of the dump D3. Each magnet generates a bending angle of 2° at the maximum beam momentum of 20 GeV/c. With respect to the previous version [10], the only change consists in the sign of the deflection angle.

b) Six quadruples are used to focus the beam. Three of them are focusing quadruples (of type QFS) and three are defocusing ones (of type QD). Quadruples of the same type have the same focusing strength. This feature allows the connection of them in series, thus reducing the number of independent power converters needed.

c) Three bending magnets (of type MCA) are used to deflect the beam to the right by an overall bending angle of 6°. Each of them generates the same deflection angle.

d) Two corrector magnets (of type M100) are installed to control the beam trajectory.

With this choice of geometry, the proton beam intersects the axis of the TOF pipe at an angle of 10°. In Fig. 2.3 the old layout is reported, while in Figs. 2.4 and 2.5 the new layout of the FTN transfer line is shown.

With respect to the previous version [10], the following differences can be found:

a) Three bending dipoles have been added to set the beam parallel to the TT2 axis and thus to form an angle of 10° with the TOF axis.

b) Five quadruples have been added in order to provide the necessary focusing strength.

c) Two corrector magnets have been added to provide the necessary control over the beam trajectory.

d) The overall length of the beam line is about 90 m, with an increase of 50 m with respect to the previous version [10].

2.3 BEAM LINE OPTICS

As in previous reports [10-12], the starting point for the optics study of the new transfer line is the standard optics configuration, used for the fast extracted beam at 26 GeV/c delivered by the PS machine [13]. This optics have been scaled down for the 20 GeV/c operation foreseen for the TOF Facility.

The quadruple FT16.QFO375 is powered by an independent power supply. It has been separated from the string of focusing quadruples of the TT2 line since the installation of the stripper foil for the ion beam, just upstream. Hence, this magnetic element can be used to focus the proton beam on the target. The six quadruples installed in the FTN line are divided into two families (focusing and defocusing).

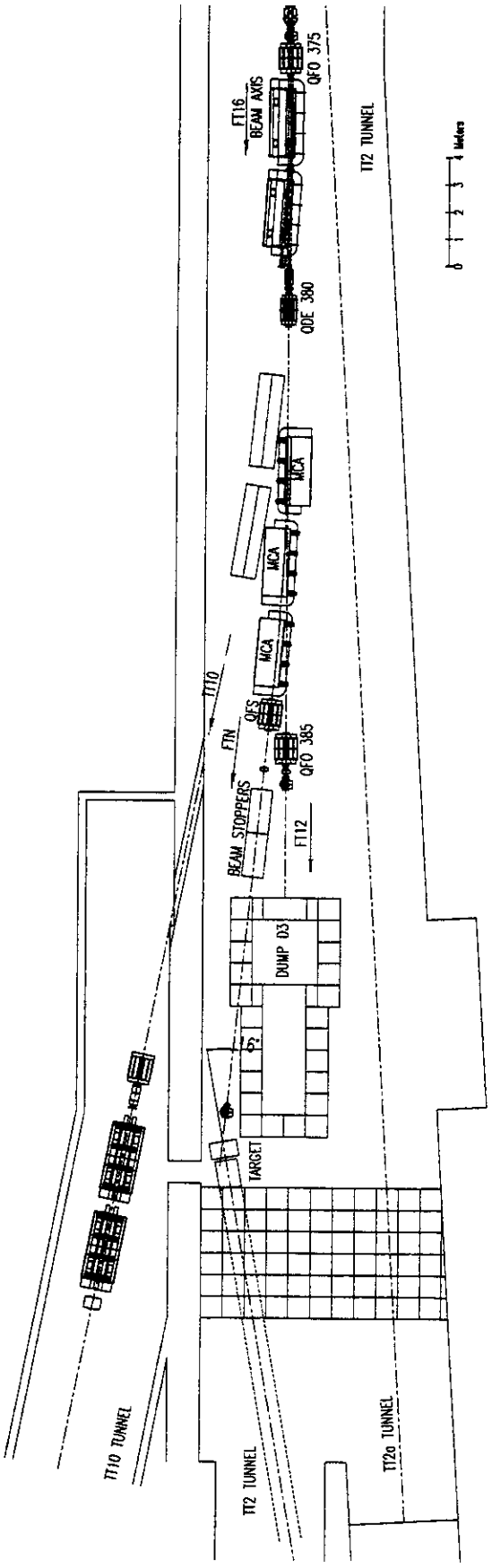

Figure 2.3: Overall layout of the FTN transfer line presented in the feasibility study.

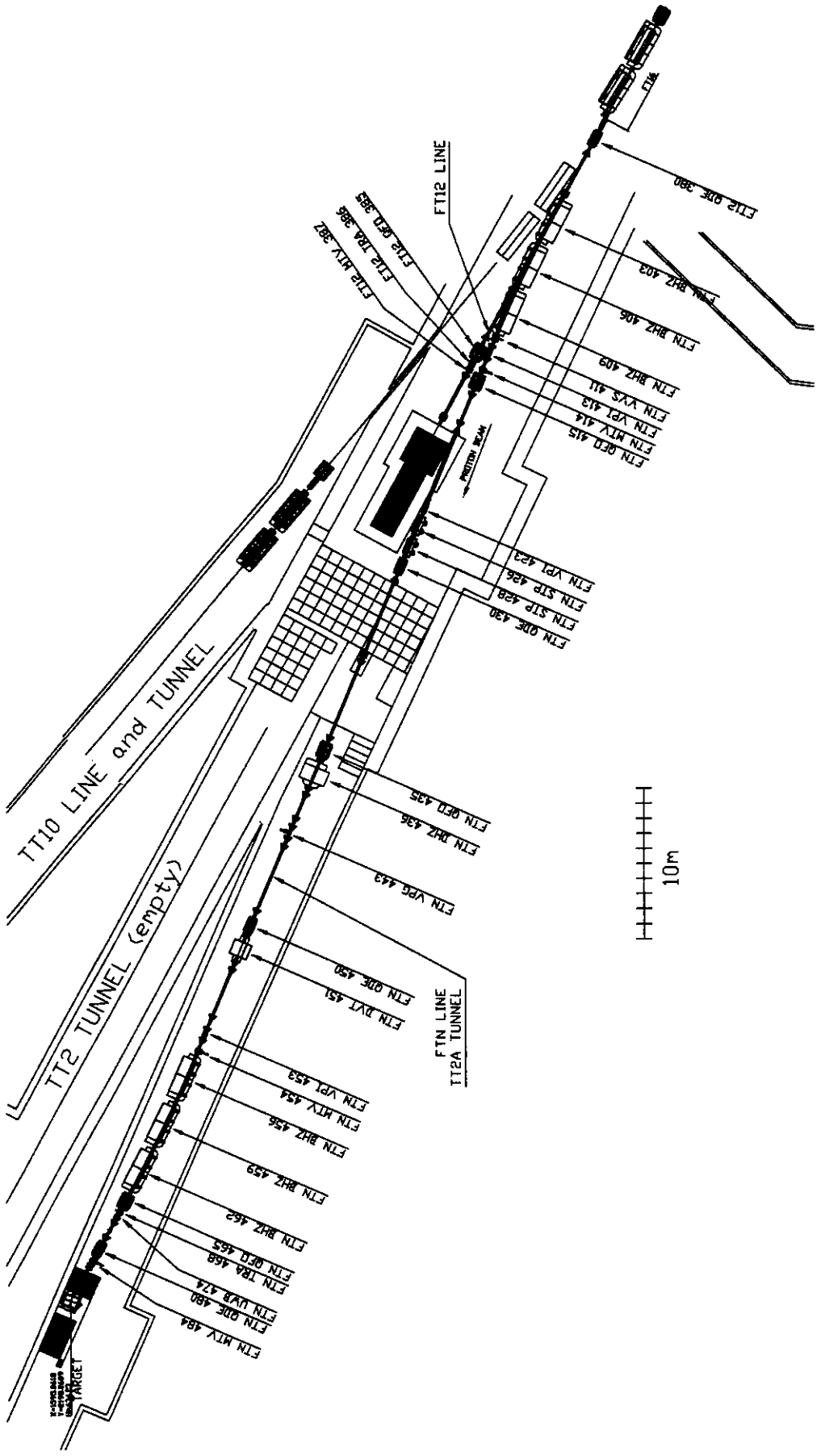

Figure 2.4: Layout of the new version of the FTN transfer line to be installed in the TT2 tunnel.

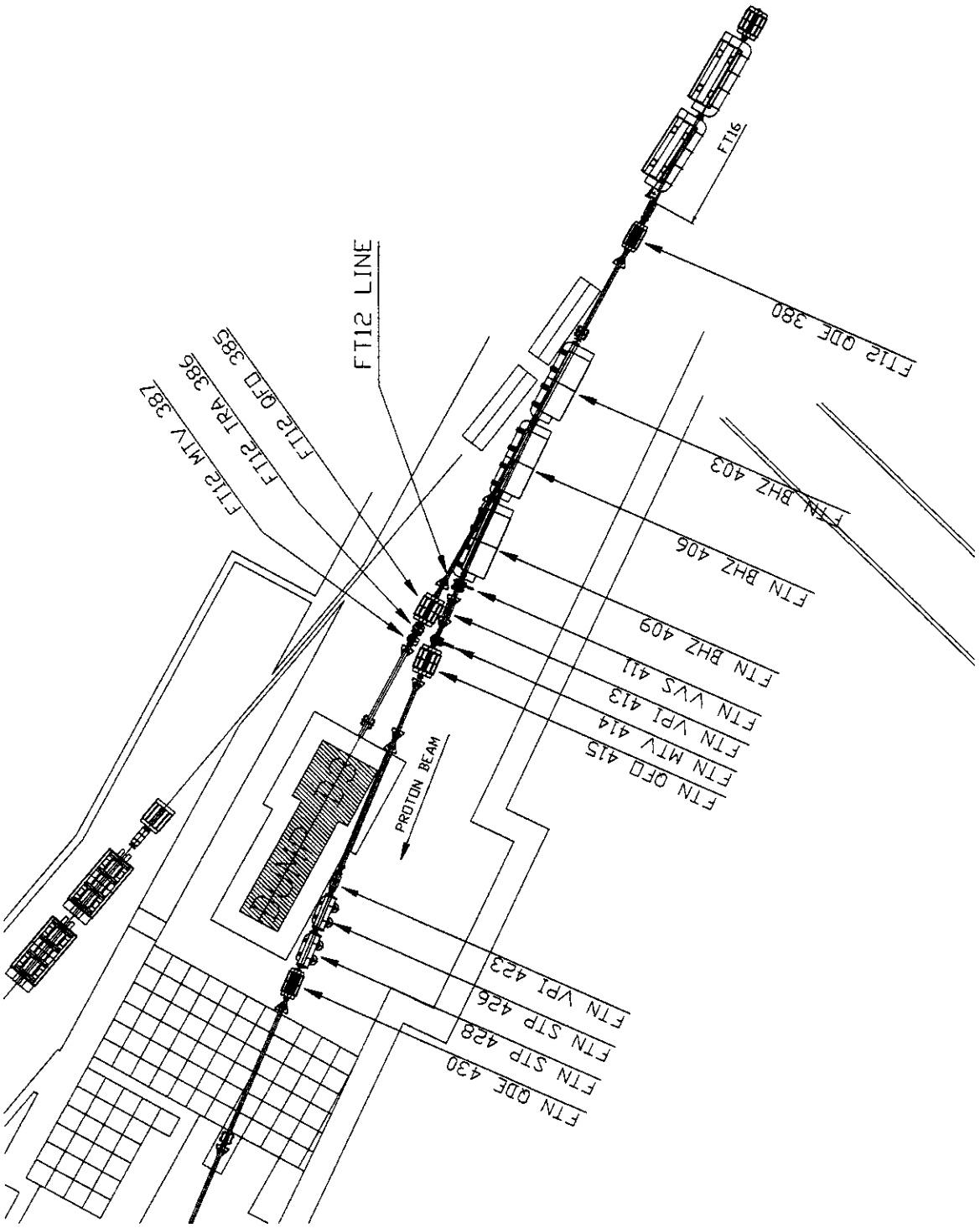

Figure 2.5: Detailed view of the new FTN transfer line near the dump D3.

To improve the control of the beam size and dispersion function at the target location, it has been decided to install two quadruples downstream from the last group of three bending magnets.

The computation of the optics has been carried out by using the *MAD* program [14]. In Fig. 2.6 the optical parameters, β–function, dispersion and beam envelope are shown. In Table 2.1 the beam parameters used for the computation of the beam envelope are reported, together with the beam size at the target location.

Table 2.1: Beam parameters used for computation of beam envelope.

Transverse parameters		Longitudinal parameters		Beam size at target	
ε_H (1σ) [mm mrad]	1.88 π	Δp/p	$\pm 3 \times 10^{-3}$	σ_H [mm]	7.8
ε_V (1σ) [mm mrad]	1.41 π			σ_V [mm]	5.6

One can see that the horizontal beam size has increased with respect to the previous version [10] ($\sigma_H \approx 2.4$ mm), while the vertical one is slightly reduced ($\sigma_v \approx 6.1$ mm). This is mainly due to a chromatic effect in the horizontal plane, as the value of the dispersion function at the target location is rather large, as well as the spread of the beam momentum. The beam size, however, is within the acceptance limit of the TOF collaboration (total beam size of the order of 30 mm).

The location of the two corrector magnets has been optimised by taking into account the optics and the available power converters (see next section for more details). The horizontal corrector has been placed near the second focusing quadruple to exploit the large value of the β-function. For the same reason, the vertical corrector has been installed near the second defocusing quadruple. Two magnets of type M100 have been chosen, due to their magnetic strength: they will be used with a gap of 140 mm. The maximum variation in the beam position at the target location is about ± 33 mm and ± 36 mm in the horizontal and vertical planes respectively for a maximum current of 20 A.

The first beam position monitor is installed at the entrance of the first focusing quadruple of the FTN beam line. It will be used to control the beam trajectory at the exit of the first group of three bending magnets. The second monitor is placed at the entrance of the fourth bending magnet, while the third monitor is located just downstream from the last quadruple.

The first two bending magnets, which are powered in series, can be used to steer the beam on the first monitor to allow a well-corrected horizontal trajectory. Using the first string of two bending magnets one can centre the beam on the second monitor. Then, the horizontal corrector allows the final steering on the target to be performed using the third monitor.

The vertical trajectory can be corrected by using the magnet FT16.DVT353 to centre the beam on the second monitor in the FTN transfer line and then using the vertical corrector installed in FTN together with the last monitor.

The new geometry of the transfer line has changed the co-ordinates of the intersection point between the axis of the FTN line and the axis of the TOF tube.

In Table 2.2 the co-ordinates of such a point are listed, as computed by the *MAD* program and then translated into the standard CERN co-ordinate systems.

Table 2.2: Co-ordinates of the intersection point of the FTN axis and the axis of the TOF tube computed using the MAD *program and expressed in the standard CERN co-ordinate system.*

X [m]	Y [m]	H [m]
1595.9564	2198.2357	434.2401

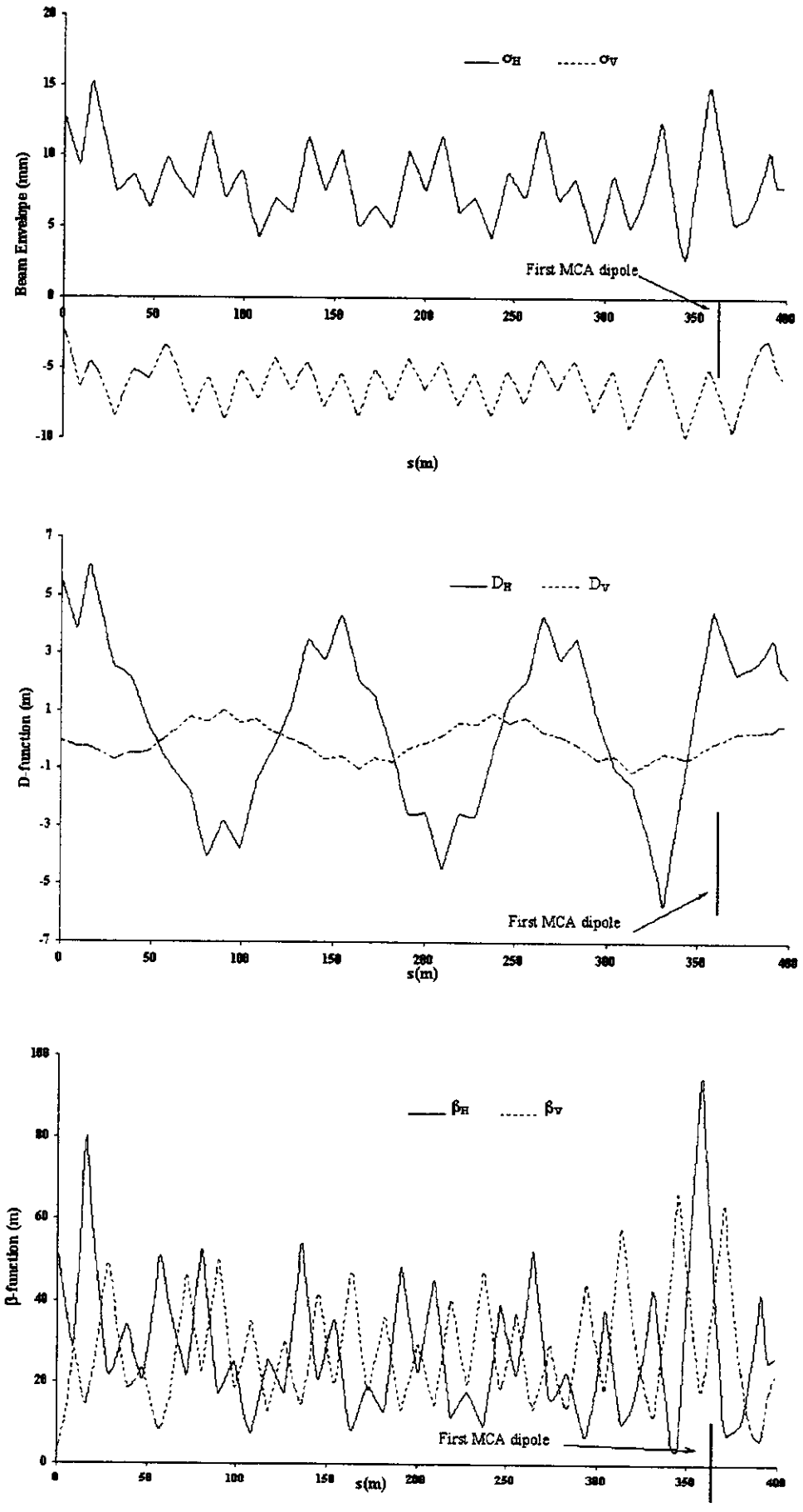

Figure 2.6: Optical parameters and beam envelope for the new layout of the FTN transfer line.

2.4 POWER CONVERTERS

In Ref. [12] it was proposed to use two power converters for the three bending magnets installed in the FTN transfer line. The first bending magnet was connected to one power converter, while the remaining two magnets were connected in series to the second power converter. This choice was imposed by the need of having a short switching time for the first bending magnet in order to allow a pulse-to-pulse modulation (ppm) mode for this magnet.

The main philosophy of this scheme has also been retained for the new layout. Only minor modifications have been introduced. One power converter (type R22.01), formerly used for Dump D2, will be used to power the first two bending magnets. This will allow the power converter to be operated in ppm mode with a switching time shorter than 1.4 s, but not faster than 1.2 s, between the operational value of 895 A and the zero value used to send the beam to the dump D3. A second power converter (type R22.02), also used formerly for dump D2, will be used for the remaining bending dipoles, i.e. the four MCA elements. The total resistance of the whole string of magnets does not allow a ppm operation, but this does not seem to be a serious limitation.

As far as the quadruples are concerned, they cannot be connected in series with the two strings of focusing and defocusing elements of the TT2 transfer line. In fact, as already mentioned in [12], the existing power converter is not able to ensure a fast cycling of the magnet string. On the other hand, two power converters of type N can be recuperated from the PS stock. They power the string of three focusing quadruples and the string of three defocusing respectively.

The two corrector magnets can be powered using separate power converters, available in the PS stock, delivering 250 A maximum current (the maximum current sustainable by M100 type dipoles is 675 A). Unfortunately, this type of power converter does not decrease the current to zero, the minimum value being 8-10 A. Obviously, this is not acceptable for corrector magnets. Therefore, the only solution consists in using power converters of type L10, supplying a maximum current of 10 A. This type of power converter works around zero-current and can be modified in order to deliver up to 20 A. The possibility of modifying such power converters in order to supply up to 50 A is being studied.

The rearrangement of building 269 combined with the rejuvenation of the low voltage distribution system allows all power converters of the FTN transfer line to be housed in that building.

The actual values of the current needed by the main magnetic elements (dipoles and quadruples) used to generate the nominal optics are listed in Table 2.3. In addition to the elements in the FTN transfer line, the quadruple FT16.QFO375 is also included.

Table 2.3: List of the actual values of the current for the various magnetic elements in the FTN line, including the last quadruple of the TT2 line.

Element type	**Current [A]**
Quadruple FT16.QFO375 (TT2)	246.15
Dipole MCA (FTN)	895.00
Quadruple QD (FTN)	167.70
Quadruple QFS (FTN)	236.80

2.5 INSTRUMENTATION

As far as instrumentation is concerned, there are no major modifications with respect to what was reported in [10-12].

A beam current transformer similar to that installed in the FT12 line will be installed downstream from the second group of bending magnets. The resistive wall pick-up should be installed in the same region.

The only difference with respect to the previous study consists in the number of scintillating screens: in the present configuration it is mandatory to have three beam position monitors installed along the transfer line in order to be able to control the beam trajectory. The first one should be located downstream from the first group of bending magnets, the second one in between the two groups of bending magnets, and the last one just upstream of the lead target block.

2.6 COOLING AND VENTILATION

The new layout of the FTN transfer line could have an impact on the cooling and ventilation infrastructures in the TT2A tunnel. In fact, contrary to the previous version [10], the majority of magnetic elements will be installed in the TT2A tunnel, downstream from the shielding wall near dump D3. These elements will be used in DC mode in order to relax the constraints on the performance of the power converters. Hence, a careful analysis should be carried out to determine whether new infrastructure is needed.

A summary of the power dissipated by the different magnet elements used for the FTN line is listed in Table 2.4. In this Table, the maximum power dissipated by the different magnets is reported, which is obtained by taking the minimum value between the maximum current delivered by the power converter and the maximum current sustainable by the magnet.

Table 2.4: Summary of maximum power dissipated in TT2 and TT2A tunnel.

	Magnetic element	I_{max} [A]	R [Ohm]	P_{max} [kW]
TT2 tunnel	Three DC dipoles (MCA)	1500	0.016	72.00
	One DC quadruple (QFS)	470	0.064	30.08
	One DC quadruple (QD)	300	0.062	18.60
			Total P_{max}	120.68
TT2A tunnel	Two DC quadruples (QFS)	470	0.064	60.16
	Two DC quadruples (QD)	300	0.062	37.20
	Two DC correctors (M100)	20	0.200	8
	Three DC dipoles (MCA)	1500	0.016	72.00
	Sweeping magnet (M200)	800	0.200	128.00
			Total P_{max}	305.36

In order to accommodate the heat loads coming from the magnets and electronic equipment, a ventilation system must be provided inside the TT2A tunnel. The existing installation has been out of service for 6 years now and its present state does not allow it to be used any more. Therefore, a small air-handling unit is proposed and will replace one of the existing devices. Some ducts must be modified accordingly. The air handling unit will operate on full recirculation air and it will be equipped with a chilled water cooling coil (for mode 'BEAM ON'), an electric heating coil (for mode 'BEAM OFF') and filter class EU4. In Table 2.5 the parameters

concerning the water flow and the pressure drop for the different magnetic elements in the new FTN transfer line are listed.

Table 2.5: Details concerning the water flow and the pressure drop of the magnetic elements installed in FTN.

Element type	Water flow[1] [l/min]	Pressure drop [bar]
Dipole MCA	20	5
Dipole M100	44	3.5
Quadruple QD	10	6
Quadruple QFS	10	8

The demineralised water must be supplied to the magnets located in both the TT2 and TT2A tunnels. Since one of the magnets installed in the TT2 tunnel represents higher-pressure losses, the water will come from Booster station (higher Δp available). For the rest of the magnets, the water will be supplied from ISR cooling station (located in building 378).

In order to deliver the required water flow some modifications of the existing pipeline should be performed, they will be comprised of:

a) A connection of the ISR distribution ring to the station in building 378.

b) A new distribution pipeline in tunnels TT2 and TT2A.

c) Connections of the existing pipeline for the sweeping magnet.

Apart from this work, there will also be a water flow measurement provided for the two tunnels. It will be connected to the TCR and/or TOF control room in order to assure good surveillance (alarms). Some of the demineralised water will be used as a primary source of cooling energy for the lead target situated in the TT2A tunnel.

2.7 VACUUM SYSTEM

The situation of the current vacuum system installed in the PS transfer line FT16 can be summarised as follows:

- p(FT16-10.VGP1) ~ 3×10^{-8} mbar
- p(FT16-10.VGP2) ~ 4×10^{-9} mbar
- p(FT16-20.VGP1) ~ 8×10^{-9} mbar
- p(FT16-30.VGP1) ~ 4×10^{-9} mbar

For the layout of the new FTN line, it has the following consequences:

a) Due to the distributed pumping speed (pumping groups and ion pumps) of the FT 16 line, and the fact that the overall length of the FTN line has been increased by approximately 50 m with respect to the previous version, it will be necessary to create a new vacuum sector.

b) A sector valve (FTN.VVS411), should be installed directly downstream from the three MCA bending magnets, in order to separate the transfer line FT16 from FTN.

[1] The water flow is referred to a temperature increase of 30°

c) One pumping group (FTN.VPG443), used for the pre-vacuum, should be positioned approximately in the middle of the beam line. It consists of a standard 600 l/s turbo-molecular pump and a 25 m^3/h primary pump.

d) Two vacuum gauges are foreseen for measurements.

e) One manual valve is foreseen for venting the sector.

f) Numerical simulations have shown that at least three 410 l/s ion pumps (FTN.VPI413/433/453) are necessary to guarantee an average H_2 pressure of about 2×10^{-8} mbar in the FTN line, which is in total agreement with the FT16 line layout. Spare flanges are foreseen along the beam line to increase the pumping speed if necessary.

The calculated pressure distribution along the transfer line FTN is shown in Fig. 2.7.

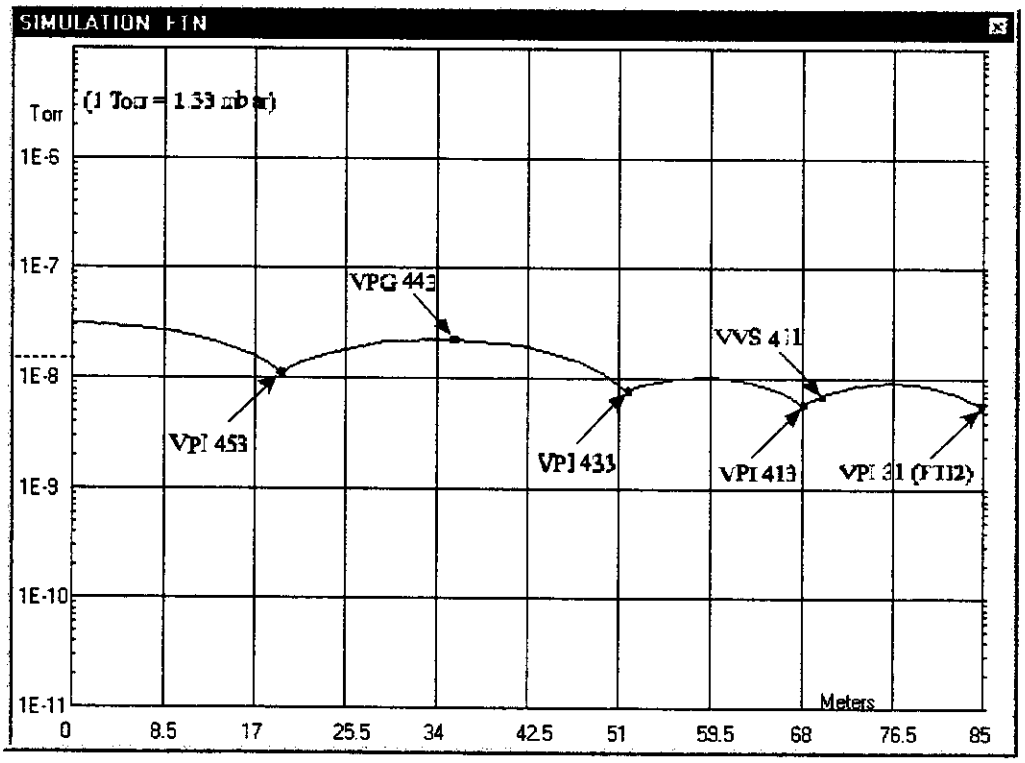

Figure 2.7: Pressure simulation for the FTN transfer line.

2.8 SAFETY ASPECTS

To comply with the safety rules in force at CERN, two beam stoppers have to be installed in the FTN transfer line. They are located downstream from the dump D3 at the end of the TT2 tunnel (see Fig. 2.5). The option consisting in installing two beam stoppers (of type XTDV) in air (see Refs. [10-12] for more details) has been dropped. At the start-up of the facility, the beam stoppers will be under vacuum.

In Table 2.6 the list of hardware needed for the new configuration of the FTN transfer line is presented. Some comments concerning the power converters are also reported.

With respect to the Table presented in [12] and in the feasibility study [10], two scintillation screens have been added. This is the natural consequence of the new

layout. The increased length of the FTN transfer line necessitates the presence of three beam position monitors to allow an optimal control of the beam trajectory.

Table 2.6: List of hardware to be installed in the TT2 and TT2A tunnel.

	Description	Availability	Comments
Beam transport	Six MCA dipoles	In stock	Two strings: one of two magnets and one of four magnets
	Three QD quadruples	In stock	One string of three magnets
	Three QFS quadruples	In stock	One string of three magnets
	Two M100 dipoles	In stock	Corrector dipoles
Beam instrumentation	Beam current transformer	To be purchased	Same as the one installed in FT12 line
	Three scintillation screens	To be purchased	Same as the one installed in FT12 line
	Wide band pick-up	To be built	Bunch shape monitor
Safety	Two beam stoppers	To be built	In vacuum

2.9 IMPACT ON THE FT12 TRANSFER LINE

As far as the FT12 transfer line is concerned, the proposed layout of the FTN beam line does not require any further modification with respect to [10, 12]: the quadruple FT12.QFO385 has to be moved downstream to allow the installation of the bending magnets. The instrumentation already present in this transfer line, a beam current transform and a scintillation screen, has to be moved just downstream from the new position of the quadruple FT12.QFO385.

Furthermore, it is foreseen to replace the section of beam pipe installed downstream from the scintillation screen with a new section, greater in diameter.

3. THE LEAD TARGET

An overall optimisation of the layout made of a lead spallation target of length h, diameter R followed by a water moderator of thickness W, has been performed for the neutron emission angle of 10° from the proton beam direction, as set by the configuration of Ref. [7]. As a result of a general trade-off between neutron flux and $\Delta\lambda$ resolution, we have chosen the parameters h = 40 cm, R = 40 cm and W = 5 cm [8].

Detailed calculations show that the power dissipation in the target gives rise to an increased temperature and therefore requires cooling. In fact, about half of the beam power will dissipate into the lead block and will require a (closed circuit) water cooling because, in the 'final phase' with 4 PS pulses, 8 kW are dissipated in total. The temperature in the centre will reach 180 °C. This cooling water will be also used as a moderator. The complete target, once activated, can be removed, with its support, by a crane and closed into a concrete blockhouse inside an old ISR gallery.

3.1 TARGET ZONE

The target zone is the most demanding part of the TOF project since it requires not only the critical coupling of the water moderator with the vacuum of the TOF tube by means of a special window, but also a sophisticated shielding and a highly performing removal procedure.

The lead target is mounted into a stainless steel support, which is an integral part of the whole target system; i.e. both parts will always be handled together. This system is immersed inside a water container, which is mounted directly onto the TOF tube. This container is not supported at the bottom as long as the target is away and will only sink by 2 mm onto a concrete support once the target is entered, due to the weight of the target.

The target zone is surrounded by marble and concrete blocks, some moulded and fixed and some removable if access is needed to the target zone. Marble has the advantage over concrete in that it becomes less radioactive. The concrete blocks are charged with 1% of boron in order to capture neutrons outside of the direction of the time of flight tube more efficiently. This shielding is shown in Fig. 3.1. The form and size of the shielding was decided according to simulations (see §9).

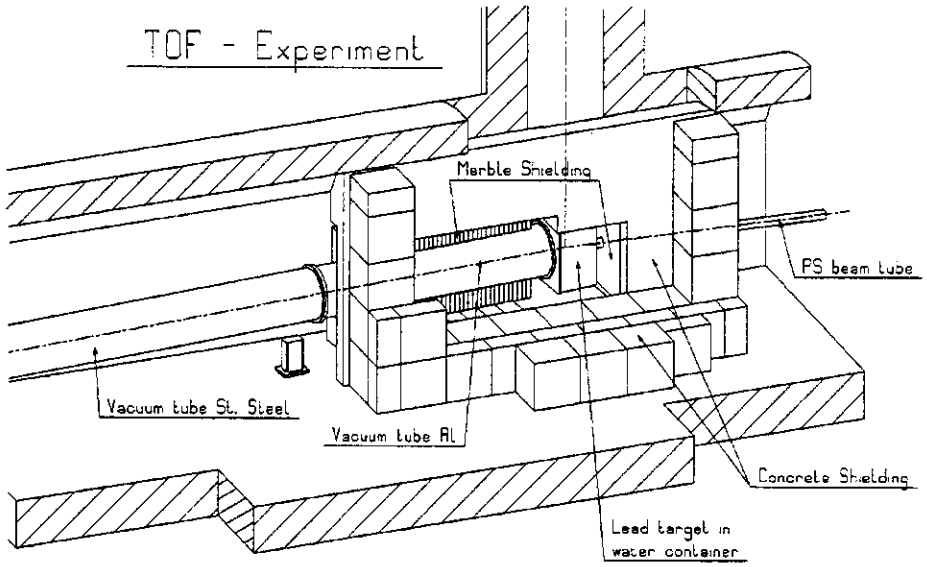

Figure 3.1: View of the target zone with the different shielding parts.

If, for any reason, somebody has to enter the target zone, the target will have to be taken out. The target will be removed through the vertical aperture, of 1.3 m in diameter, joining an ISR gallery on top of it. It will be placed in a concrete bunker and stocked in the corridor or transported in a storage zone.

3.2 LEAD TARGET AND SUPPORT

The lead for the target will be taken from the TARC experiment [17]. Pure lead (99.99%) was chosen to ensure that impurities have a negligible effect on the neutron flux. Information on the concentration levels for 11 elements were obtained by measurements (see Table 3.1).

Table 3.1: Summary of measured impurity concentrations for manufactured lead blocks. The systematic error is the error quoted by the laboratory, which performed the measurement; the third column shows the spread between all measurements of a given sample. The total error is the quadratic sum of the two contributions.

Element	Concentration (ppmw)	Error spread (ppmw)	Syst. error (ppmw)	Total error (ppmw)
Na	0.006	0.007	0.0001	0.0075
Mg	0.003	0.005	0.0006	0.005
Al	0.02	0.01	0.004	0.01
Cu	0.09	0.2	0.01	0.2
Ag	3.78	0.6	0.07	0.6
Cd	0.09	0.04	0.006	0.045
Te	0.215	0.09	0.025	0.09
Sb	0.14	0.14	0.006	0.14
Tl	4.6	1.3	0.3	1.4
Bi	19.0	2.8	0.3	2.8
Au	0.0009	0.0002	0.00035	0.0004

Although the target size optimisation favoured a circular cross section in the beam direction, a square shape of 800 mm length of side will be constructed because it is extremely difficult to machine lead to a round shape. Therefore nine blocs of $300 \times 300 \times 600$ mm^3 are needed in order to construct such a target and to reach the optimal size as defined in [8]. For this, the length of the central block and of the block below will be reduced to 400 mm. The shorter central block now provides the right depth. The shorter block below the central block is needed in order to extract the target from the water tank. In order to cope with the 1.18% of slope of the time of flight tube in the tunnel, all the lead blocks are machined to 0.676° with respect to the vertical line at the outlet face. The complete target is shown in Fig. 3.2.

The complete target is put on a stainless steel support (Fig. 3.3) which allows handling and transportation. The support is part of the target and has to be changed if a new target is to be installed.

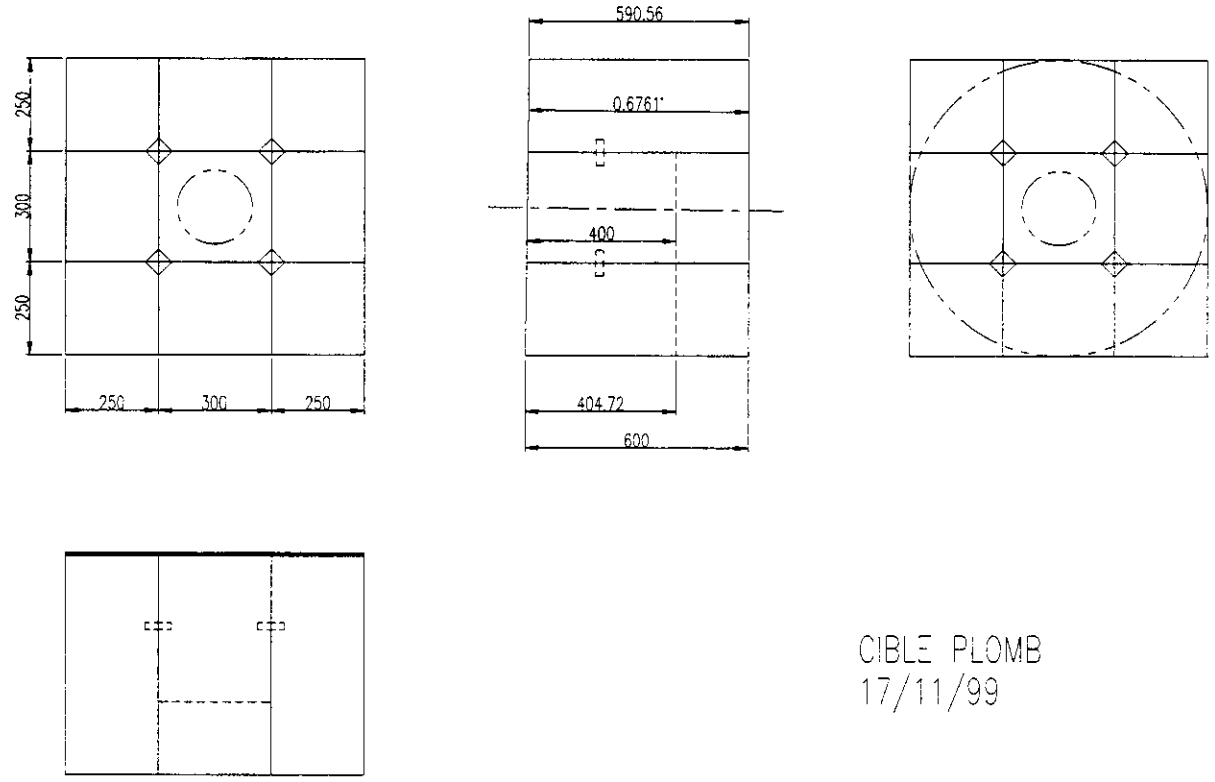

Figure 3.2: View of the lead target.

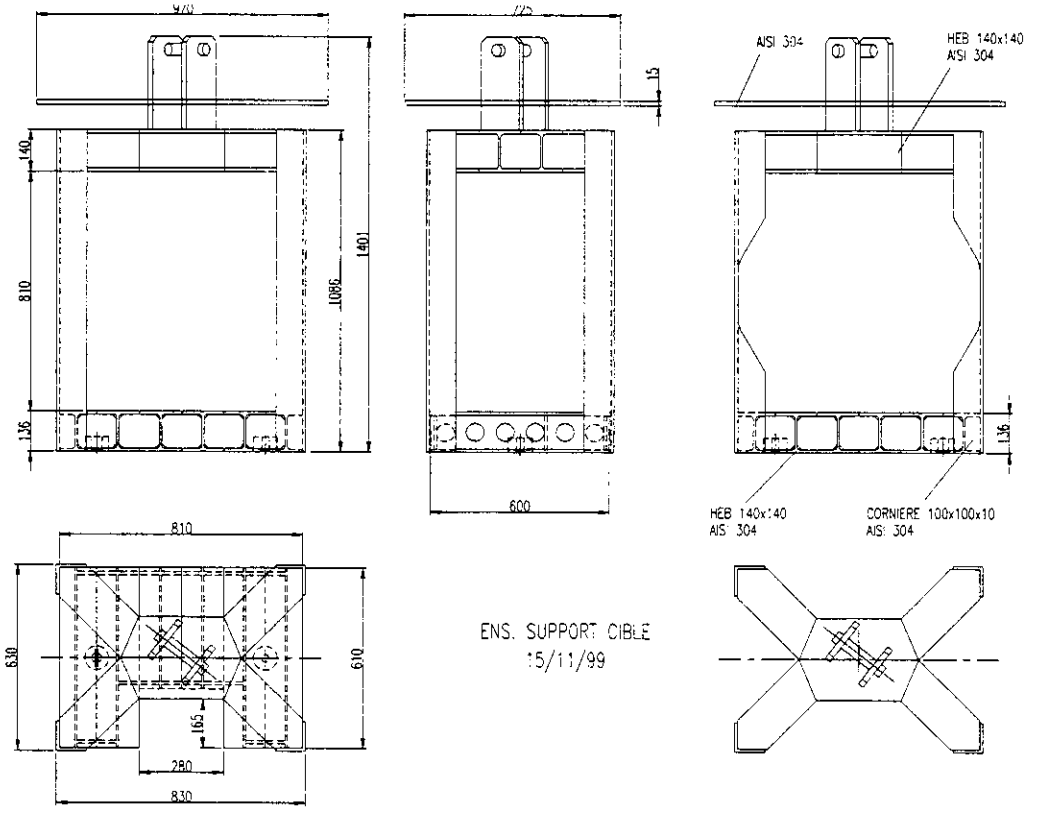

Figure 3.3: View of the stainless steel support for the lead target.

3.3 THE COOLING

The target assembly is put into a tank (Fig. 3.4) filled with demineralised water. The water is needed for two reasons: neutron moderation and cooling of the lead target. To avoid unnecessary activation the tank is made out of an aluminium alloy (ISO Al-Si1-Mg-Mn 6082). At the entrance face, a 2 mm thick window of 200 mm in diameter, set back 205 mm in comparison with the tank wall, is directly machined into the aluminium alloy. This reduces the amount of water to 30 mm to be traversed by the proton beam and avoids unnecessary interactions. This window, however, requires the lower lead block to be shortened also, as has been mentioned in 3.2. At the exit face of the tank the distance between the wall and the lead target is 50 mm, providing the necessary amount of water for the moderation of the neutrons. The water tank is covered by a stainless steel plate, which is mounted directly onto the stainless steel support and will be removed with it (see Fig. 3.3). It is clear that the water will also be activated by the radiation from the beam and the target (see 8.2). Therefore, after one year's operation, the complete water circuit will be emptied and the water transported to a radioactive waste storage.

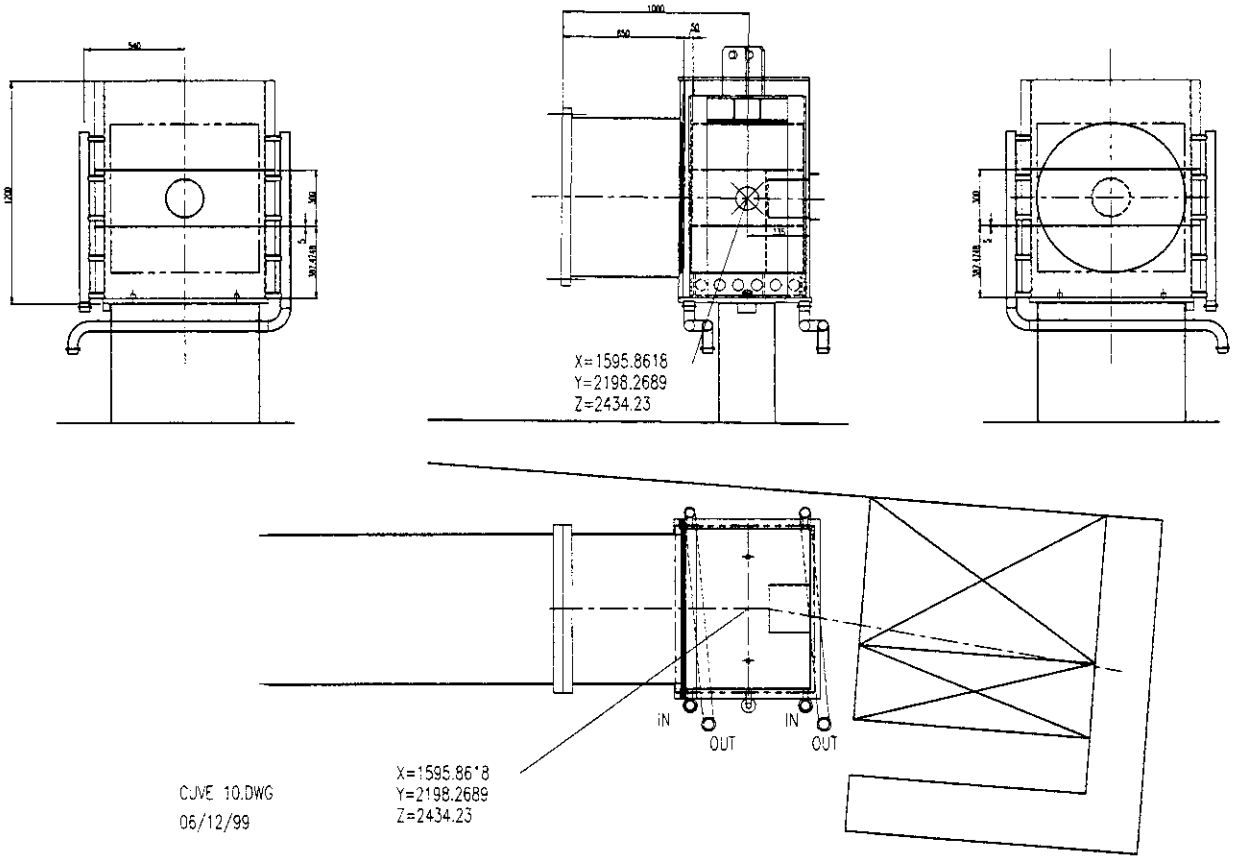

Figure 3.4: View of the water tank with the connections for the demineralised water. At the exit face, the 1 m long Al tube is shown. The lead target is shown with a hatched line.

The purpose of the cooling system is to evacuate the heat produced inside the target. The heat dissipation in the target is expected to reach a maximum of 8 kW if 4 pulses from the PS reach the lead target during 14.4 s. Therefore, the cooling system is designed starting from this basic figure. The temperature inside the target and the heat of the target's outer face have been simulated for a water flow of 6 l/s and a water temperature of 30 °C, with the result shown in Fig. 3.5.

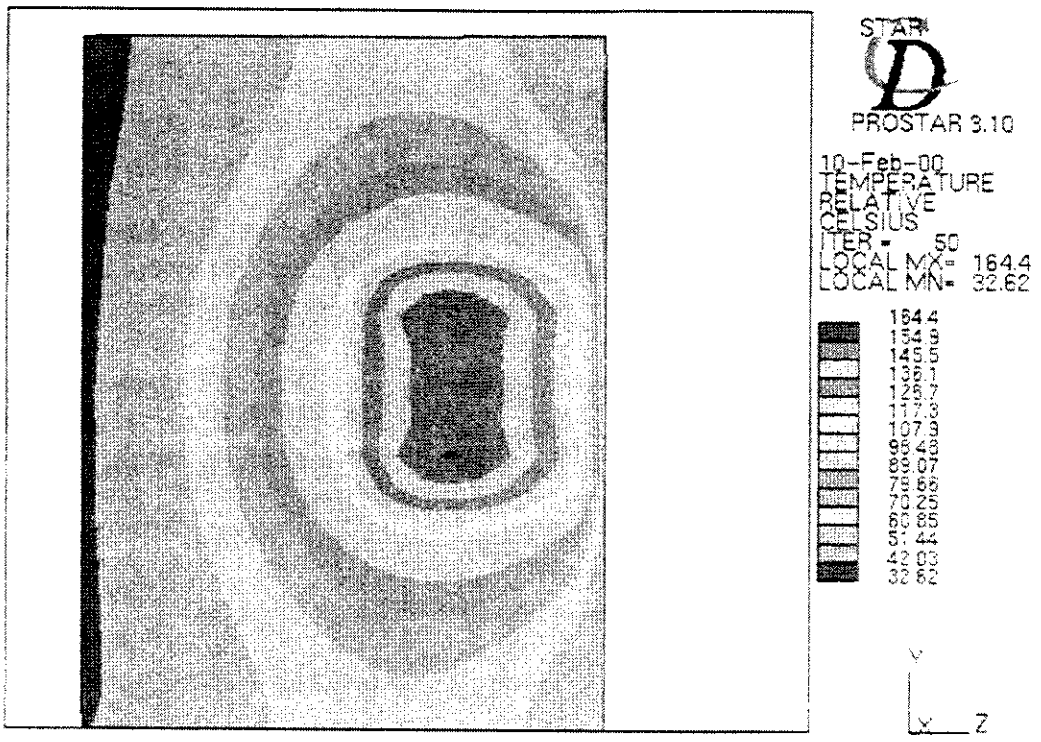

Figure 3.5: Temperature distribution inside the lead target for a water flow of 6 l/s and a water temperature of 30°C.

3.3.1 Principle of the target cooling system

The principle of the cooling system is described in Fig. 3.6. It is a hydraulic circuit mainly constituted of a heat exchanger and two independent loops:

- The first one (primary loop) is connected to the inlet and return lines of the magnet cooling circuit,
- The second one (secondary loop) is connected to the target's tank and provides the water flow in it.

The water is demineralised in both loops.

On the primary loop side, the heat exchanger is connected to the inlet and the return line of the magnet cooling circuit. The differential pressure between these two lines is about 8-12 bar with an absolute pressure of 10-14 bar at inlet line and 2-3 bar at return line.

On the secondary loop side, the heat exchanger is connected to the target tank, which will be open to the atmosphere. The target tank will act as an expansion vessel. The pressure is about 1 to 1.5 bar in the secondary loop.

The water temperature at the primary loop inlet is about 28-31 °C. This loop is on the cold side of the heat exchanger and cools the water down in the secondary loop at a temperature of about 35 °C.

The flow rate in the secondary loop is set at a constant value (about 22 m^3/h).

The secondary loop is filled-up via a derivation coming from the primary loop. A water level control close to the target tank commands a solenoid valve (VM02) opening, fixed on the derivation.

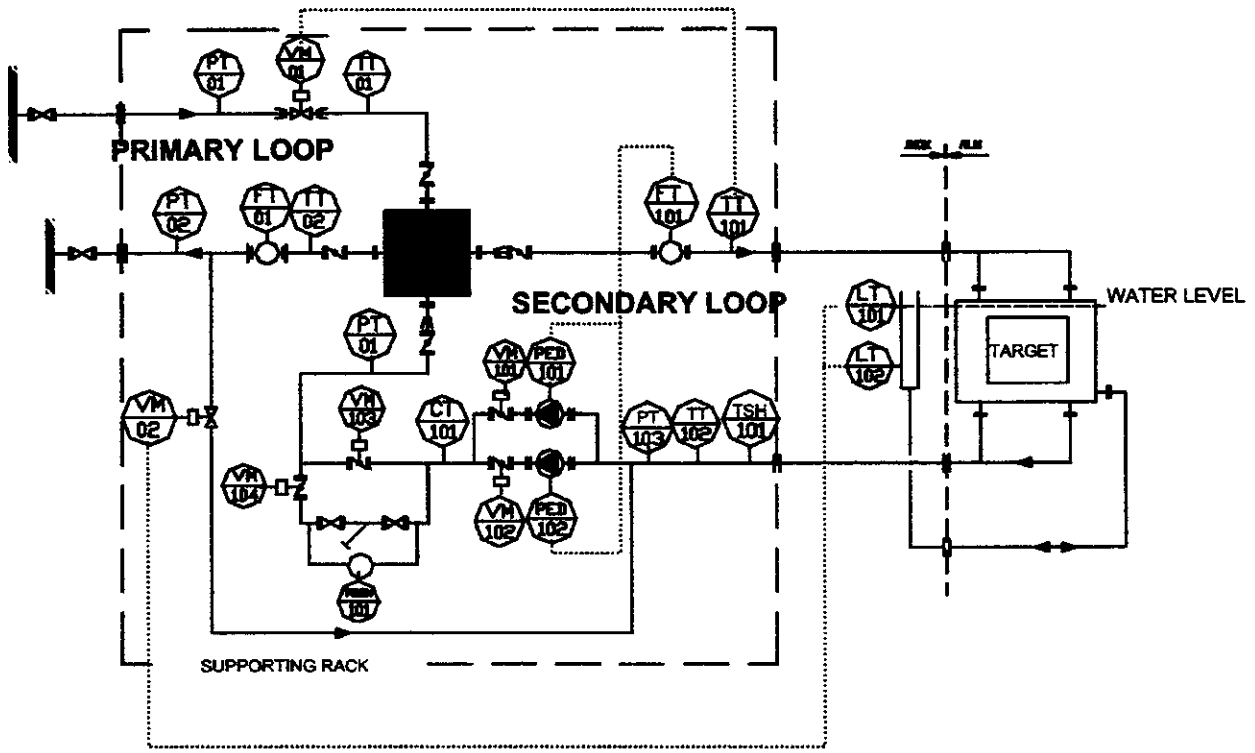

Figure 3.6: Principle schematic of the cooling circuit.

3.3.2 Main features of the control and regulation system

The control system will use a PLC, supervised, via an Ethernet communication, by a PC located in the control room. This PC will use the Wizcon supervision Software.

The regulation valve (VM01) controls the flow rate on the primary loop in order to obtain the right temperature (measured by the temperature transmitter TT101) on the secondary loop; this control is done via a PLC.

Two identical pumps (PED101 and PED102) will be installed in parallel. Only one will be in operation normally and will be backed up by the other in case of breakdown; two electrically actuated butterfly valves (VM101 and VM102), will allow flow in one pump or the other.

A flowrate meter transmitter (FT101), installed in the secondary loop, will control the pump velocity – via the PLC – in order to have a flow rate in the loop of about 22 m^3/h.

A cut-off differential thermostat (TSH101) will be installed to prevent any temperature rise over 50 °C. The free potential contact will be dealt with by the regulation and control system.

3.3.3 Installation of the cooling system

All the elements contained in the dashed frame of Fig. 3.6 are built separately on a supporting rack (see Fig. 3.7). This rack is then brought in situ and connected to the target tank and to the magnet cooling circuit. This rack is located directly at the dump D3 inside the TT2A tunnel.

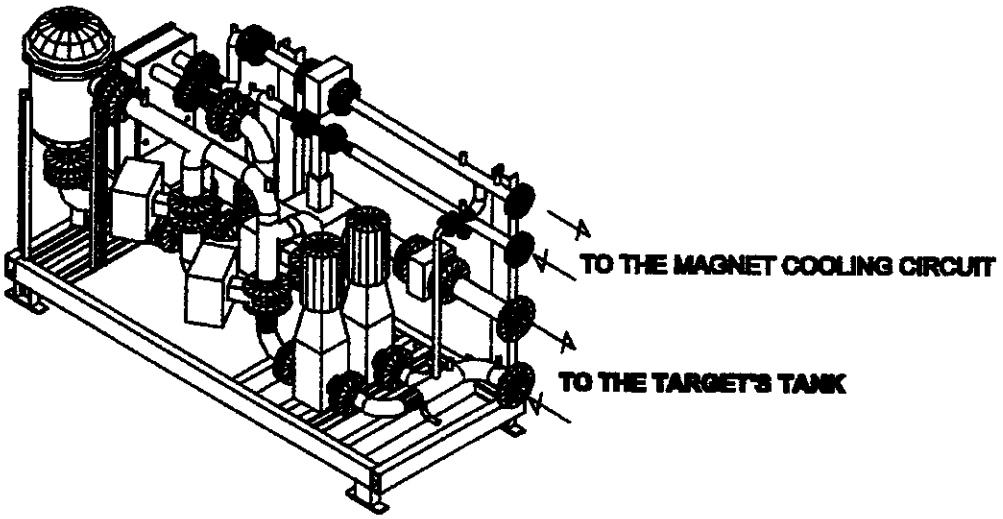

Figure 3.7: Elements of the cooling system on the supporting rack.

3.4 THE WINDOW

The aluminium alloy (AA 6082) window of 800 mm diameter is fixed onto the face of the water tank (Fig. 3.8) which separates it from the time of flight tube. The window is welded directly onto a 250 mm long aluminium alloy tube. A Helicoflex ring provides the necessary leak tightness between the water and the vacuum inside the time of flight tube. A flange is welded onto the end of this, which connects directly to the time of flight tube. This construction allows the easy mounting of the window from the outside of the tank and the easy removal of the tank from the target zone.

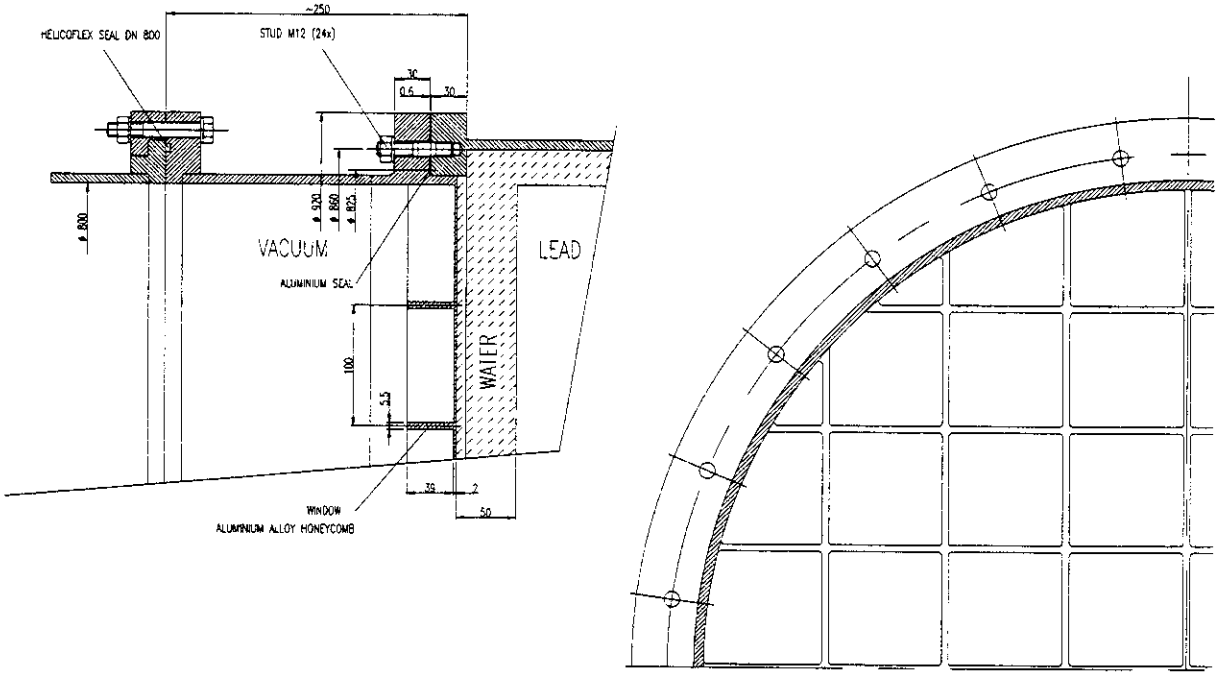

Figure 3.8: Aluminium alloy window welded to a 250 mm long aluminium alloy tube and fixed on the tank and the time of flight tube. On the right side the grid structure of the window is shown.

The window itself represents a critical part of the project. On one hand it must be solid enough to separate the water from the vacuum (pressure difference = 1.2 bar) and remain flat (maximum deflection allowed in the centre ≤ 2 mm) in order to guarantee a constant water moderation of 5 cm, therefore not affecting the energy resolution. On the other hand it should be as light as possible to avoid neutron scattering and made of the right material not to absorb too many neutrons. Furthermore, it should be radiation resistant since the dose rate accumulated in one year could reach a few 10^6 Gray depending on the running period.

We have chosen the aluminium alloy as material for the window instead of carbon fibre because of the lack of information on the resin and glue used in its construction. On one hand, this lack of information could result in a distorted and inexplicable neutron spectrum and on the other hand the strong radiation in this region may change the mechanical rigidity leading to the possible breakage of the window. The Al alloy window has the advantage that the material composition is known, therefore also the neutron spectrum, and that the mechanical stability is not influenced by the radiation.

The window itself is made of a 2 mm thick plate, reinforced by a grid 40 mm thick with sides of 10 cm in length. The struts of the grid have a thickness of 5.5 mm. This window will be machined in one piece from a thick Al alloy plate. The 'equivalent' total thickness of the Al alloy is 6.17 mm. The face of the window with the grid is mounted towards the vacuum tube. The deformation of the window amounts to 1.96 mm in the centre. However more simulation studies should be done to optimise the window.

Concerning the neutron scattering and absorption inside the window the simulation shows a 15% gain in the neutron intensity (Fig. 3.9) and a 10% loss in neutron energy resolution (Fig. 3.10) compared to the configuration described in [9].

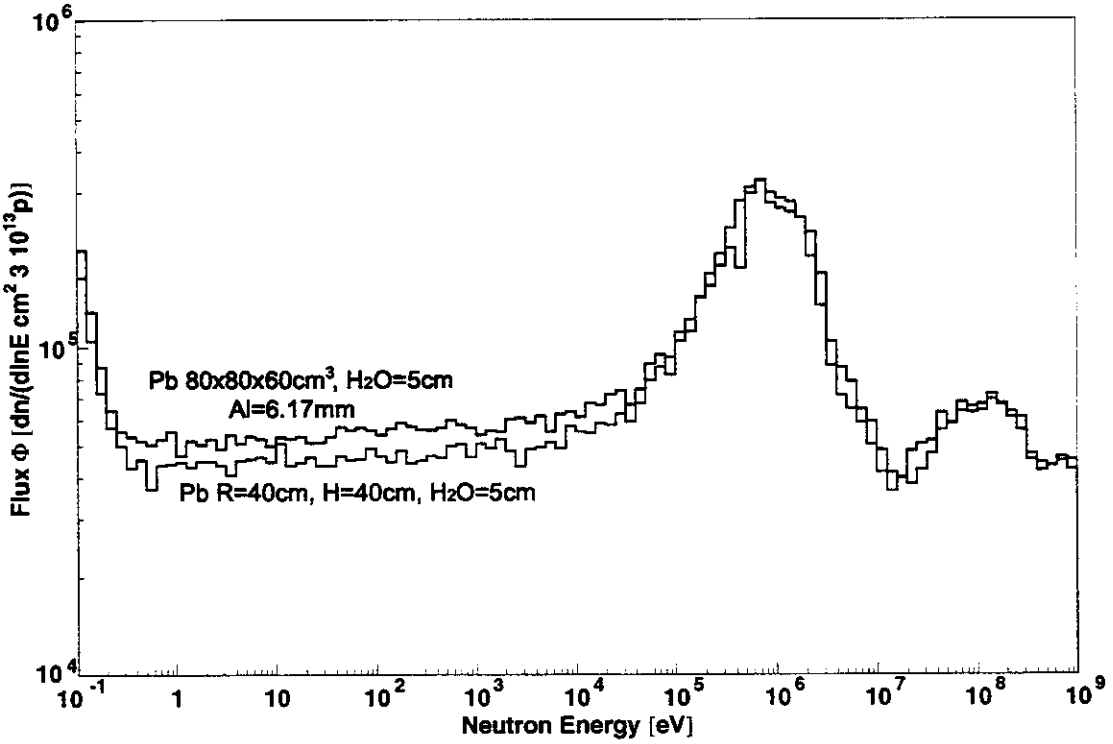

Figure 3.9: Neutron flux versus neutron kinetic energy for the actual configuration compared to the configuration in [9].

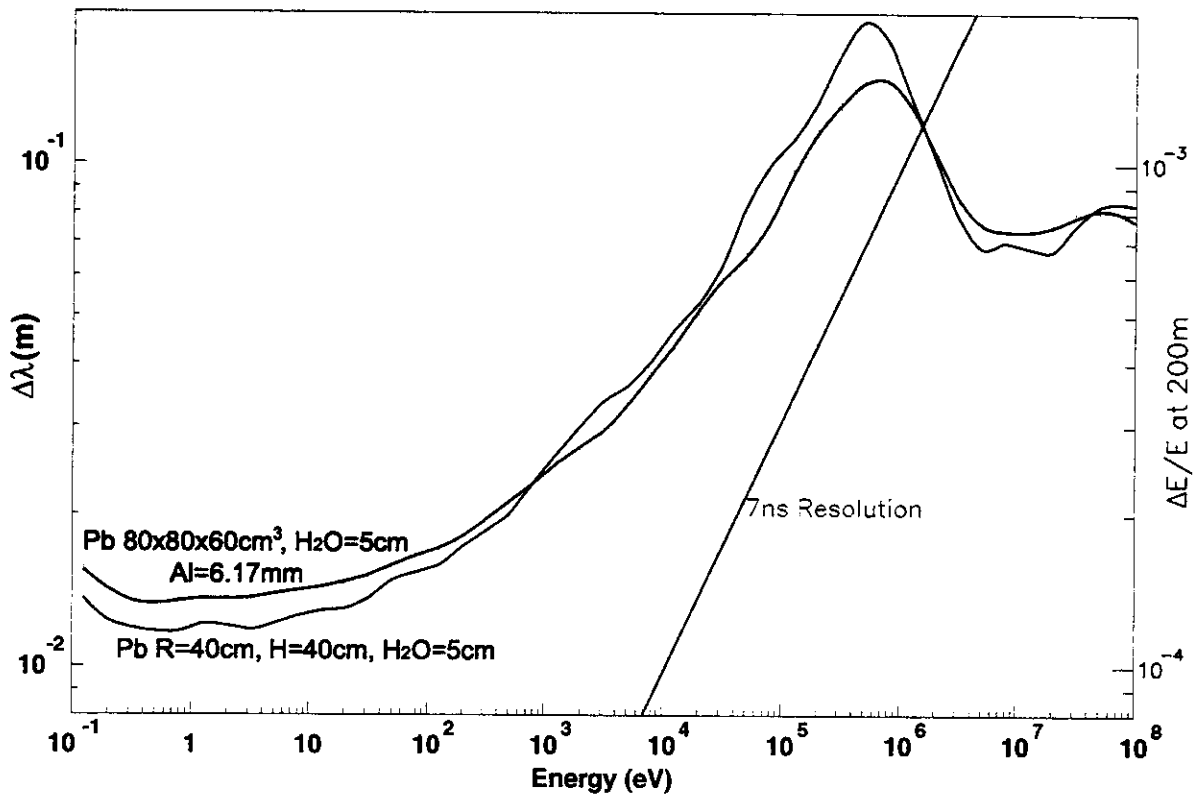

Figure 3.10: Neutron energy resolution versus neutron kinetic energy for the actual configuration compared to the configuration in [9].

3.5 THE HANDLING OF THE TARGET

The target on its stainless steel support will be lowered through the 1.3 m diameter shaft inside the water tank. During the operation of the TOF facility, this shaft is completely closed off by concrete blocks, and on top, in the ISR gallery, an additional iron shielding is necessary to keep the radiation below 1 μSv/h. During the 3-month yearly shutdown, the target might be extracted if maintenance work is necessary at the target station. This is a complicated operation since the target has an activity of 10 Ci after one month of operation and one month of cooling down (see 8.1). Therefore, the concrete blocks have to be removed from the shaft whereby the hook of the crane is fixed automatically in the eyes of the concrete blocks with the help of a television camera. Once the target is removed from the shaft it is placed in a concrete blockhouse and enclosed in concrete. Once the new run period starts, either a new target will be used or the old one can be placed back in the water container following the same procedure.

4. THE TOF TUBE

The time of flight tube will start directly behind the window and end where the rising floor of the TT2A tunnel touches the tube thus allowing a length of 200 m (Fig. 4.1). It is at an angle of 10° with respect to the proton beam direction in order to minimise the collection of unwanted secondary particles. A sweeping magnet at a distance of ≈ 150 m removes all the remaining charged particles. At the end of the tube an area should be excavated in order to house the detectors.

4.1 THE STAINLESS STEEL TUBE

As described in 3.4, the window and the 250 mm long aluminium alloy tube, 800 mm in diameter, is directly mounted onto the water tank (see also Fig. 3.8). Then a 3885 mm long aluminium alloy tube, 800 mm in diameter, is flanged onto this short tube and traverses the 2 m of marble in front of the target. From there, a stainless steel 304 L tube with different sectors, as described in Table 4.1, constitutes the time of flight tube which is represented in Figs. 4.2a, b, c.

Table 4.1: Characteristics of the various sectors of the time of flight tube. The lengths of the different sectors include some bellows.

Sector number	Material	Length [m]	Int. diam. [mm]	Thickness [mm]
1	Al alloy AA 6082	4.135	800.00	8.00
2	st. steel 304L	65.750	796.96	7.92
3	st. steel 304L	68.350	596.90	6.35
4	st. steel 304L	61.372	396.88	4.76
	Total	199.607		

The first 24 m of the stainless steel tube is divided into two parts with vacuum flanges at the end. This allows their removal during shutdown if the shielding of the target area has to be removed by forklift. In the second of the 12 m pieces, three additional windows, 600 mm in diameter, are mounted on the side. This allows measurements to be taken in the future much nearer to the target with elements, which need a high neutron intensity because of their small cross section, i. e. reaction rate.

At the end of the 800 mm diameter tube, a reduction piece of 600 mm diameter is welded. On this reduction piece, 4 windows are mounted which allow monitors to be inserted. Immediately after there is an iron shielding with a cross section of 1.80×1.80 m^2 where the left side, (seen in beam direction), is reduced to the available space to the tunnel wall. This iron shielding is embedded in 40 cm of concrete.

The next reduction with 4 windows reduces the tube from 600 mm in diameter to 400 mm in diameter. A similar iron shielding of 1.20×1.20 m^2 and 1 m long is again embedded in concrete with a total thickness of 2 m (Fig. 4.3). This time, however, the shielding fills the whole tunnel in order to remove as much background as possible. Only on the right side, a 1.6 m wide shielding is made such that it can be easily dismounted in a shutdown to allow a forklift to go through in case work has to be executed in the tunnel. Access to the tunnel is provided through the chicane.

After the shielding the 400 mm diameter tube runs through the sweeping magnet and can end at the detector station. Actually the TOF collaboration defines an additional collimator at a distance of ≈ 180 m from the target where again a reduction in tube diameter is foreseen depending on the type of experiment to be conducted.

The detector station inside the excavated basin has still to be defined as well as a special cavern of ≈ 8 m length with shielding and chicanes for trapping neutrons and to protect the detectors from back-scattered neutrons.

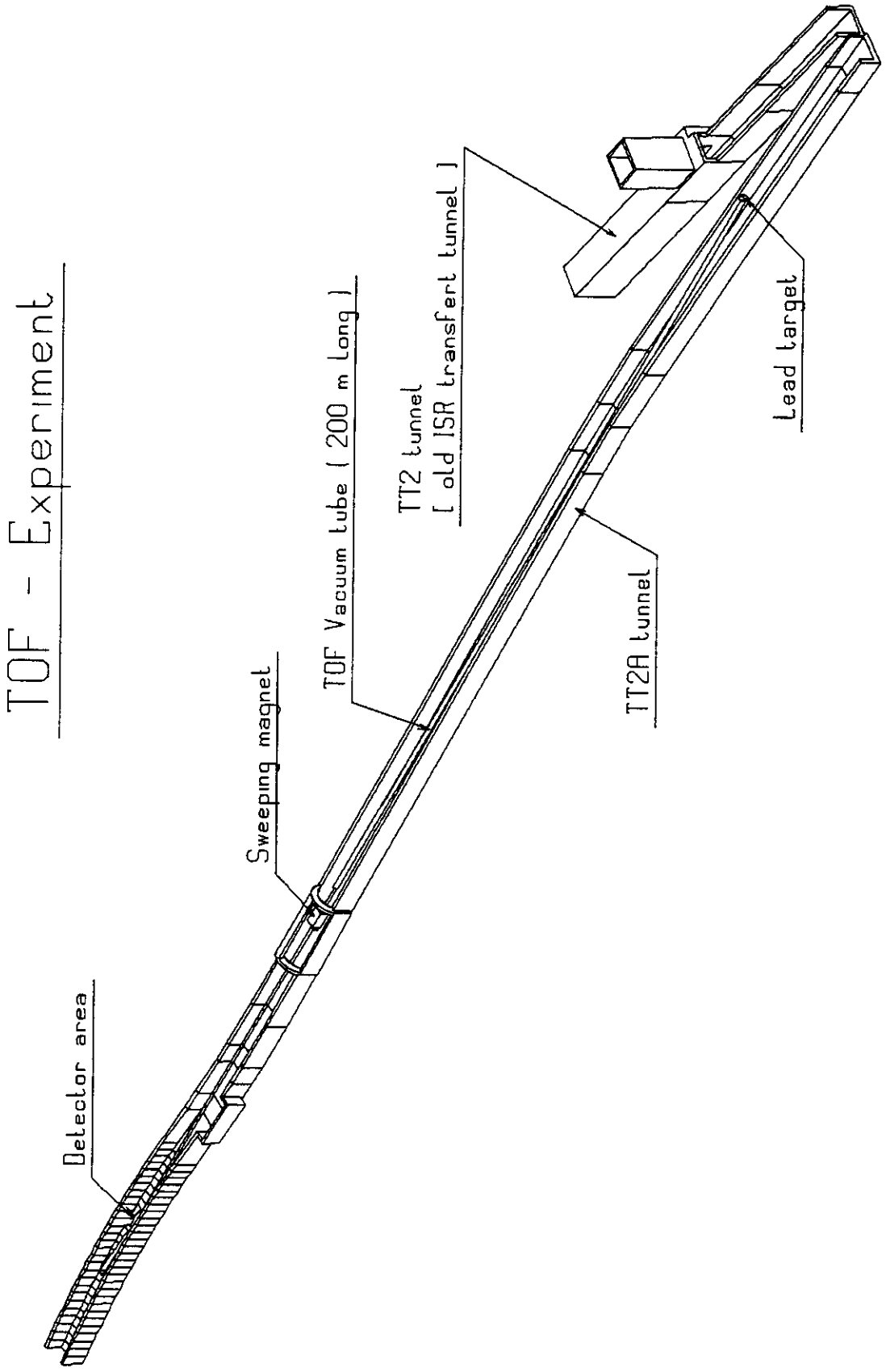

Figure 4.1: Perspective view of the time of flight tube inside the TT2A tunnel with the sweeping magnet.

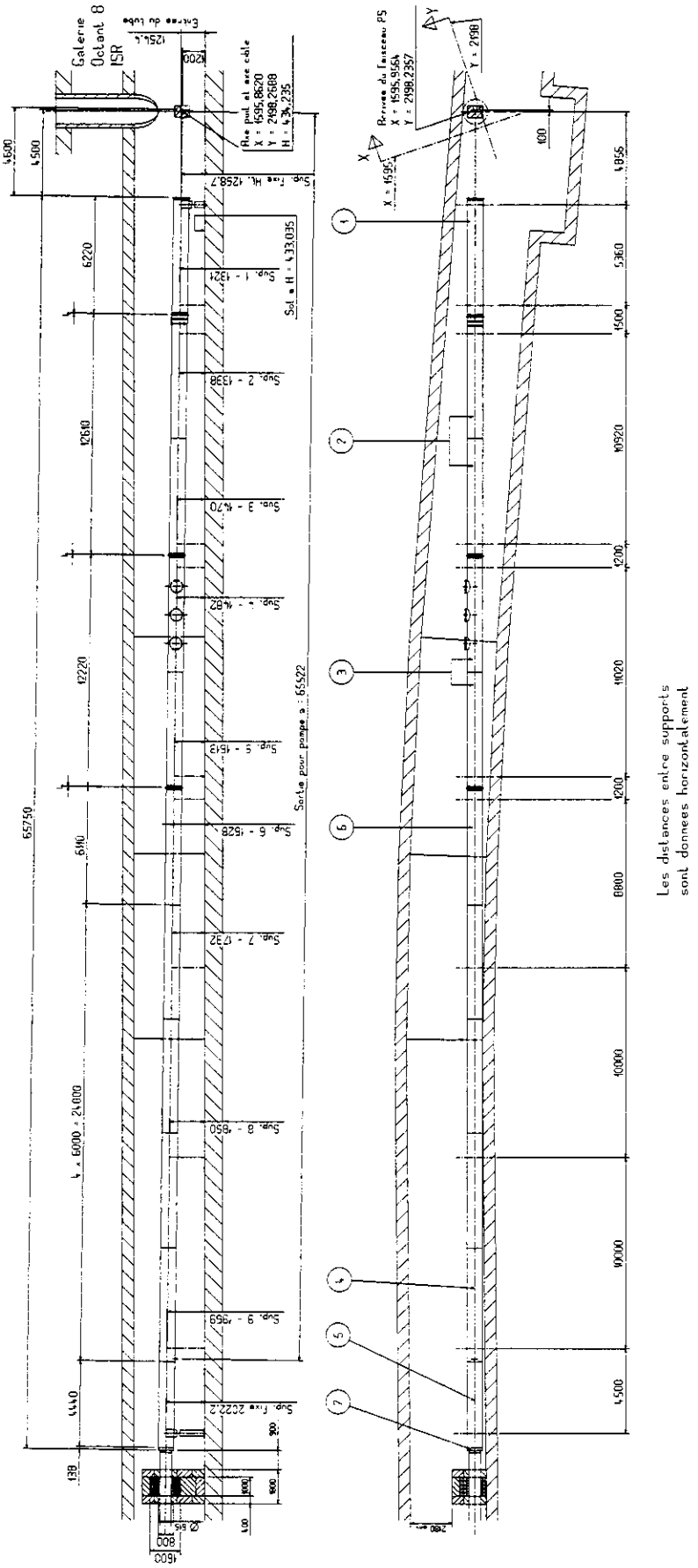

Figure 4.2a: Sector 1 and 2 of the time of flight tube with the shielding at the reduction from 800 mm in diameter to 600 mm in diameter.

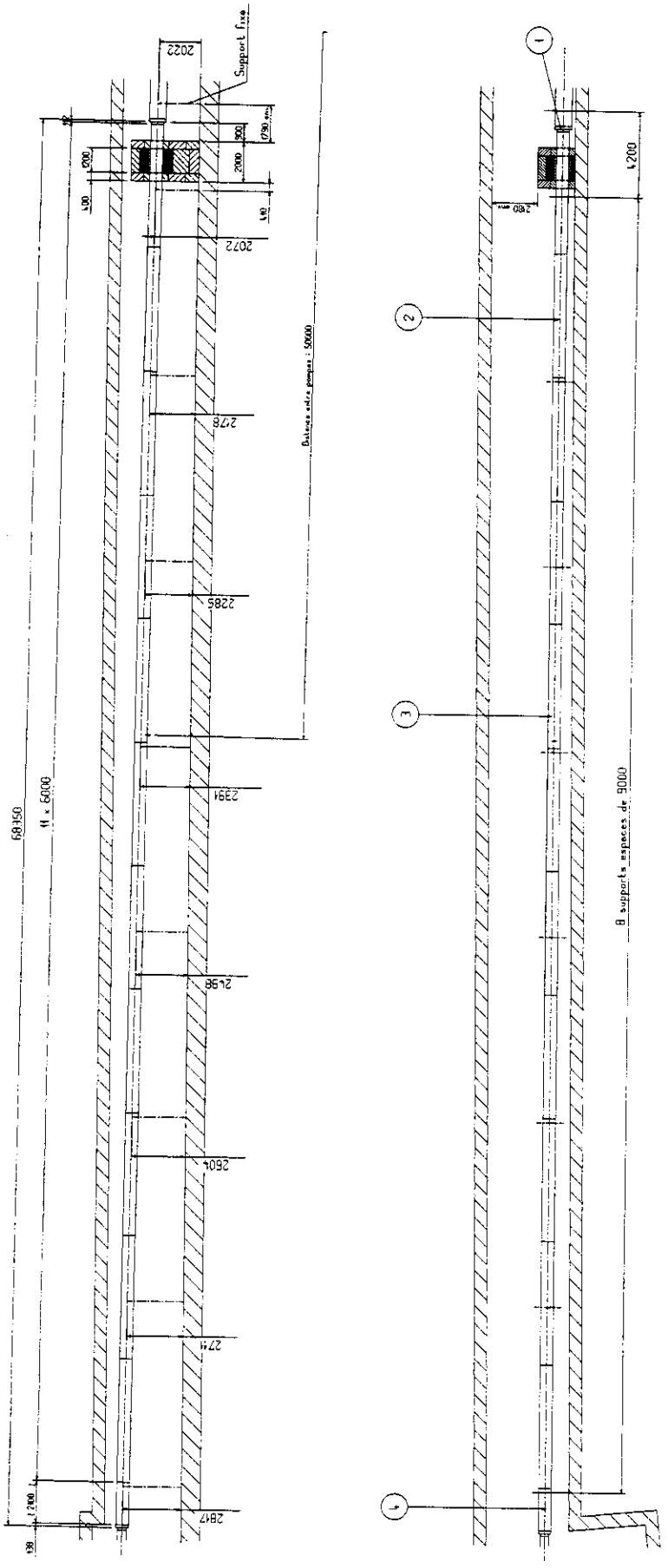

Figure 4.2b: Sector 3 of the time of flight tube.

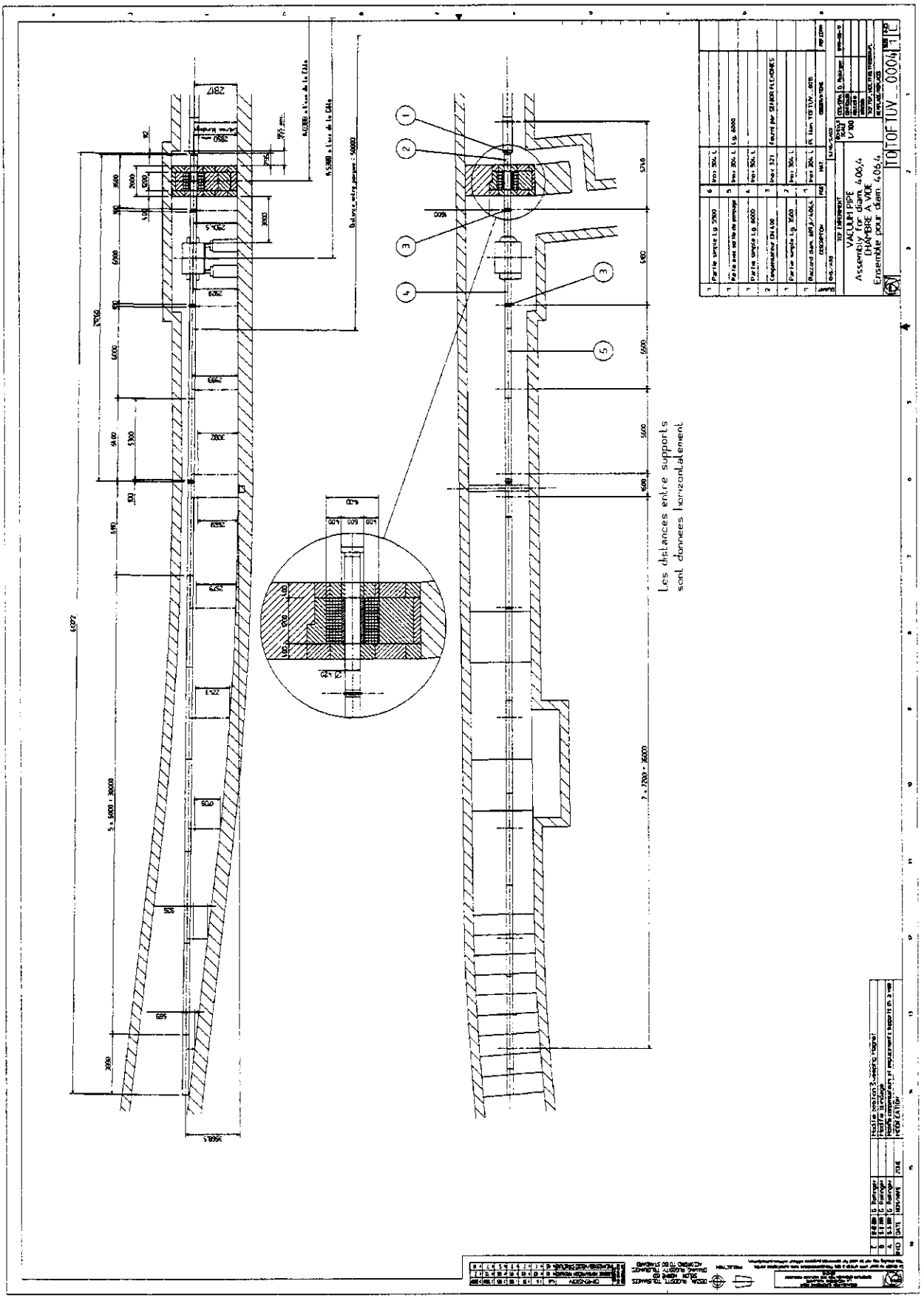

Figure 4.2c: Sector 3 and 4 of the time of flight tube with the shielding at the reduction from 600 mm in diameter to 400 mm in diameter and the sweeping magnet.

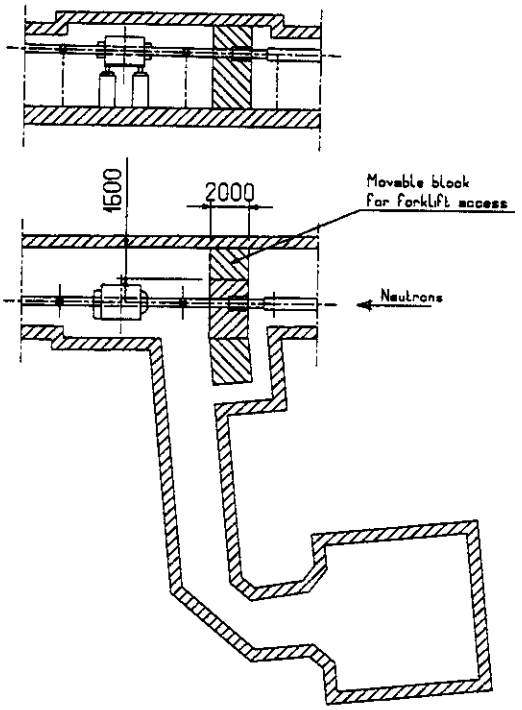

Figure 4.3: Shielding at the reduction from 600 mm in diameter to 400 mm in diameter and the shielding magnet.

4.2 THE VACUUM

In contrast to the FTN line, the vacuum requirement for the TOF tube is only 1 mbar. By using three, double stage, rotary vane pumps (35 m^3/h) this pressure will be reached in less than 10 hours (Fig. 4.4). For vacuum measurements, six Pirani gauges will be installed along the tube.

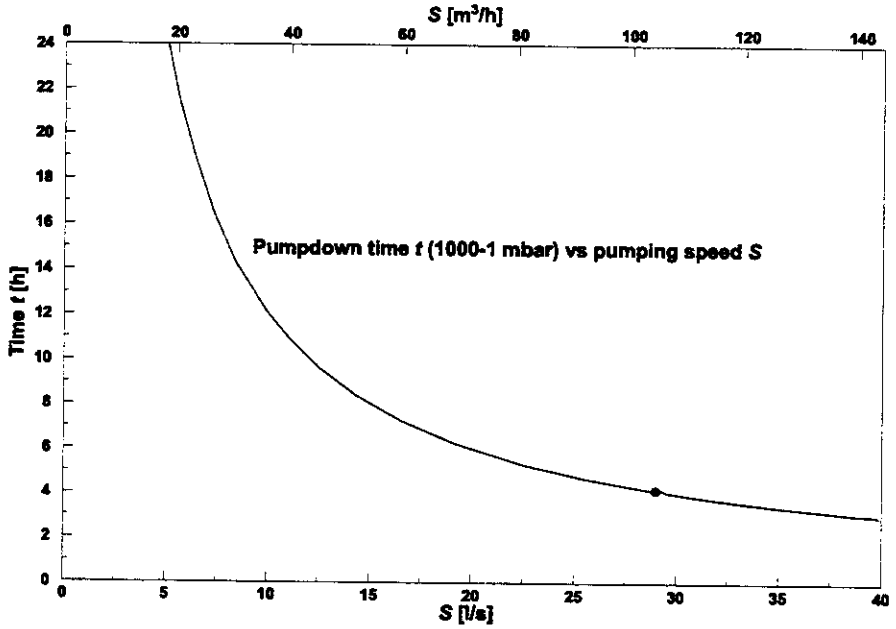

Figure 4.4: Pumping time for the time of flight tube.

At the detector side (the end of the TOF tube) a standard valve of DN 400 (~ 5 s closing time) or DN 200 (~ 2 s closing time) will mechanically protect the window. It should also be connected to the access control.

4.3 THE SWEEPING MAGNET

The natural choice consists in using a dipole magnet to sweep away the charged particles that contaminate the neutron beam. This magnet is a standard M200 magnet, which was in beam transfer lines at the PS. Only the gap has to be opened to 410 mm in order to allow the time of flight tube to pass through.

4.3.1 General characteristics of the sweeping magnet

The angular acceptance of the beam line can be computed under the assumption that the decays in flight of the charged particles generated by the spallation process can be neglected. Using this hypothesis, the geometry of the beam line allows estimating the maximum angle θ_{max} of a charged particle reaching the sweeping magnet located L meters from the beginning of the line, namely

$$\theta_{max} \approx \frac{d_i + d_{mag}}{2L}$$

where d_i represents the diameter of the beam pipe at the entrance of the beam line and d_{mag} the diameter at the magnet location. Furthermore, a deflection angle given by

$$\theta_{def} \approx \frac{d_{mag}}{(1-L)}$$

allows the deflection of charged particles travelling parallel to the beam pipe axis and near its walls so that they hit the opposite side of the pipe *(l-L)* metres downstream from the sweeping magnet. Hence, the maximum deflection angle to be produced by the magnet should be given by

$$\theta_{mag} = \theta_{max} + \theta_{def} \approx \frac{(1-L)d_i + (1+L)d_{mag}}{2L(1-L)}$$

Neither the position L of the sweeping magnet nor the parameter l can be chosen freely. In the new version of the TOF channel, the position of the sweeping magnet has been changed with respect to the previous layout. Realistic values of the parameters L and l are now 140 m and 15 m respectively. Then one obtains

$$\theta_{mag} = 26.67 \text{ mrad}$$

To determine the actual strength of the required magnetic field, it is necessary to evaluate the maximum kinetic momentum p_{max} of the charged particles to be deflected. In Fig. 4.5a the distribution of charged particles as a function of their energies and their arrival time at 200 m (Fig. 4.5b) is shown for three different products of the interaction between the proton beam and the lead target.

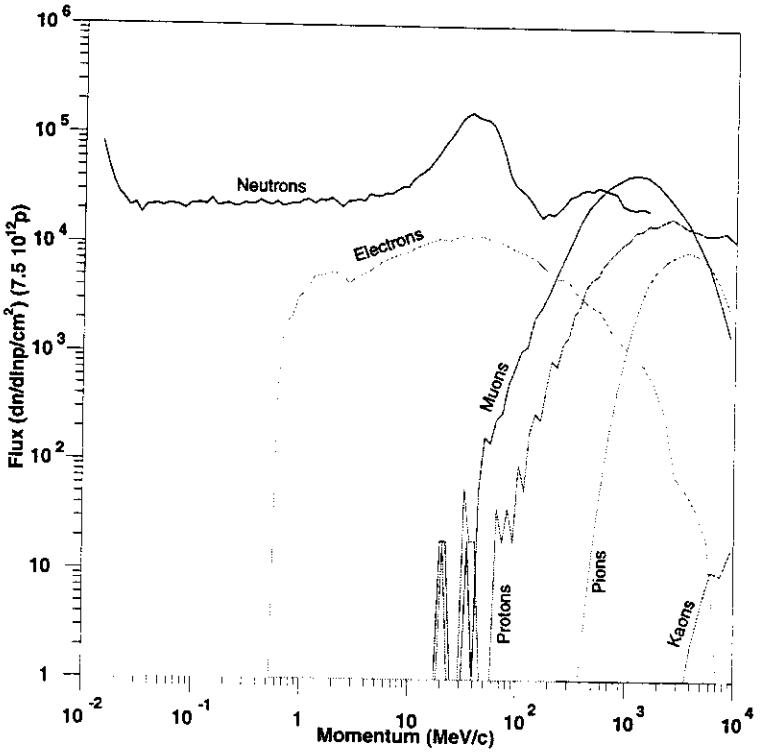

Figure 4.5a: Fluxes of the charged secondary particles produced by the spallation process as a function of their momentum.

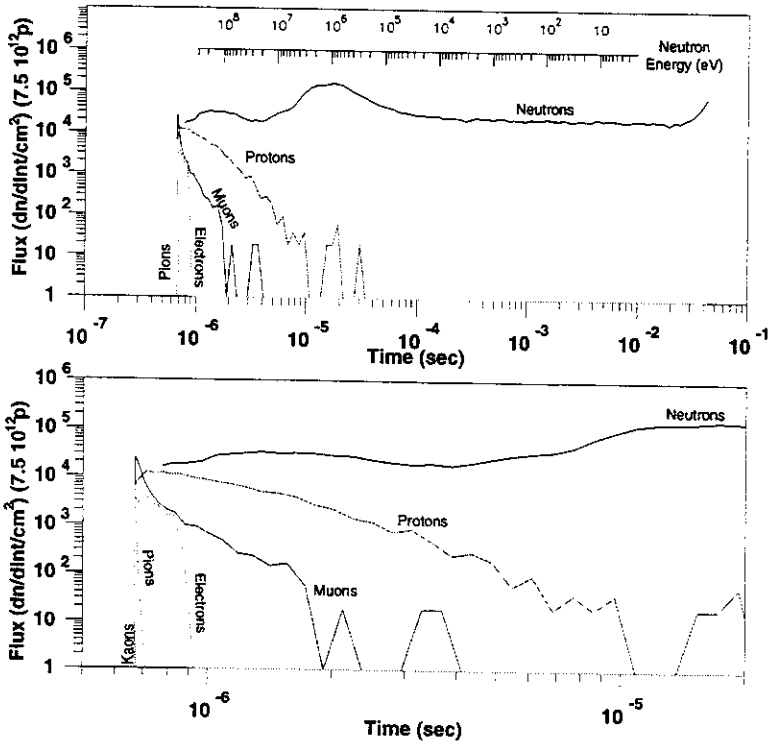

Figure 4.5b: Fluxes of the charged secondary particles produced by the spallation process as a function of their arrival time at 200 m. In the upper part, the energy is also shown. The lower picture is a magnification for times between 1 μs and 10 μs.

All three distributions show a rather sharp fall for a value of the kinetic momentum p of about 10 GeV/c. Therefore, it has been decided to define the cut-off at the value p_{max} = 10 GeV/c. From this, one obtains the integrated magnetic field of the sweeping magnet, namely

$$(Bl)_{mag} = \theta_{mag} \times (B\rho)_{max} = 1.03 Tm$$

As a remark, a hypothetical secondary particle having a kinetic momentum equal to 20 GeV/c would reach the pipe walls about 30 m downstream from the sweeping magnet under the effect of the computed angular kick $(Bl)_{mag}$.

4.3.2 Performance simulation of an electromagnetic sweeping magnet

To reduce the costs, the approach has been to look for a suitable magnet among those available in the CERN stock. The best candidate is the M200-type magnet [16]. This is a 2-metre long magnet with a variable height gap. The gap size can be changed by varying the width of a special spacing plate installed in the iron yoke (see Fig. 4.6), the spacing plate is clearly visible on the left side of the magnet yoke. This would allow the gap to be increased up to 440 mm by simply inserting a specially designed ARMCO spacing plate 330 mm thick.

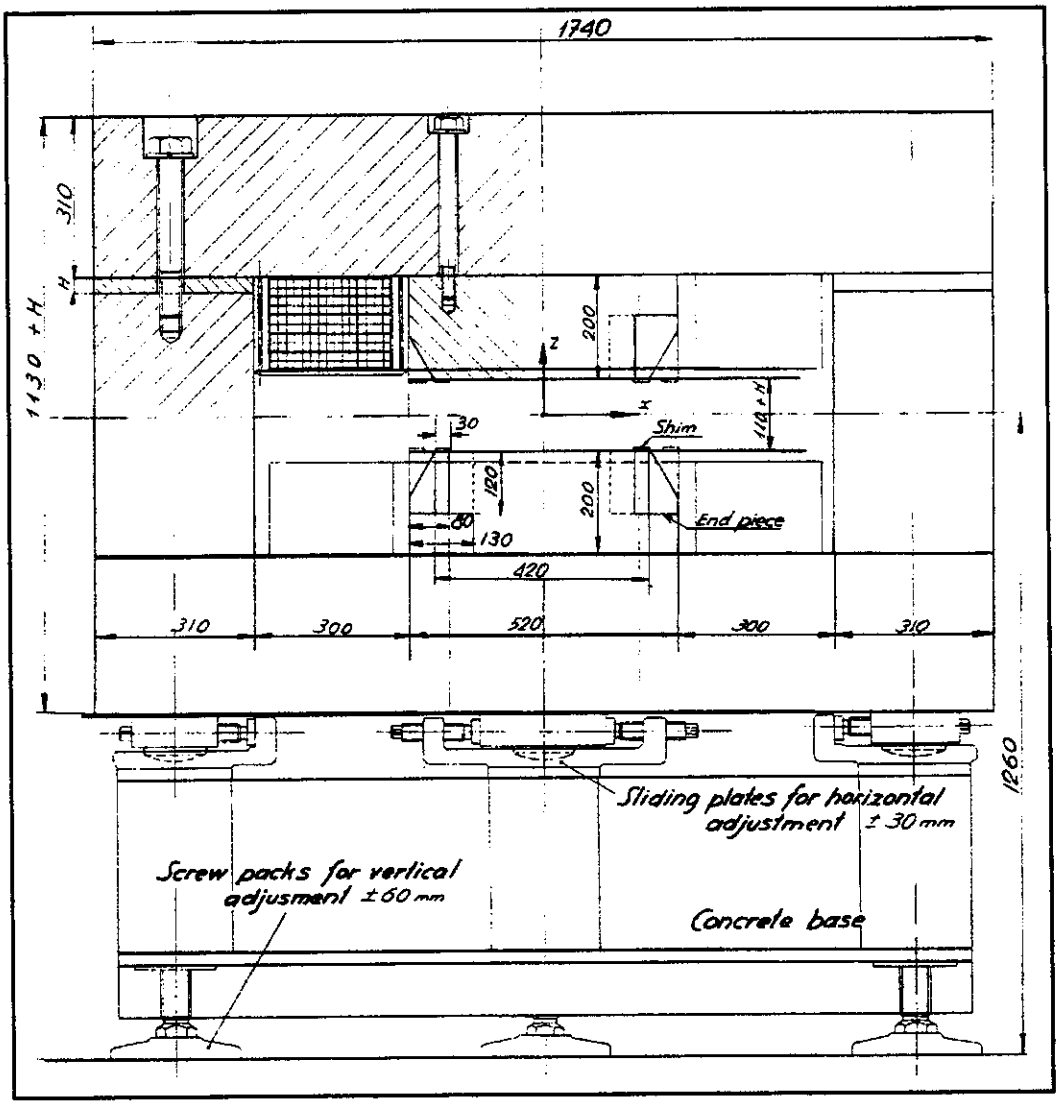

Figure 4.6: Mechanical layout of the M200-type magnet used as sweeping magnet.

This magnet exists in two versions: with straight poles or tapered poles. In order to have enough room to install the vacuum pipe inside the yoke, it has been decided to use the straight pole type.

As far as the magnetic field is concerned, the maximum integrated field is about 3.63 T m. A simulation of the magnetic performance of this type of magnet has been carried out using the OPERA program (for more details on the results of the numerical simulations see Ref. [15]). In Fig. 4.7, the mechanical layout (upper part) is shown together with the field map (centre part) and the homogeneity with respect to the peak field value of 1.77 T (lower part): the field drop in the transverse direction at the pole end is about 5%. This result allows the accuracy of the simulation to be estimated. The measured peak field is 1.73 T and this value agrees with the result of the numerical simulations within 2%. Therefore, one can be confident that the model used is also capable of correctly simulating the situation with an increased gap size. The main parameters of the M200-type magnet are summarised in the Table 4.2.

Table 4.2: Main parameters of the M200-type magnet.

Type	**2 m bending magnet. Straight poles.**
Pole face [mm^2]	2000×520
Gap height [mm]	110, 140 (nominal), 170, 200
Bending power [T m]	3.63
Resistance at 20 °C [Ohm]	0.195
Max. temperature	40 °C at inlet and 80 °C at outlet
Max. power [kW]	140
Water flow [l/min]	66
Weight of magnet [Kg]	30000
Weight of base [Kg]	6000

The increase in the gap size will result in a drop of the magnetic field produced, which is approximately proportional to the ratio of the two gap sizes. Therefore, it is expected to have an overall reduction by a factor of three with respect to the nominal layout (140 mm gap size). The numerical simulations shown in Fig. 4.8 confirm this trend: in the upper part, the distribution of the field lines is plotted on the transverse plane. In the centre part, the field homogeneity is shown in the form of a contour plot, while in the lower plot it is reported the field homogeneity as a function of the transverse coordinate.

The peak field reaches a value of 0.75 T, thus giving an integrated field of about 1.5 T m. This is a rather conservative estimate, as the magnetic length will be bigger than the mechanical length of the magnet, due to the very large gap size. The field homogeneity is about 10%, but this is not a major source of concern in this specific case. In fact, the field quality is not relevant as long as the minimum integrated field is high enough to deflect the charged particles and this is certainly the case for the field drop obtained with numerical simulations. For this reason, the possibility of modifying the shims in order to improve the field quality has not been taken into account.

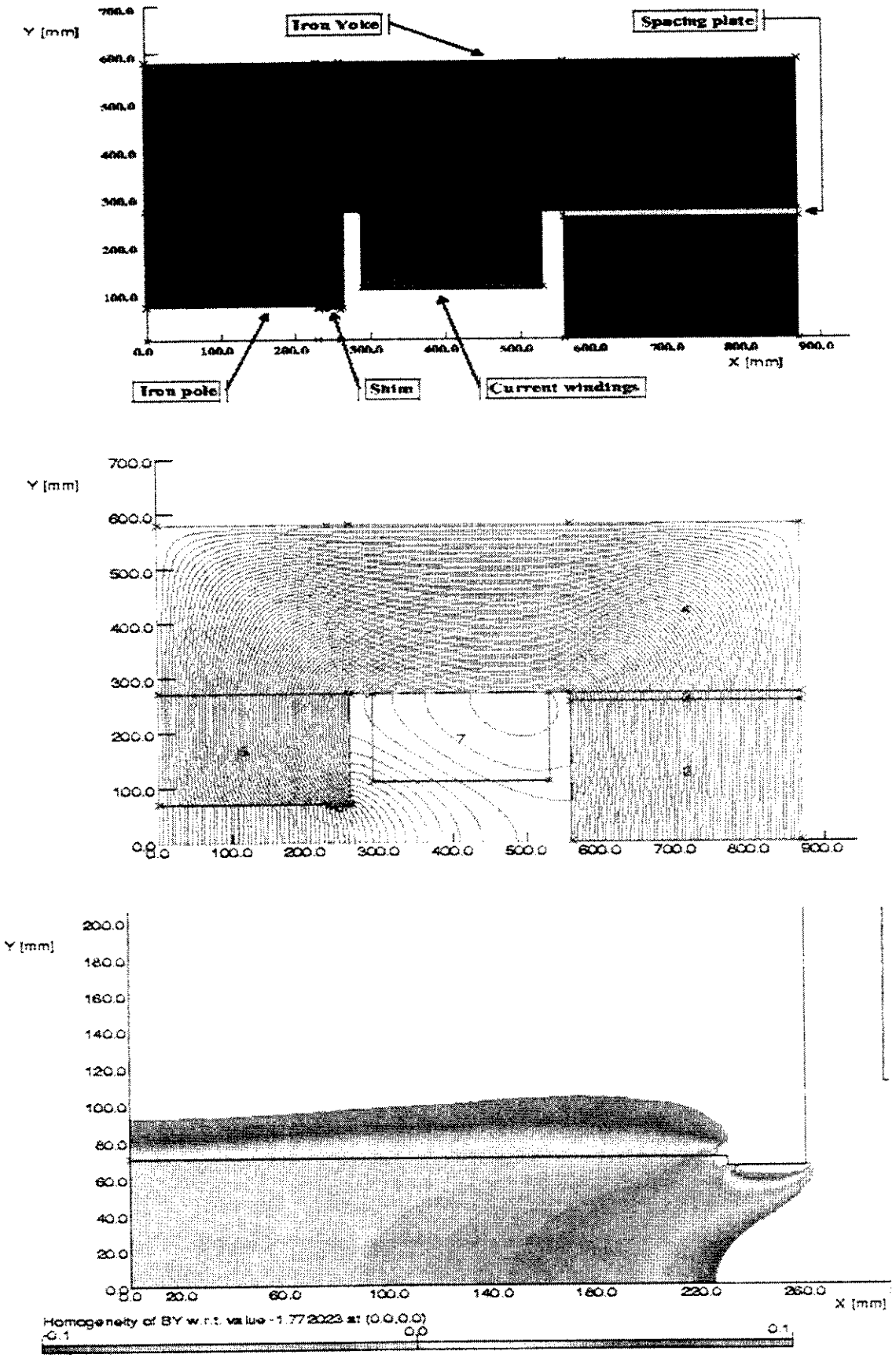

Figure 4.7: Layout of the M200-type magnet. The geometry is shown in the upper part. In the centre part, the field map is shown for the standard configuration (140 mm gap), while in the lower part the field homogeneity with respect to the peak value is shown.

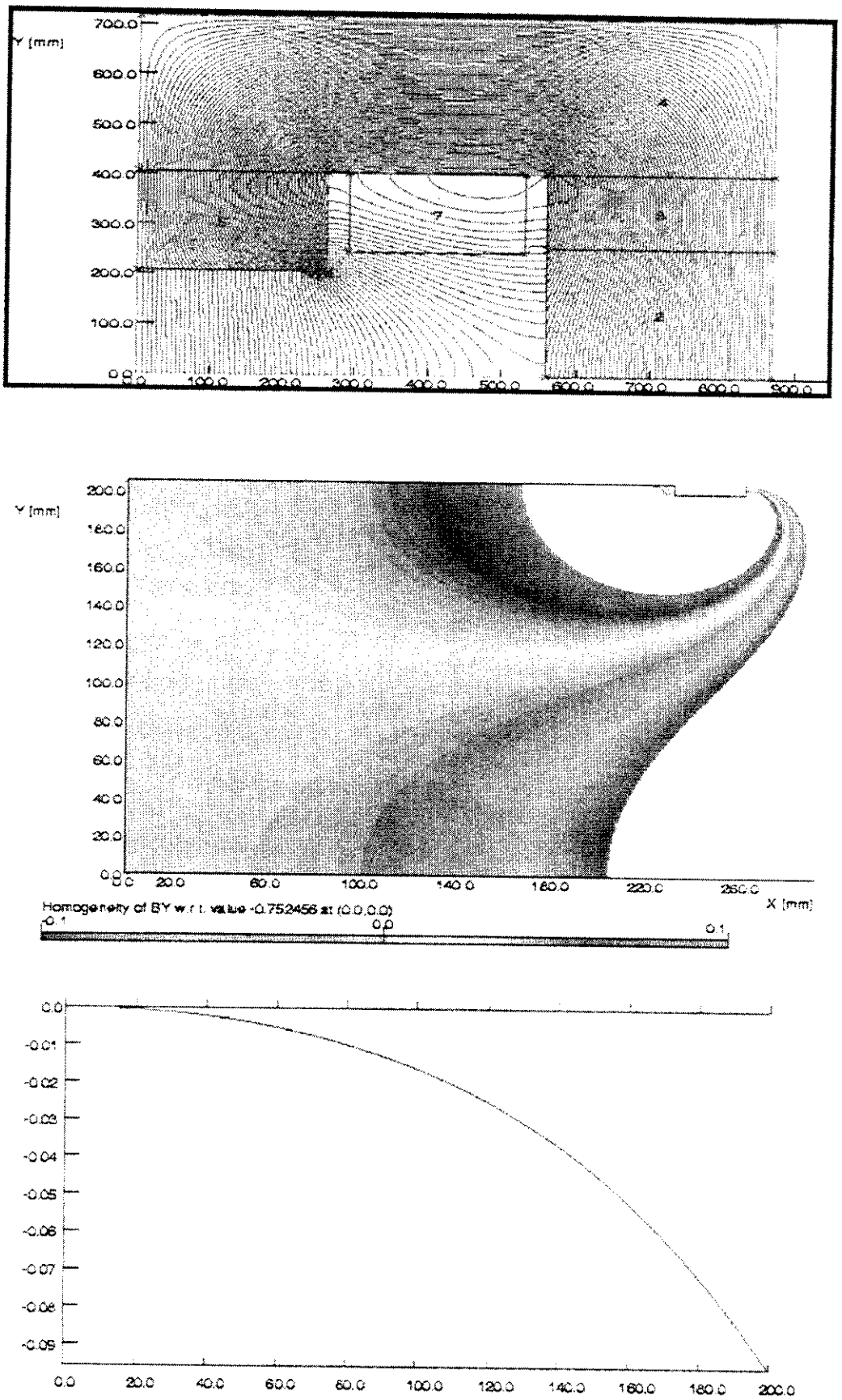

Figure 4.8: Magnetic properties of the M200-type with 410 mm gap. The field lines are shown in the upper part. In the centre part, the contour plot of the field distribution in the magnet gap is plotted. In the lower part, the field homogeneity is presented.

An important point is that such a magnet has already been installed in regions with a high degree of radioactivity (primary areas of the East Hall). However, one should keep in mind that the weak point, as far as radiation hardness is concerned, is the resin used for the magnet coils. Typical values of integrated doses sustainable by the resins used to build coils are of the order of 5×10^7 Gy [18].

The water-cooling should pose no problems since the water supply is taken from the TT2 tunnel. The power dissipated by the magnet during normal operation requires the presence of a ventilation system in the TT2A tunnel, in order to avoid a temperature rise in the whole tunnel.

Finally, it has to be mentioned that the power converter can also be recuperated from the PS stock.

5. CIVIL ENGINEERING WORK

The realisation of the TOF project makes four different civil engineering interventions necessary:

5.1 BEAM DUMP D3

In the previous study reports, [10, 12] a heavy program of civil engineering activities was required in order to allow the installation of the FTN transfer line and of the TOF beam pipe. In the new configuration, most of the items have been removed from the list. The only activity left concerns the dump D3: despite the efforts made to find a solution where the deflection point of the FTN transfer line is shifted further upstream with respect to the previous design, no feasible configuration has been found. In fact, not far from the point where the TT2 and FTN transfer lines start to diverge, are located the bending magnets to deflect the beam towards the SPS machine via the TT10 transfer line.

Therefore a hole should be drilled in the concrete blocks on the left-hand side of the dump D3 to let the beam pipe pass through, as foreseen in [10, 12].

5.2 TARGET ACCESS SHAFT

In order to allow the installation and the removal of the target, an access shaft of 1.3 m diameter and ~ 5 m height had to be constructed between the TT2A tunnel and an overlying ISR gallery.

The volume between the tunnel and the gallery being fully filled with concrete, the shaft has been executed by drilling spaced holes along the perimeter of the shaft, between which the concrete has been sawn.

The plug of ~17 tons has been sectioned in pieces and lifted with a gantry crane, installed over the shaft.

In the lower part of the shaft, a concrete support has been made for the plugs foreseen to close the hole.

5.3 TARGET SHIELDING

The shielding around the target under the shaft is divided in two parts: one part fixed, the second removable.

The fixed part is partially made out of marble, essentially for the volumes surrounding the incoming proton vacuum pipe and the outgoing neutron TOF tube. The rest (floor, columns and roof) is made out of concrete loaded with 1% of boron.

The thickness of the shielding on the proton side is 1.9 m and 3.2 m on the forward direction.

The movable part is made out of standard concrete blocks (80 cm thick) followed by boron loaded blocks (40 cm thick).

5.4 EXPERIMENTAL AREA

A pit and a trench are planned at the end of the tube, in the zone where the tunnel TT2A has an upward gradient.

The details of this intervention are still to be defined. To date, the following dimensions are proposed:

Pit: $4 \times 4 \times 2$ m^3 (length × width × depth)

Trench: $8 \times 1 \times 1.5$ m^3 (length × width × depth)

6. ELECTRICAL WORK

6.1 GENERAL CONSIDERATIONS

The installation of the TOF project in tunnel TT2A requires the following electrical work:

- Installation of two rectifiers and two corrector magnets in station 24 (Bldg. 269) and a rectifier for the *sweeping magnet* whose final destination remains to be determined.
- Installation of an electrical switchboard in the TOF control room to supply all general electrical services in the zone.
- Electrical supply of the target cooling station in the tunnel from station 24.
- Installation of stand-by lighting and new normal lighting in TT2A tunnel.
- Installation of emergency stop buttons in the TT2A tunnel.
- Pulling of different control cables mainly between PS and TT2A tunnel.

6.2 DESCRIPTION OF WORK

Specific electric work of this project, which will be completed by the ST/EL group are the following:

6.2.1 Station 24 (Bldg. 269)

- Removal of EBD1*24 switchboard in order to leave space for the rectifiers to be installed.
- Removal of a 48 V charger EAU131*24. This space will be assigned to the corrector racks.
- Supply 48 V loads from the 48 V distribution board ECG1*23 in station 23.
- High voltage disconnection of transformer EMT103*24 feeding the EBD1*24 switchboard.
- Disconnection and earthing of all the low voltage connections concerning the switchboard EBD1*24 and the transformer EMT103*24.
- Installation of 160 A feeders and cables from Y-T8 board feeding the two rectifiers to be installed.
- Installation of 100 A feeders and cables from Y-T8 board supplying the two correct racks to be installed.

6.2.2 Station 23 (Bldg. 214)

- Installation of an EBD3*23 board intended to recover loads from the general services panel to deposit in station 24.
- Transfer of all EBD1*24 loads to a new EBD3*23 switchboard.
- Transfer of the 48 V charger EAU131*24 load to the ECG1*23 switchboard.

6.2.3 Station 66 (Bldg. 273)

- Refitting of the existing feeder with a new 630 A circuit beaker and new cable link from ERD4*66 switchboard for the rectifier of the *sweeping magnet*.
- Refitting of the existing feeder with a new 250 A circuit beaker and new cable link from EBD2*66 switchboard for a new general services switchboard in TOF control room.

6.2.4 Tunnel TT2A

- Installation of a new 15 kW link from EAD11*24 switchboard feeding the target cooling station.
- Installation of a general services board in the TOF control room.
- Installation of normal lighting.
- Installation of stand-by lighting.
- Installation of emergency stop buttons.

7. CONTROLLED ACCESS

7.1 GENERAL CONSIDERATIONS

The realisation of the TOF facility implies the implementation of safety systems ensuring personnel and equipment protection. The purpose of this document is to give a general overview of the access control and machine interlock safety systems foreseen. This document will be considered as a first draft based on the actual definition of the project infrastructure. The different layers of the safety systems and the access operation principles will be described.

7.2 SAFETY CONSIDERATIONS

At CERN the areas under radiation control are divided in two families:

- Primary Beam Areas,
- Secondary Beam Areas.

These areas are submitted to the following safety rules:

- Access to the areas under radiation control must be forbidden and nobody should be present in these areas during beam exploitation.
- Should the beam be absent, the machine should be switched off and the level of resident radiation must be acceptable before access to such areas.

In order to cope with these rules an Access Control System and a Machine Interlock System are to be provided for each family of beam area:

7.2.1 Access Control Systems - ACS

The Access Control System controls the equipment (doors, separating grids, shielding walls,...) wrapping and parcelling out a primary beam area. All this equipment is called (following the INB Regulations) Important Safety Components of the access (ISC-access).

7.2.2 Machine Interlock Systems - MIS

The Machine Interlock System manages the equipment (i.e. beam stoppers, magnets power supply, other machine equipment involved in the safety,...) in charge of beam circulation. All this equipment is called (following the INB Regulations) Important Safety Components of the machine (ISC-machine).

The safety concept is based on the interlock of these two systems:

- Under the Machine Interlock System exploitation all the Important Safety Components of the access should be bolted in a 'SAFE' position and a 'VETO' signal inhibits and prevents any access procedure. In the case of an emergency, the ISC-machine is immediately stopped if a door is opened.
- In the same way, under the Access Control System exploitation, all the Important Safety Components of the machine should be stopped ('SAFE' position) and a 'VETO' signal inhibits and prevents the engaging of the power supply.

7.3 SAFETY SYSTEMS OF THE TOF PROJECT

The architecture of an industrial network can be divided in the following layers: the *Equipment Layer*, the *Control/Safety Layer* and the *Supervision Layer*. Hereafter are the layers foreseen for TOF's safety systems.

A. Secondary Beam Area

This area (see Fig. 7.1) being considered as a Secondary Beam Area, access is allowed following the procedure of an experimental area's access. In this area the detector of the experiment is located.

The *Equipment Layer* is made of the following items:

- 1 Secondary Beam Area Access Points equipped with:
  - one *personnel* access door - PPE1,
  - one *material* access door - PPX0,
  - a film-badge reader,
  - one monitor (assistance to the users),
  - a panel signalling the access mode,
- 2 grids (PPX1, PPX2) used as emergency exits and a sector grid,
- 2 search hardware systems dedicated to the patrol of the area divided in two sectors,
- Hardware interfaces, switches, contacts... dedicated to the generation of the ISC-access/machine safety signals (access equipment, bending magnet, beam stoppers, PS extraction, other ...),
- Cabling/hardware interfaces related to the acquisition of the safety signals (access and machine equipment).

The *Control/Safety Layer* is made up of the following items:

- A hardware fail-safe industrial network based on 3 Programmable Logic Controllers,
- Its communication network Profibus or Ethernet TCP/IP -based.

The *Supervision Layer* is made of the following items:

- An Ethernet *TCP/IP-based* communication network,
- One workstation running the access application program,
- One PC located in the access point dedicated to the access procedures.

Access exploitation principle

During machine exploitation (ISC-machine ON), the Access Point is bolted in order to prevent any access to the area (CLOSED MODE). As soon as the ISC-machine is off, the authorised users set the Access Points into a SUPERVISED MODE thus granting the access to the machine. The users are identified by the system (by insertion of the film-badge in the film-badge reader) and, if they're authorised, the door is automatically released. Before turning into data acquisition exploitation, the area will be patrolled by the users.

B. Primary Beam Area

This area (see Fig. 7.1) being considered as a Primary Beam Area without Access Point (therefore without direct audio and video supervision), the access is allowed following a specific procedure.

The *Equipment Layer* is made up of the following items:

- 2 grids (D204, D201) used as entrance points,
- 2 doors (D202, D203) dedicated to the parcelling of the target area,
- 6 search hardware systems dedicated to the patrol of the area,
- Hardware interfaces, switches, contacts... dedicated to the generation of the ISC-access/machine safety signals (access equipment, bending magnet, beam stoppers, PS extraction, other ...),
- Cabling/hardware interfaces related to the acquisition of the safety signals (access and machine equipment).

The *Control/Safety Layer* is made up of the following items:

- A hardwired fail-safe network based on the existing safety system of the PS Primary Beam Areas,
- Its communication network,
- The integration in the existing PS safety system of an additional safety chain.

The *Supervision Layer* is made up of the following items:

- The existing PS-CO Ethernet *TCP/IP-based* communication network,
- The existing ACSPS1 workstation running the access application program.

Access exploitation principle

The absence of Access Points hampers the access procedure to the primary beam area. Any access to this area is possible using one unique key located in MCR under the responsibility of the operators. In addition, a TIS/RP technician should grant the access after the verification of the resident radiation of the area.

Of course, all grids will be equipped with emergency passage devices (in both ways) for evacuation of the area in the case of an emergency.

The activation of any emergency passage device will also stop (in addition of all machine equipment dedicated to TOF), the extraction from the PS.

A specific access procedure around the target area will be defined with TIS as soon as possible.

7.4 REMARKS

- A more detailed study concerning the ventilation of the primary area is needed in order to define the door location.
- TIS/RP recommendations need to be clarified regarding the access to the target area.

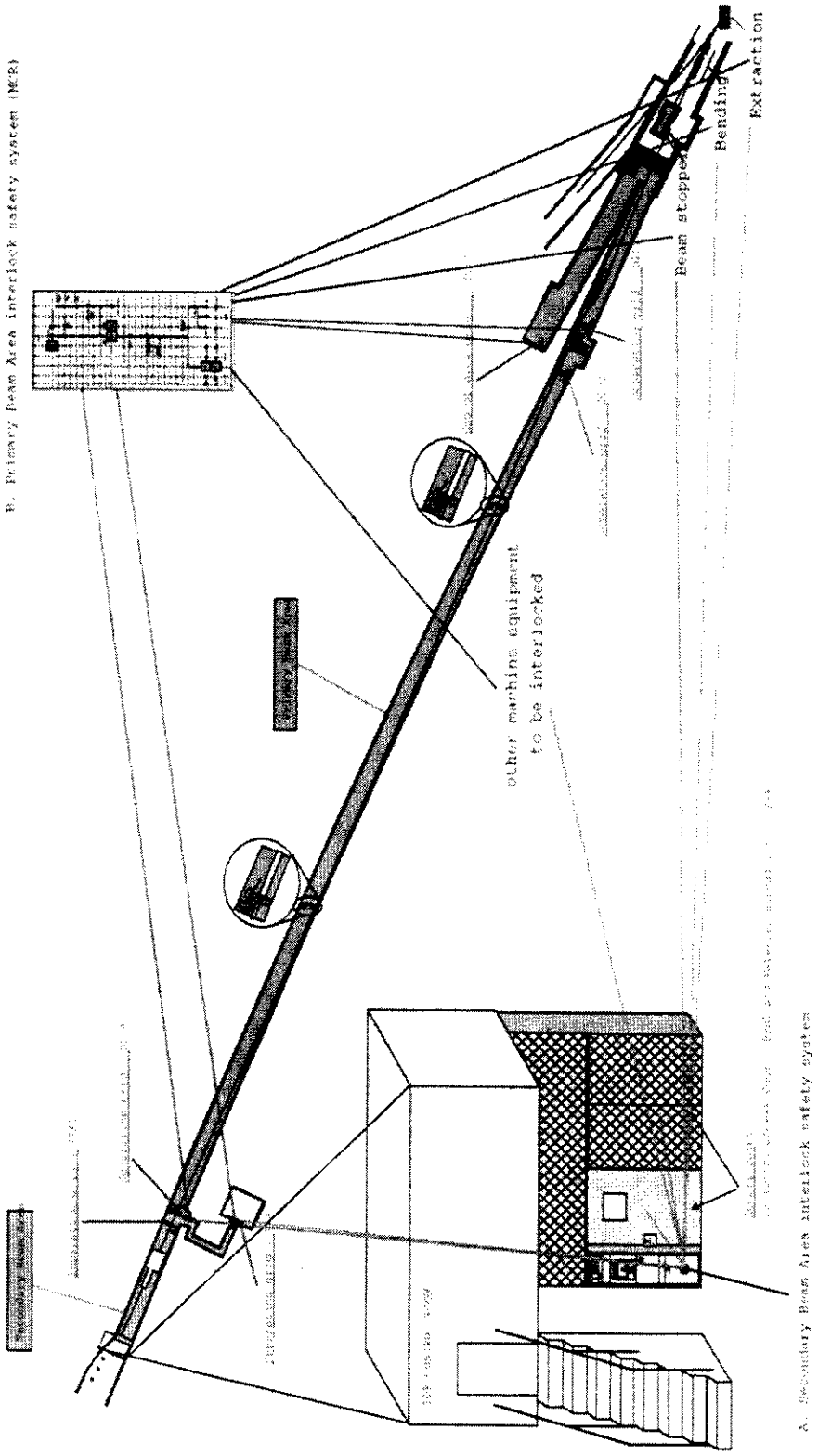

Figure 7.1: Schematic layout of the Access Control equipment location.

8. SIMULATION STUDIES ON ACTIVATION

The TOF facility uses a high intensity proton beam which, through the spallation process, produces a high flux of charged particles, gammas and neutrons. One of the main concerns is clearly the radioprotection of such a facility. Therefore

intensive simulation studies were undertaken to calculate the activity and dose at different places of the TOF facility.

The important points of this simulation cover the following topics:

- activation of the lead target,
- activation of the cooling water,
- dose around the target area,
- dose near the sweeping magnet.

In this and the following paragraph 9, the different above-mentioned topics will be treated in more detail.

8.1 ACTIVATION OF THE LEAD TARGET

8.1.1 Simulation conditions

The geometry used in the simulation is shown in Fig. 8.1. The dimensions of the lead target are 80 cm in height, 80 cm in width, and 60 cm in depth. The niche of dimensions 40 cm × 30 cm × 20 cm in the back face is taken into account. The front face plane is at an angle of -0.676° with respect to the vertical.

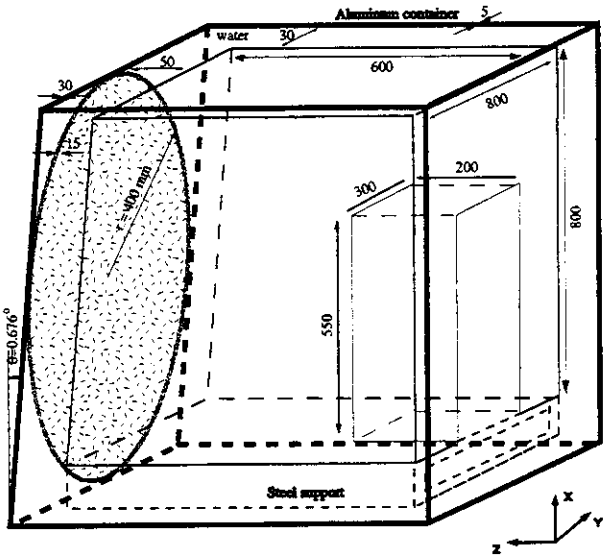

Figure 8.1: Geometry of the TOF target used in the simulation.

The target lying on a steel support is submerged in water and contained in an aluminium alloy vessel. The water layer surrounding the lead is 3 cm except at the front face of the target where it is 5 cm thick. The walls of the aluminium container are 0.5 cm thick, the front wall is tilted at the same angle as the lead and is 3.0 cm thick.

The origin of the system is in the centre of the lead target; the proton beam travels in the Z direction with an incident angle of 10°, the X axis is vertical and the Y axis points to the right. The 24 GeV energy proton beam, which is the maximum possible energy, hits the lead target at the point (x = 0, y = -1.7632 cm, z = -10 cm).

8.1.2 Activity of the target

We scored the residual nuclei produced by inelastic hadronic interactions in the lead volume. The intensity of the beam is about 0.7×10^{13} protons per pulse. We have considered 2 cases, one with a pulse every 14.4 s and another one with 4 pulses every 14.4 s. Furthermore, we have considered two irradiation periods, one of

1 month, and one of 9 months. The decay of the nuclei starts from the beginning of the irradiation, the beam intensity is supposed to be constant, of the order of 4.86×10^{11} protons per second, and 1.94×10^{12} protons per second respectively. The total activity of the lead target is given in Fig. 8.2; at the end of the irradiation, the activity is about 850 Curies for one pulse. After 1 year of cooling, the total activity is around 1 Ci for 1 month's irradiation time, and about 7 Ci for 9 months irradiation time. For 4 pulses the values are four times larger.

The dose equivalent rate after 1 month of irradiation time and one day of cooling, is estimated on the front face of the lead target about 25 Sv/h. This result is obtained by using the ω factor giving the dose rate in contact with an extended surface in rem/h; this factor is applied to a *star density rate* (hadron inelastic interaction given per cm^3/s) calculated in Monte-Carlo programs (FLUKA [19] in our case); this star density is deposited for an irradiation period followed by a given cooling time [20].

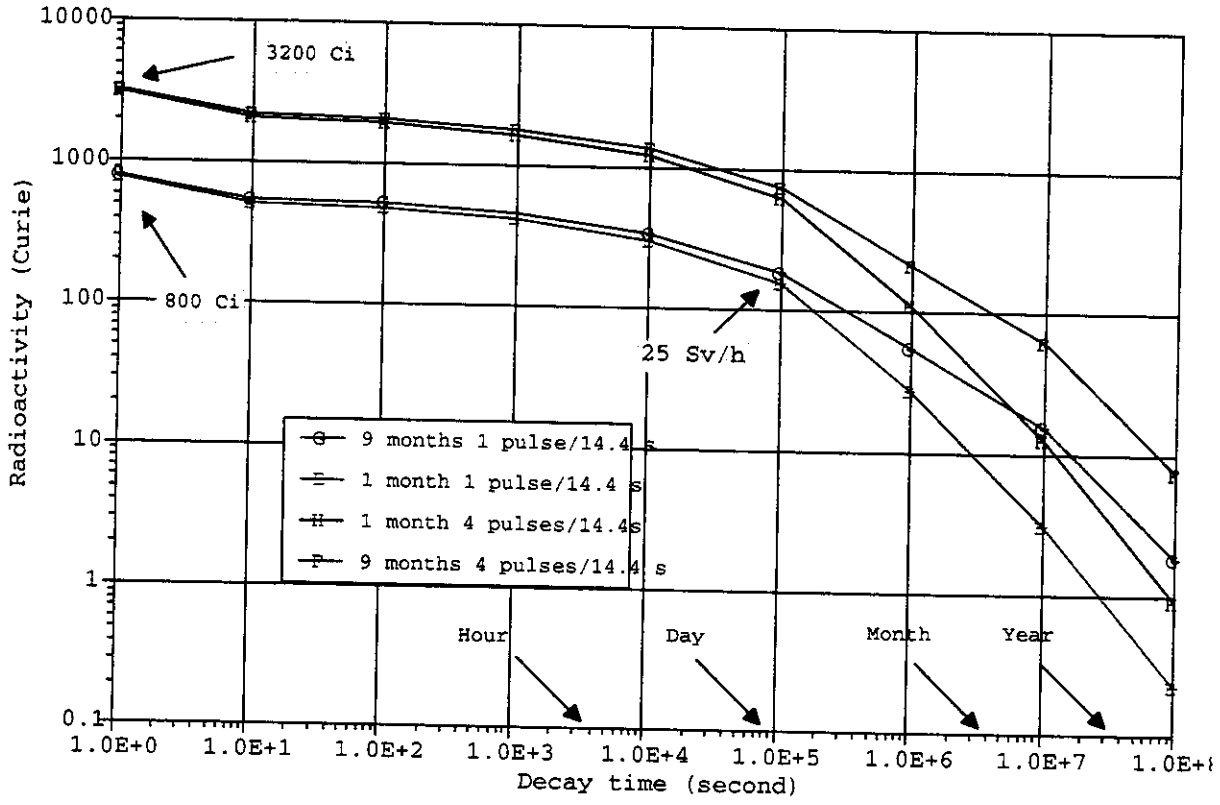

Figure 8.2: Total activity of the lead target for an irradiation period of 1 month and 9 months irradiation versus cooling time, for 1 and 4 pulses.

8.2 ACTIVATION OF THE COOLING WATER

The same conditions as described previously for the lead activation have been used.

An estimation of the total volume of water used for the cooling system is about 700 l, the aluminum container is filled with 20% of this volume; Fig. 8.3 shows the total activity of the water inside the container after 1 and 9 months irradiation for 1 pulse and 4 pulses per supercycle. The activity decreases rapidly after 1 day because of the short half-life of the nuclei present after the shutdown.

We can reasonably assume that the activity of the whole water volume is five times less than the activity shown in Fig. 8.3 given for the water inside the container, as this water is permanently circulating in a cooling system.

The nuclei dominating the activity are given in Table 8.1 (1 month's irradiation); After 1 day of cooling, the activity is mainly due to ^{7}Be and tritium, with 53.3 d and 12.33 y half-lives respectively.

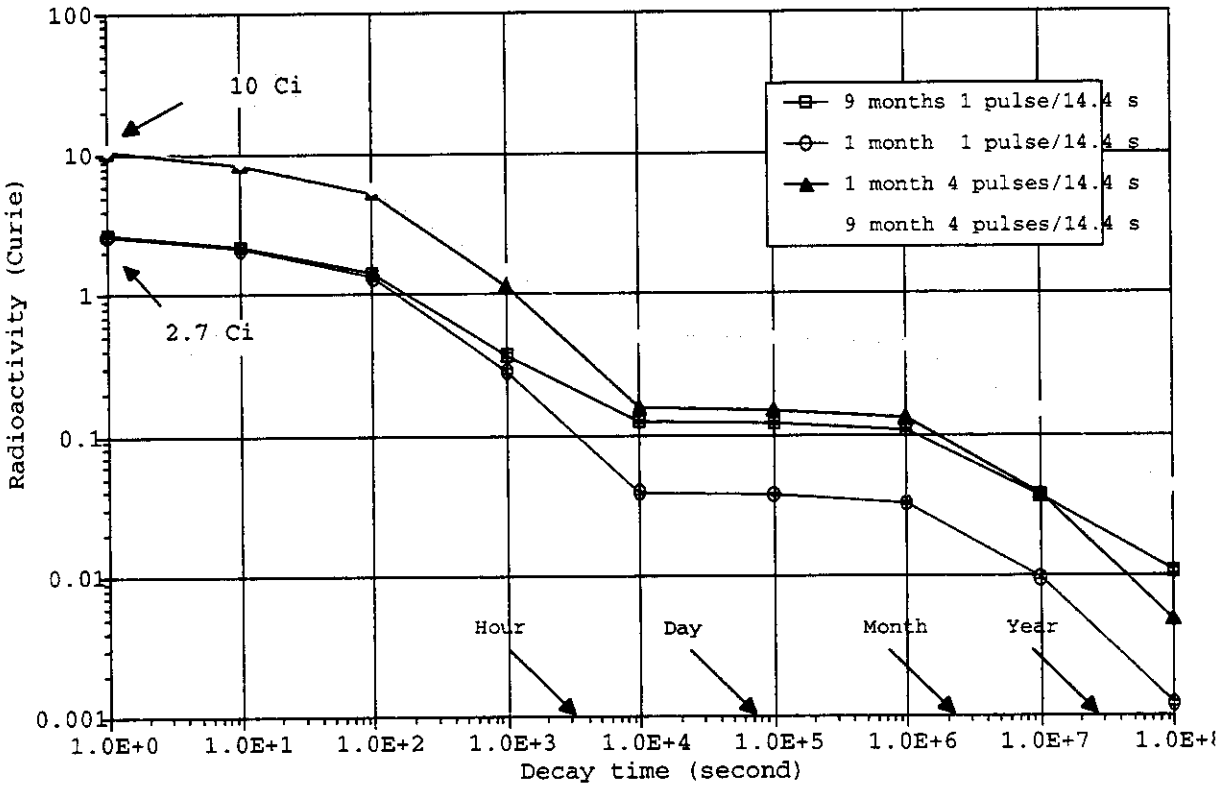

Figure 8.3: Activity of the water inside the aluminium container, after 1 month and 9 months irradiation versus the cooling time, for 1 and 4 pulses.

$T_{cooling}$	A	Z	Bq/cm^3	A (%)	Mode
Day	7	Be (53.3 d)	9509.3	96.14%	EC
	3	H (12.33 y)	381.2	3.85%	β^-
Month	7	Be	6521.2	94.49%	EC
	3	H	379.5	5.50%	β^-
Year	7	Be	89.16	19.79%	EC
	3	H	360.7	80.06%	β^-

Table 8.1: Nuclei dominating the activity of the water inside the aluminum_container submitted to 1 month's irradiation time.

9. RADIATION SAFETY

9.1 TARGET SHIELDING

The TOF lead target is situated at a depth of 9 m under the ISR tunnel, which is a supervised area. The dose rate allowed in this region must be less than 2.5 μSv/h; the design value for the shielding was taken at 1 μSv/h. FLUKA [19] simulations were performed to determine the shielding requirements.

The TOF target will be removed from the TT2A tunnel via a shaft set in concrete and linking a service tunnel located in-between TT2A and the ISR, which will serve as a storage area for the target. The concrete thickness between TT2A and this service tunnel is 5.5 m (Fig. 9.1). FLUKA simulations were performed to estimate the dose in the ISR during the TOF operation.

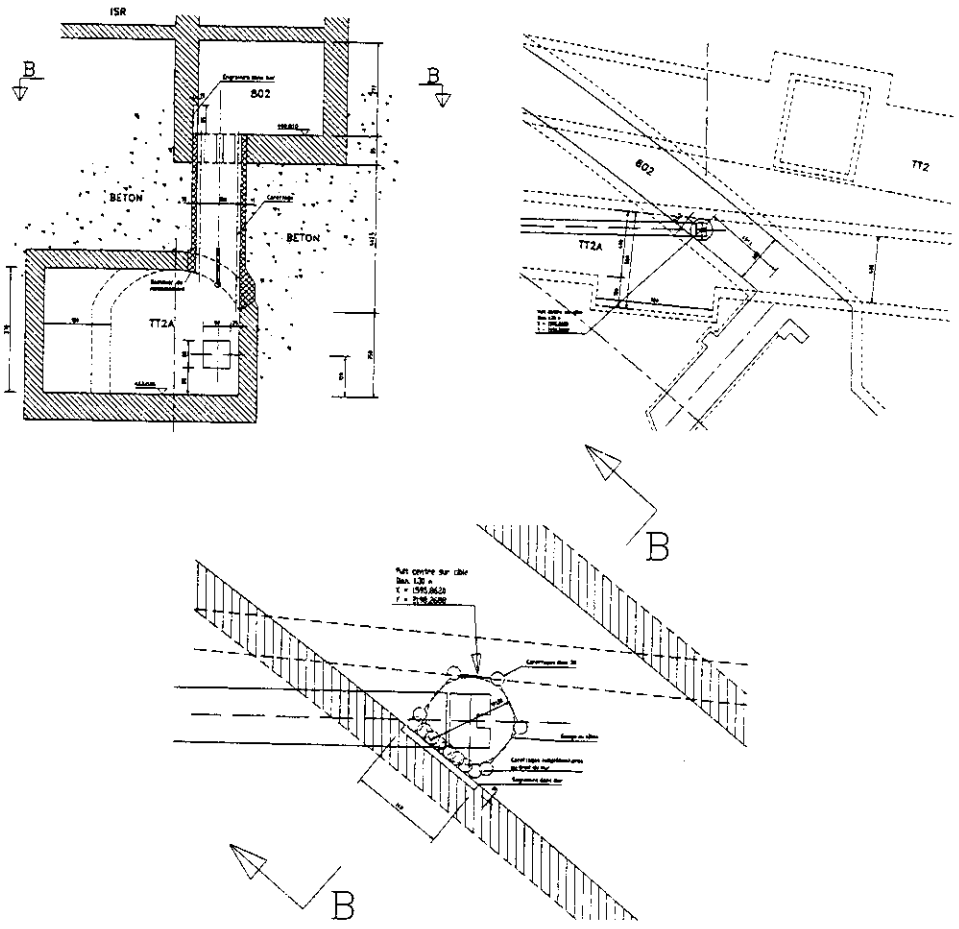

Figure 9.1: Shaft dug in concrete to extract the TOF target from the TT2A tunnel.

9.1.1 Simulation conditions

The origin of the coordinate system is at the centre of the lead target; the proton beam travels in the Z direction with an incident angle of 10°, the X axis points vertically and the Y axis points to the right, as shown in Fig. 9.2. The 24 GeV proton beam hits the lead target at the point with coordinates x = 0, y = -1.7632 cm, z = -10.0 cm. Only neutrons have been followed without any energy cut-off, using neutron cross-sections of 72 groups from 19.6 MeV to thermal energy.

9.1.2 Dose from neutrons transmitted through the shaft

The geometry used for the simulations is shown in Fig. 9.2. The 130 cm diameter shaft has been filled with 4.55 m of concrete (from x = 243 cm up to x = 698 cm), divided into nine slices for biasing purposes, seven, 50 cm thick slices (n° 2 to 8) and the last two slices (n° 9 and 10) of 32.5 cm thickness. The composition of the concrete used for roofs, walls and the shielding is given in Table 9.1, its density is 2.35 g/cm^3. A concrete slice (n° 11), 40 cm thick and 150 cm in diameter, was put on top of the shaft in the target storage area.

Table 9.1: Concrete composition used in the FLUKA simulations.

Elem.	H	C	O	Na	Mg	Al	Si	K	Ca	Fe
(%)	1	0.1	52.9	1.6	0.2	3.4	33.7	1.3	4.4	1.4

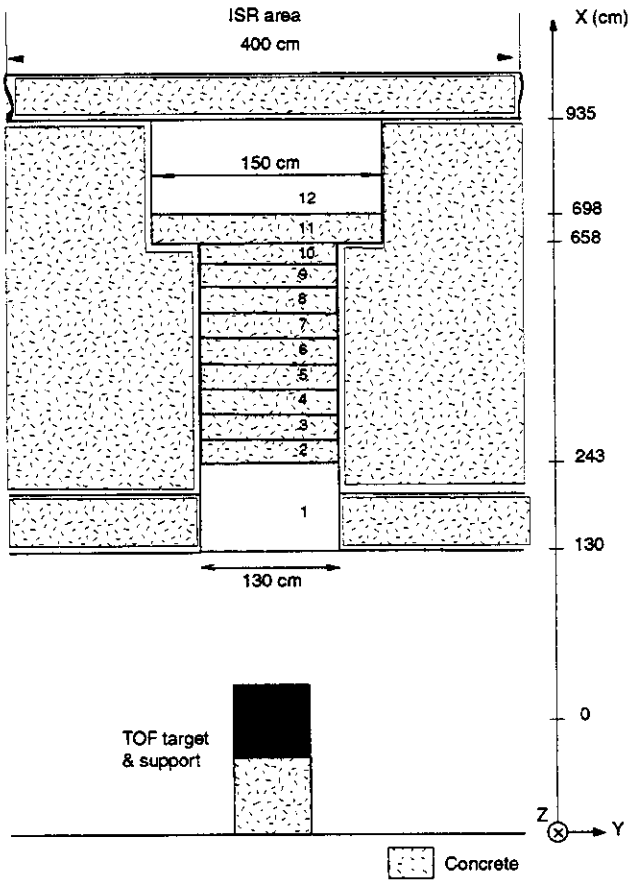

Figure 9.2: Geometry of the shaft used in the FLUKA simulation.

The neutron energy deposition was scored by region (from 1 to 12) and given in GeV/proton. This number was then divided by the volume of the region (cm^3) and by the density of the material in kg/cm^3. An average quality factor of 5 was applied to convert dose in Gray in Sievert. We have considered 1 pulse and 4 pulses every 14.4 s with an intensity of 7×10^{12} protons per pulse.

The dose equivalent rates obtained with this 4.95 m concrete shielding are given in Table 9.2. The dose equivalent rate in region 1, 1.3 m above the target and before any shielding is about 80 Sv/h for 1 pulse and 11 mSv/h for 4 pulses.

Table 9.2: Dose equivalents with concrete inside the shaft.

Region	Volume (cm^3)	GeV/proton	Gray/proton	Sv/h 1 pulse	Sv/h 4 pulses
1 (air*)	1493238.25	1.44×10^{-4}	1.3×10^{-14}	78.8	315
2 (concrete)	663661.45	4.84×10^{-3}	5.0×10^{-16}	3.11	12
3 (concrete)	663661.45	6.25×10^{-4}	6.4×10^{-17}	0.40	1.6
4 (concrete)	663661.45	1.40×10^{-4}	1.4×10^{-17}	0.09	0.4
5 (concrete)	663661.45	4.46×10^{-5}	4.6×10^{-18}	0.03	0.1
6 (concrete)	663661.45	1.57×10^{-5}	1.6×10^{-18}	0.01	0.04
7 (concrete)	663661.45	3.15×10^{-6}	3.2×10^{-19}	2×10^{-3}	8×10^{-3}
8 (concrete)	663661.45	1.56×10^{-7}	1.6×10^{-20}	0.1×10^{-3}	0.4×10^{-3}
9 (concrete)	431379.95	1.54×10^{-7}	2.4×10^{-20}	0.15×10^{-3}	0.6×10^{-3}
10 (concrete)	431379.95	3.10×10^{-7}	4.9×10^{-20}	0.3×10^{-3}	1.2×10^{-3}
11 (concrete)	706858.35	1.24×10^{-6}	1.2×10^{-19}	0.7×10^{-3}	2.8×10^{-3}
12 (air)	**4188135.70**	$\mathbf{1.4 \times 10^{-8}}$	$\mathbf{4.3 \times 10^{-19}}$	$\mathbf{2.7 \times 10^{-3}}$	$\mathbf{11 \times 10^{-3}}$

*density of air = 0.001225 g/cm^3

9.1.3 Dose from neutrons outside the shaft

In this case, slices 2 to 10 of the shaft were considered as 'blackhole' FLUKA material, in which any particle is killed when crossing it. This simulation was performed to estimate the dose equivalent rate due to the neutrons passing through the concrete around the shaft in a 1.35 m thick crown. The contribution of these neutrons is negligible, less the 1 µSv/h, as shown in Table 9.3. For 4 pulses it exceeds 1 µSv/h. Measurements in the first year should clarify whether additional shielding is needed to bring the dose down to ≤ 1 µSv/h.

Table 9.3: Dose rate from neutrons passing around the shaft.

Region	Volume (cm^3)	GeV/proton	Gray/proton	Sv/h 1 pulse	Sv/h 4 pulses
1 (air)	1493238.25	9.65×10^{-5}	8.4×10^{-15}	53	212
11 (concrete)	706858.35	1.1×10^{-8}	1.1×10^{-21}	6.6×10^{-6}	26×10^{-6}
12 (air)	4188135.7	3.5×10^{-12}	1.1×10^{-22}	0.7×10^{-6}	3×10^{-6}

9.1.4 Shielding with iron and concrete

The dose equivalent rate in the ISR with the shaft 'plugged' with 4.95 m of concrete is clearly far too high. To reduce it to the design value, additional shielding has to be installed on top of the target. A shielding consisting of 1.6 m iron plus 0.8 m concrete placed in the service tunnel in-between the shaft and the ISR, will reduce the dose equivalent rate to below 1 µSv/h.

9.2 SHIELDING OF BASEMENT OF BUILDING 287

A room situated in the basement of building 287, located at the same level of the TT2A tunnel, is routinely occupied by personnel belonging to EST/SM. This room is linked to TT2A by a tunnel which serves as an emergency exit and therefore cannot be completely blocked off. The way to reduce neutron streaming from TT2A into building 287 is to install a properly designed labyrinth. As building 287 is a supervised area, the ambient dose equivalent rate in the room in the basement must not exceed 2.5 μSv/h. It will be shown below that this can be achieved with a labyrinth having two legs 5.6 m long, 0.9 m wide and about 2.5 m high.

9.2.1 Dose rate estimation from the TOF neutron beam

The room is situated at the end of a 12 m long tunnel linked to TT2A. The TOF sweeping magnet is situated near the tunnel aperture, at ≈ 150 m from the TOF target as shown in Fig. 4.3.

The total neutron background in the tunnel (outside the TOF tube) was estimated by previous calculations [21] and is shown in Fig. 9.3, which gives the total neutron background flux outside the tube versus the flight distance in the tunnel for 4 pulses per super-cycle, i.e. 3×10^{13} protons per 14.4 s.

The exit of the room in the basement of building 287 is located just after the second collimator at a distance of ≈ 150 m from the neutron source. We can therefore safely use as the total neutron background in the area, an upper limit of 10^5 n/cm^2/pulse as illustrated in Fig. 9.3.

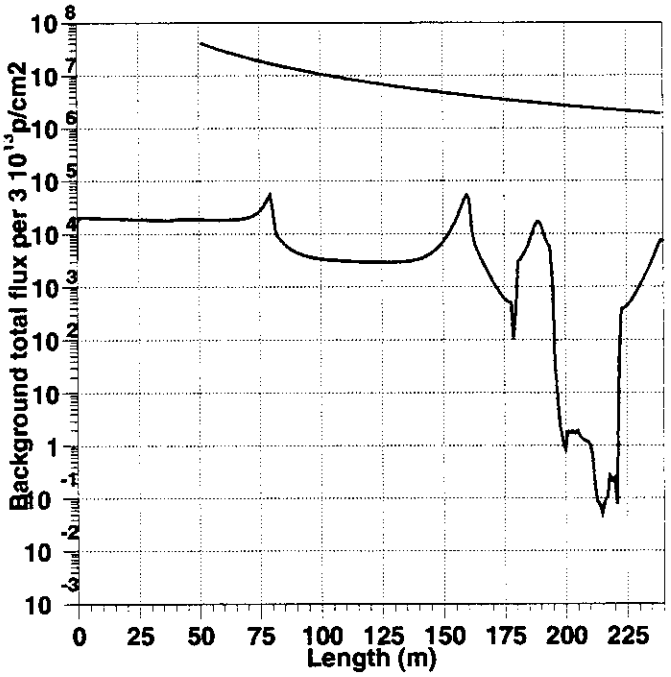

Figure 9.3: Total neutron background flux in the tunnel versus the flight distance (lower curve) and the flux inside the neutron beam tube (upper curve). The effect of the collimators is visible, with an increase in the neutron background at distances of 80 m, 160 m and 190 m.

Previous calculations [21] have also shown that the neutron background in this region has a flat spectrum, which resembles the spectrum inside the tube. We can

thus generate the neutron background spectrum from the nominal spectrum inside the tube, by rescaling with the appropriate factor so that the integral of the neutrons is 10^5 n/cm^2/pulse (Fig. 9.4a).

If we fold the neutron background fluence, with the neutron fluence to ambient dose equivalent conversion factors given by [22] (Fig. 9.4b) we obtain the ambient dose equivalent versus the neutron energy per pulse (Fig. 9.4c), which amounts to a total dose equivalent of 1.27×10^7 pSv/pulse, or 3.25 mSv/h.

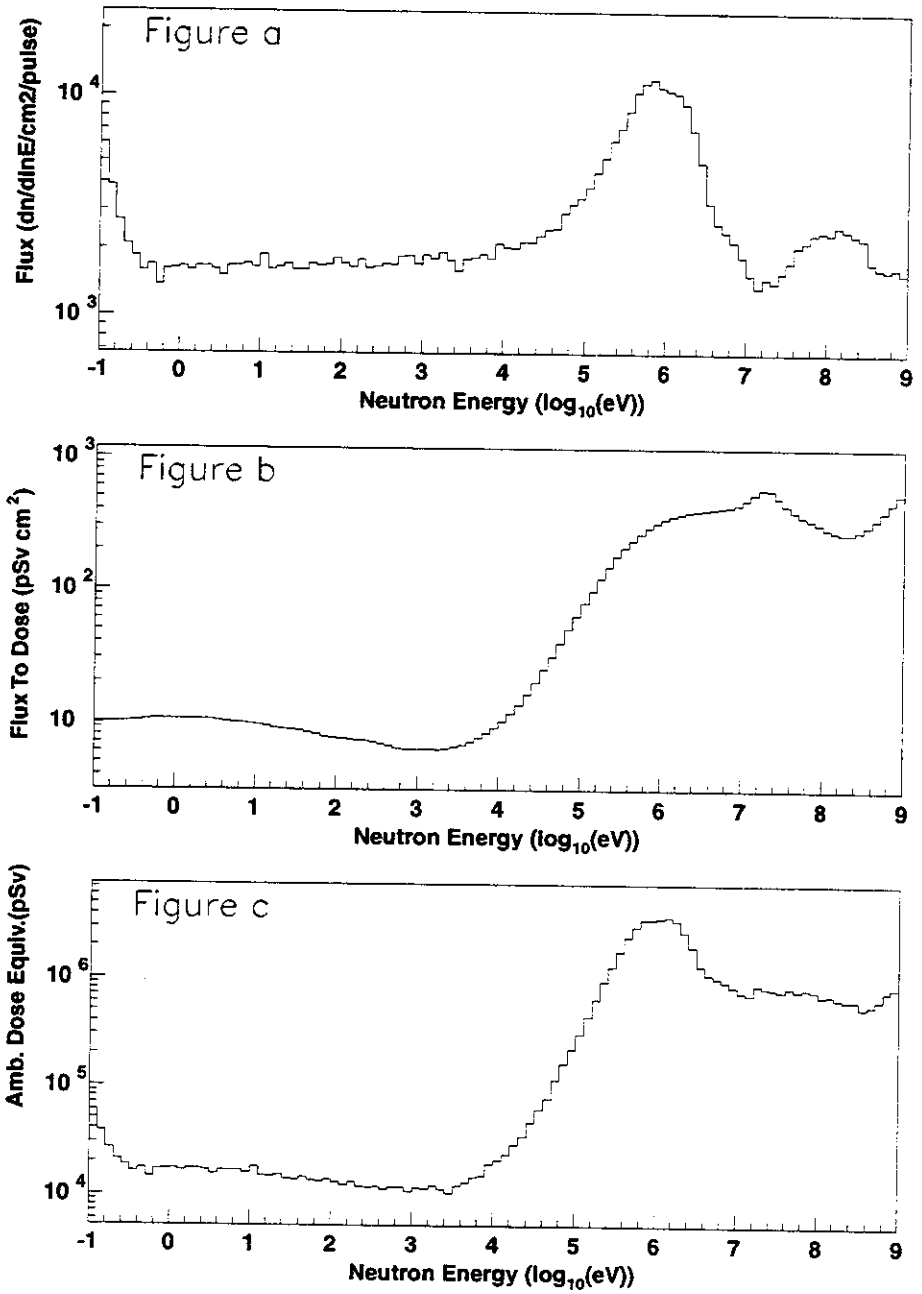

Figure 9.4: a) Background neutron flux near the second collimator; b) Neutron fluence to dose equivalent conversion factor; c) Neutron ambient dose equivalent per isolethargic bin per pulse.

9.2.2 Calculations for concrete labyrinth

The curves shown in Fig. 9.5 are used to calculate the dose attenuation after the first leg of the labyrinth [23], where d is the length of the leg and A its cross section. The length has to be chosen as twice or three times the section value; in our case, $A = 2.5 \times 0.9 = 2.3\ m^2$ (width of 0.9 m and a space of 1.60 m between the concrete chicanes have been left for a stretcher).

The data from the curve corresponding to a plane source have been used. Figure 9.6 shows the curves for the subsequent legs of the labyrinth.

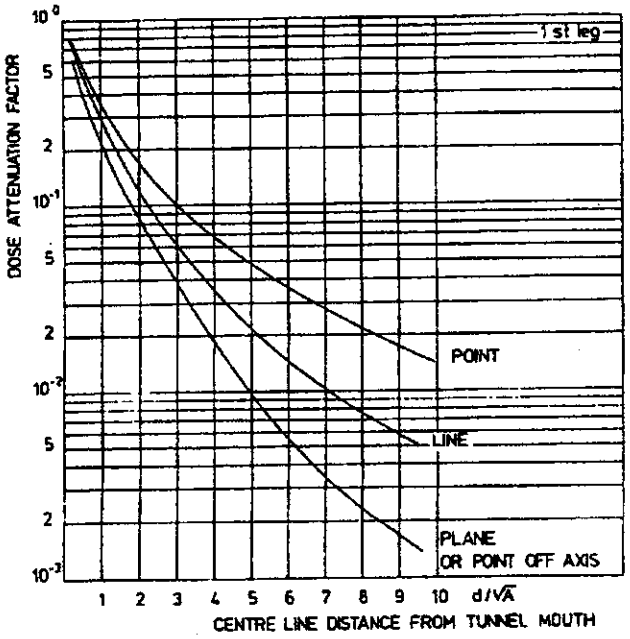

Figure 9.5: Attenuation curves for the 1st leg of the labyrinth.

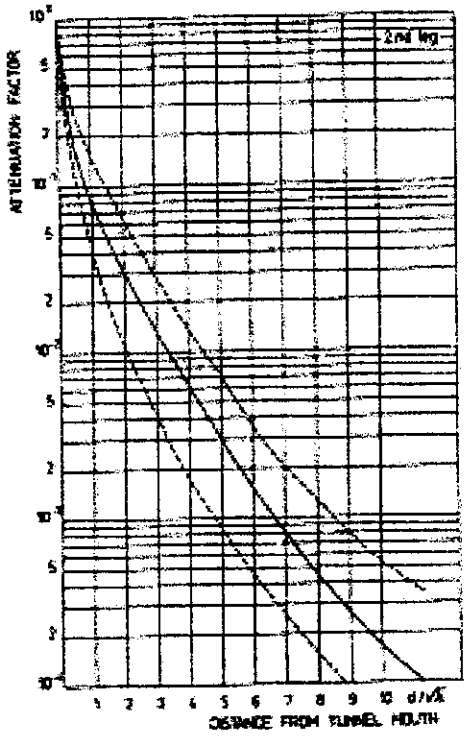

Figure 9.6: Attenuation curves for the 2nd and subsequent legs of a labyrinth.

The standard dimensions of the concrete blocks for shielding at CERN are in multiples of 40 cm in width and 80 cm long; for our purposes, the calculations have been carried out with leg lengths in multiples of 80 cm. The radiation dose equivalent rate is estimated to be less than 1 μSv/h after two legs each of 5.60 m in length and a 2.30 m^2 cross section.

The attenuation factors and results are shown in Table 9.4. The final labyrinth is drawn in Fig. 9.7. Two corners of the concrete walls will have to be cut out to allow a passage for a stretcher.

Table 9.4: Estimation of the dose rate in the labyrinth.

Leg dimensions: l = 5.60 m; A = 2.3 m^2	**Attenuation factor**	**Initial dose rate 3.25 mSv/h**	**Initial dose rate 10 mSv/h**
1st leg	0.022	71.5 μSv/h	0.25 mSv/h
2nd leg	0.009	0.6 μSv/h	2 μSv/h

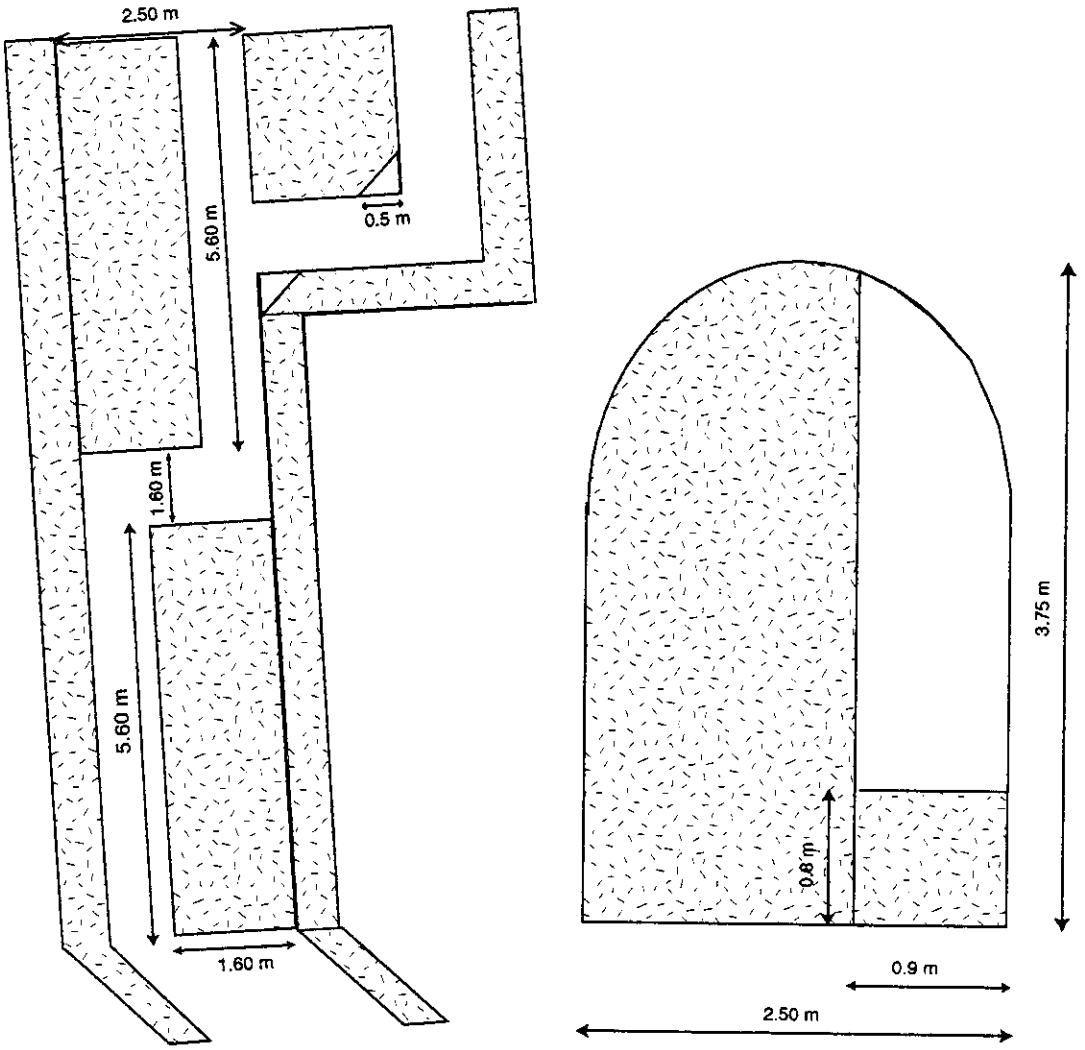

Figure 9.7: Labyrinth with three legs, but only the two 5.60 m legs have been considered for the dose attenuation calculations.

To summarise, the dose rate in the room located in the basement of building 287, at about 150 m from the TOF target must not exceed 1 μSv/h. The estimated dose rate from the neutron beam in the TOF tunnel at 12 m from this room, is 3.25 mSv/h.

This dose is estimated for 4 bunches per super cycle that is to say 3×10^{13} protons per 14.4 s. Even if the dose rate is underestimated by a factor 3, the ambient dose equivalent rate will not exceed the design value for a supervised area.

9.3 RADIATION MONITORING SYSTEM

The radiation monitoring system consists of three hydrogen-filled chambers, four ion chambers with a tissue-equivalent wall acting as induced activity monitors, and four flashing warning panels (PAD). The hydrogen-filled chambers, (known as PAX monitors) are filled to a pressure of 20 atmospheres. The induced activity monitors (known as PMI monitors) are 3 litre air chambers at atmospheric pressure. All monitors all linked to the centralised TIS/RP data acquisition system (Fig. 9.8). Radiation levels can be read remotely from an X-terminal in the TOF control room. The hourly dose equivalent rates are recorded in a database and can be retrieved at any time in the future. The monitors have two alarm thresholds, the first (A) set at 25 μSv/h (warning level), the second (B) at 100 μSv/h, which is the maximum allowable dose rate under transient conditions in a simple controlled radiation area. The PAX monitors do not have a direct interlock action on the beam (beam abort) in case alarm levels are exceeded, but the standard user interface programs are available in the PS control room and can be viewed by the PS operator.

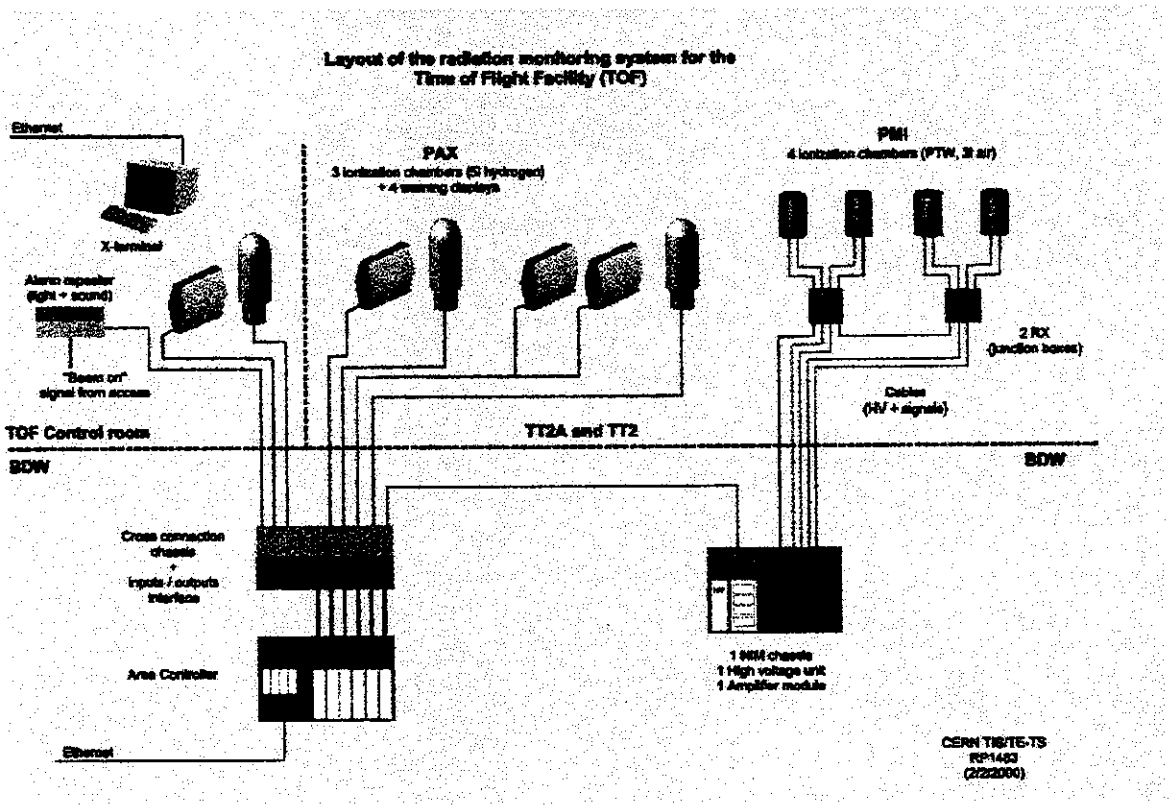

Figure 9.8: Layout of the radiation monitoring system for the Time of Flight Facility.

The positions of the radiation monitors and warning panels are shown in Fig. 9.9. One PAX is installed in the TOF control room, to monitor the stray radiation

coming from both the TT2A tunnel and from the adjacent H3 beam line transporting secondary beams from the SPS to the West Experimental Hall.

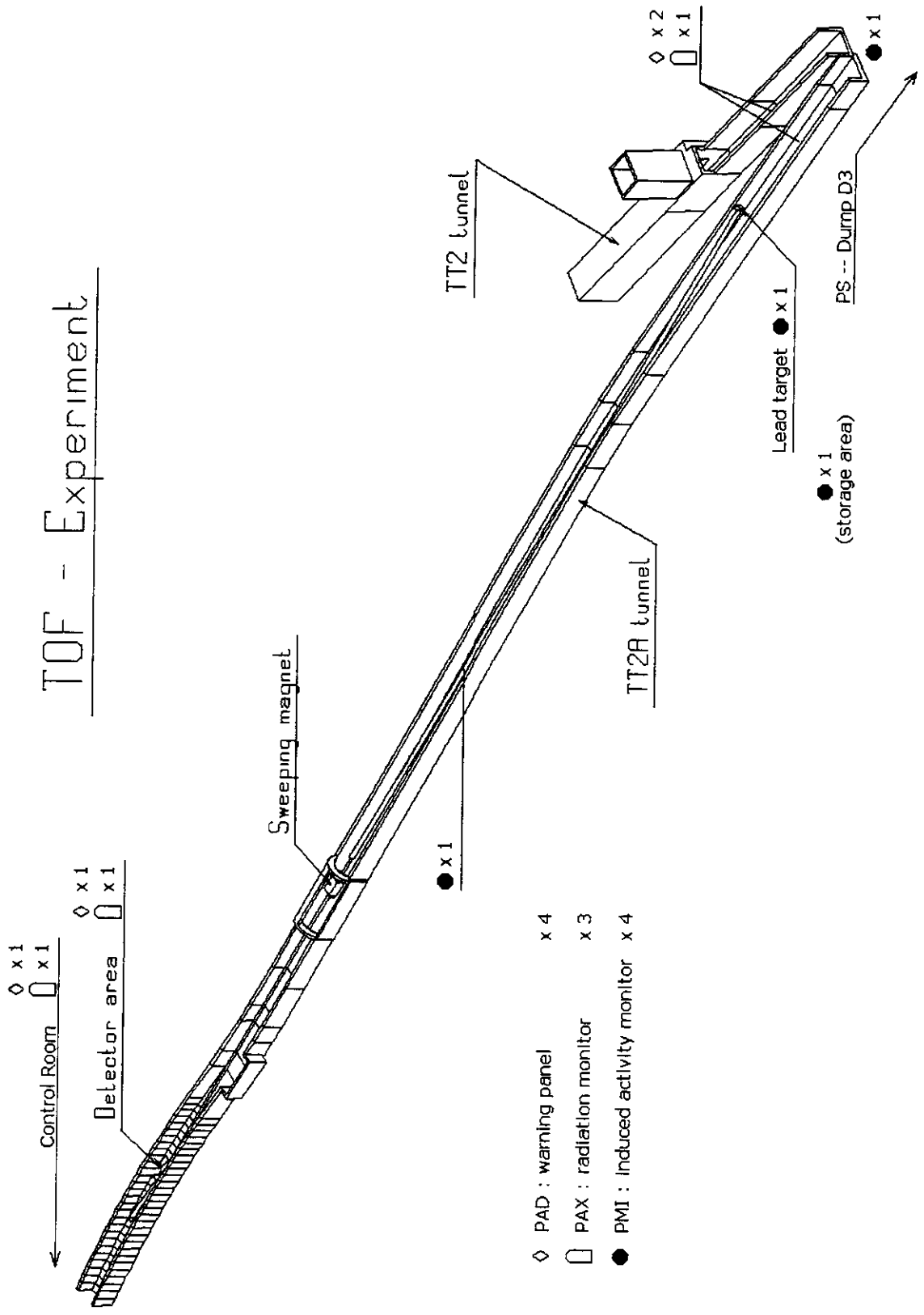

Figure 9.9: Positions of the radiation monitors and warning panels.

A warning panel installed close to it flashes if the radiation level exceeds threshold A, reinforced by an acoustic signal in case threshold B is reached. A second PAX is

installed in the TT2A; the exact location (in-between the target and the experimental area) has still to be decided. If installed in the experimental area it will also monitor any substantial induced radioactivity in the experimental equipment when the beam is not present. The third PAX is installed in the TT2 tunnel and serves two purposes. Firstly, it will monitor the stray radiation in TT2 from beam losses in the proton transfer line during TOF operation; secondly, it will detect stray radiation coming either from the PS side of TT2 or from TT10 under conditions of access (i.e. with the TOF beam off). These detectors are coupled to the Radiation Protection Group Area Controller in BDW. Two warning displays (PADs) are placed in TT2A and one in TT2. These displays are used to warn personnel of excessive radiation levels in TT2 and TT2A when access is granted, by visual and acoustic signals if the alarm thresholds are exceeded, as described above. A 'Beam On' signal is monitored by the Area Controller and the three warning panels may be enabled by this 'Beam On' signal if so desired. A summary alarm panel can be mounted in the TOF control room in order to alert operators of abnormal conditions on any of the monitors.

Four induced activity monitors (PMI) are foreseen. The first is to be installed upstream in TT2A, close to the PS shielding wall, to monitor the induced radioactivity in this part of the tunnel which is accessed by the PS personnel in case an intervention is required on the proton beam line. The second is to be installed close to the lead target, to monitor the residual radioactivity of the target before it is removed or the shielding opened. The third PMI is to be installed in the ISR service tunnel on top of the target, to monitor the radiation level when the target is being moved and stored in its 'garage' location. The fourth monitor is to be placed in the downstream part of TT2A, in-between the target station and the experimental area, to survey the radiation level due to induced radioactivity before access is granted to this section of the tunnel. The dose rates of these induced activity monitors are available on the X-terminal in the control room.

10. PROMPT PHOTONS

The distribution of photons emerging from the lead target has been simulated using the FLUKA program [19] and the geometry described in 8.1.1. The photons were propagated down to 200 m in the direction of the detector station. Their distribution as a function of energy is shown in Fig. 10.1. The photon energy spectrum extends from several keV up to several GeV. The time projection of the produced photons is shown in Fig. 10.2. One can clearly separate the gammas into two groups. The first one with times smaller than 1 μs, is the *'fast'* component resulting from the spallation process and the second one, with times $t > 1$ μs is mainly due to thermal neutron capture in the elements present in the moderator and the lead target. The *fast* photons are forwardly peaked in the proton beam direction. Because of the 10^{o} angle of the proton beam with respect to the neutron beam line, the prompt gamma flash is drastically reduced inside the neutron tube. The gammas coming from the thermal neutron capture are emitted isotropically. The photons in the first group will arrive at the detector station within 670 ns from the time of impact of the proton pulse with the lead target, well before the arrival of the fastest neutrons. Therefore, they will not interfere with the neutron cross section measurements. These photons can be also used as trigger, defining the time t_0, for the data acquisition system. The photons that are emitted after a neutron capture will reach the detector station at 200 m later, with a broad peak centred at 10^{-4} s. They will thus overlap the 20 keV neutrons. Even though their flux is 10 times lower than the neutron flux, outscattering and/or pileup effects cannot be ignored. From the

energy spectrum of these photons (Fig. 10.3), one can see that 40% of the contribution is due to the neutron capture on hydrogen (the 2.2 MeV ray); this energy is too small to produce any photonuclear interactions. Another 5% contribution is comes from photons with energies from 7 to 7.5 MeV resulting from the neutron capture on lead, on the elements of the container and on the I-beams iron and aluminium.

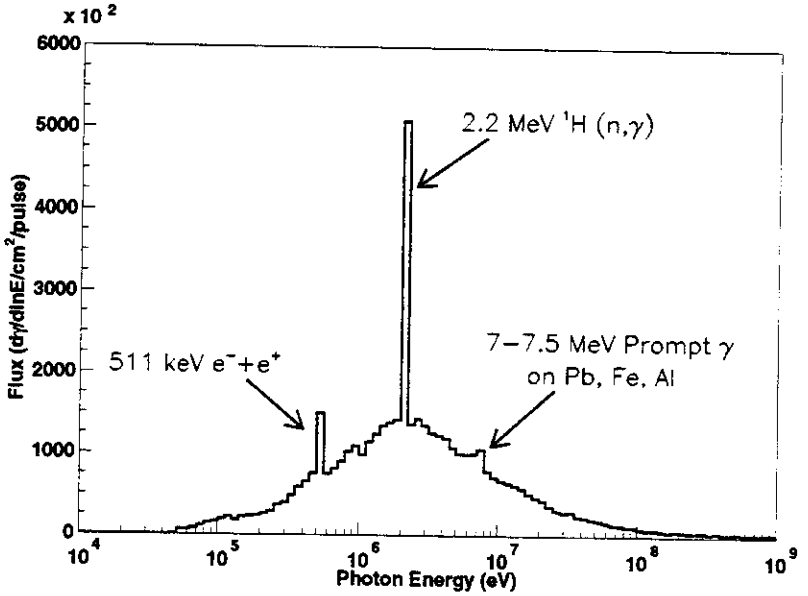

Figure 10.1: Photon distribution at the detector station 200 m as a function of energy.

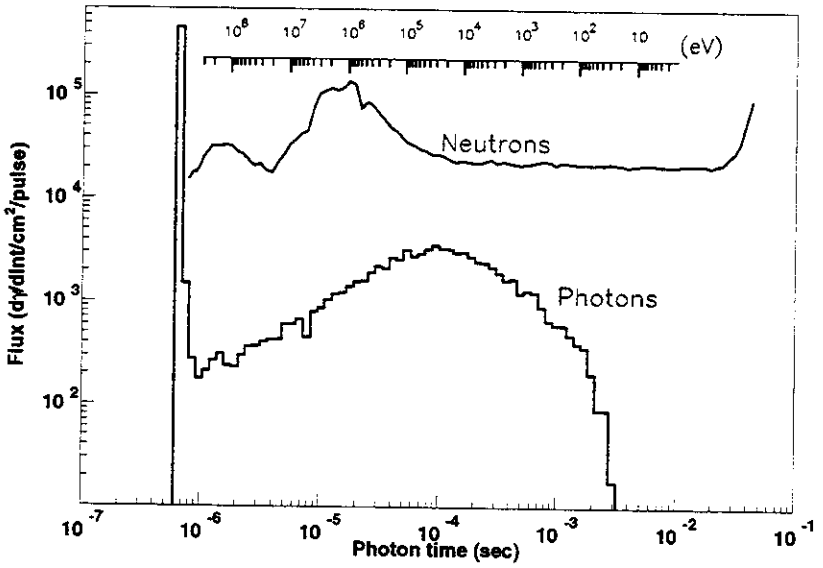

Figure 10.2: Distribution of photons as a function of their arrival time at 200 m. We can separate them into two groups. The first consists of photons with time $t < 1$ μs, coming from the prompt gammas resulting from the spallation process, and the second group $t > 1$ μs mainly due to the prompt gammas resulting from the thermal neutron captures.

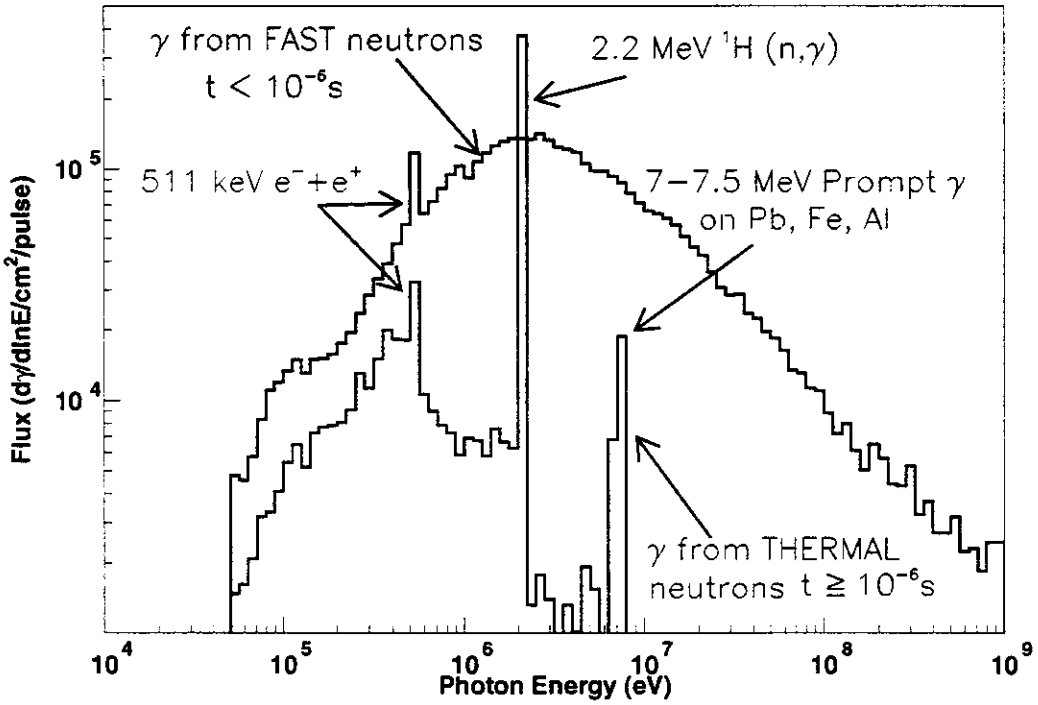

Figure 10.3: Photon distributions at 200 m, from the fast and the thermal neutrons. The thermal neutron capture on hydrogen gives rise to 2.2 MeV γs, respresenting 40% of the total gammas.

11. COLLIMATION OF THE NEUTRON BEAM

The neutron TOF measurements require a geometrically well-defined neutron beam at the sample position. A collimating system is being designed to obtain the required neutron beam diameters, and to insure that the halo of this beam will not collide with the beam pipe in the experimental area.

The beam pipe and the shieldings at the diameter reductions contribute to the beam collimation, however the main collimating elements are two collimators. One close to the sample (typically at aprox. 10 m) named as *Beam Shaping Collimator* or *BSCol*, and another one close to the second diameter reduction of the pipe, and preferably before the sweeping magnet (at about 140 m from the lead target), named *Source Screening Collimator, SSCol.*

The Beam Shaping Collimator defines the shape and size of the neutron beam at the sample position. Different apertures will be required for different sample sizes (ranging from 3 cm to 8 cm of diameter). Two solutions are being considered at the present time. On one hand, a very limited set of exchangeable cylindrical collimators which, with some simple mechanics, will allow selecting the required aperture without breaking the vacuum in the neutron pipe. On the other hand, the possibility of using a pair of flat adjustable collimators is under study. Both solutions share the same concept for the longitudinal profile of the BSCol, namely a sandwich of aprox. 1.25 m of iron or another medium Z element, preceded by 50 cm of borated polyethylene (or another light material with embedded highly capturing isotopes) and followed also by 75 cm of borated polyethylene.

The purposes of the Source Screening Collimator are to define the maximum neutron halo diameter at the sample position, by clipping the neutron source

effective area, and to reduce the background in the beam and in the experimental area, by shielding the Beam Shaping Collimator. Even though the optimal solution would require a specific SSCol for each sample size, Montecarlo studies [24, 25] have shown that it is possible to obtain configurations for this SSCol that are simultaneously optimized for the small samples and acceptable for the largest samples foreseen. This SSCol can consist of only two pieces a large (aprox. 1.25 m) iron piece and a large concrete piece after the iron

The final definition of the collimators precise positions and apertures are still under study.

12. CONTAMINATION INSIDE THE NEUTRON TUBE AND BACKGROUND IN THE DETECTOR HALL

Two types of background can degrade the neutron TOF experiments performance. First, the neutrons that arrive to the sample after interactions with materials of the tunnel (pipe, collimators, walls,...). These neutrons will not follow the energy-time relation of the main beam, which is the fundamental basis of the neutron TOF measurements. Their interaction with the samples will introduce a contamination in the measurements, usually consisting in a distortion at high energies (slow neutron interactions are attributed to faster neutrons).

The second source of background are the neutrons that reach the detector or the photons which were not produced in the sample. Both of them can generate signals in the detector that could be confused with real events.

In order to estimate the magnitude of these backgrounds, four independent detailed transport simulations were performed [26-29] by different groups and with different code systems (sharing most of the nuclear databases for cross sections and photon emission after capture, ENDF-BVI).

For these simulations a neutron beam optics was defined, following the principles of the previous paragraph but with tentative, non optimized, collimators positions and apertures.

The simulations were divided in several stages. First, the proton interaction with the lead target and the production and transport of neutrons up to the beam pipe vacuum was simulated with a combination of FLUKA [19] and the TARC-MC [30]. Second, a parameterization of the distribution on neutrons on energy, time, position and angles, at their entrance to the neutron pipe vacuum, was prepared in the form of an event generator [31]. This was required to obtain acceptable neutron source statistics in a reasonable CPU time. The neutrons generated with this parameterization were then transported through the tunnel. The photons generated by the interactions of these neutrons were also transported. The combinations of codes used in this phase are: FLUKA alone, FLUKA combined with MCNP, and GEANT 3.21.

All the simulations agree in the main features and general conclusions on the neutron beam optics, providing a sound basis and common understanding of the neutron phenomenology and on the design of its optics. The main conclusions from these simulations are:

1) In comparison with the main beam, the neutron contamination level inside the vacuum pipe is very small (10^{-6} to 10^{-5}) (see Fig. 12.1). The beam profile and beam intensity can be calculated ignoring this contribution.

2) However, the observed level of neutron background in the detector area is comparable to the fluence of neutrons scattered by the sample (for samples of a few 100 $\mu g/cm^2$, a few cm^2 and scattering cross sections of a few barns).

3) The observed level of photon background is comparable to the number of photons produced by capture in some candidate samples (for samples of a few 100 $\mu g/cm^2$, a few cm^2 and moderate capture cross sections). The ratio between the photon flux at the detector position and the neutron flux in the sample ranges between 10^{-7} to 10^{-6} (see Fig. 12.2).

4) The source of these backgrounds is identified in the high energy neutrons ~100 MeV. Typically, these neutrons will travel without interaction until they collide with the last collimator. The neutrons are then scattered and their energy is reduced. Then they enter in the front wall of the experimental room and eventually escape towards the detector area producing neutron background. Otherwise they can be captured in one of the experimental area walls producing photons that later on, and with small probability, can contribute to the photon background.

5) Two proposals have been made to reduce these backgrounds. The first consists in shielding the inner face of the experimental area walls. This avoids that neutrons and photons escape from the walls and produce background. First simulations show that a reduction of more than a factor 4 can be achieved. The second proposal is to reduce the number of neutrons colliding with the collimator close to the sample, BSCol, by appropriate modifications of the preceding optic, SSCol. The expected mitigation factors are also larger than 4.

6) Available statistics in the simulations of different groups allow, in some cases to obtain upper limits and in other cases to obtain order of magnitude of the expected background. It is also possible to estimate the ranges of the energy and time distributions of background neutrons and photons. These ranges have large overlaps with the interesting time intervals and sensitive energies.

7) However, more statistics is required before a detailed analysis of the structure of the background can be performed. This information will be required to evaluate different algorithms for signal to noise separation, and to estimate their efficiency.

More definitive conclusions will be obtained from the simulations of the final setups taking into account the different sample geometries and larger statistics. However, as already indicated, the expected background levels will be substantially smaller than the one presented above.

Three additional sources of background were identified and their simulation is still pending. First, the direct photons produced in the lead target and surrounding materials that could reach the detector or generate new particles (in their interaction with the tunnel materials) that could finally generate signals

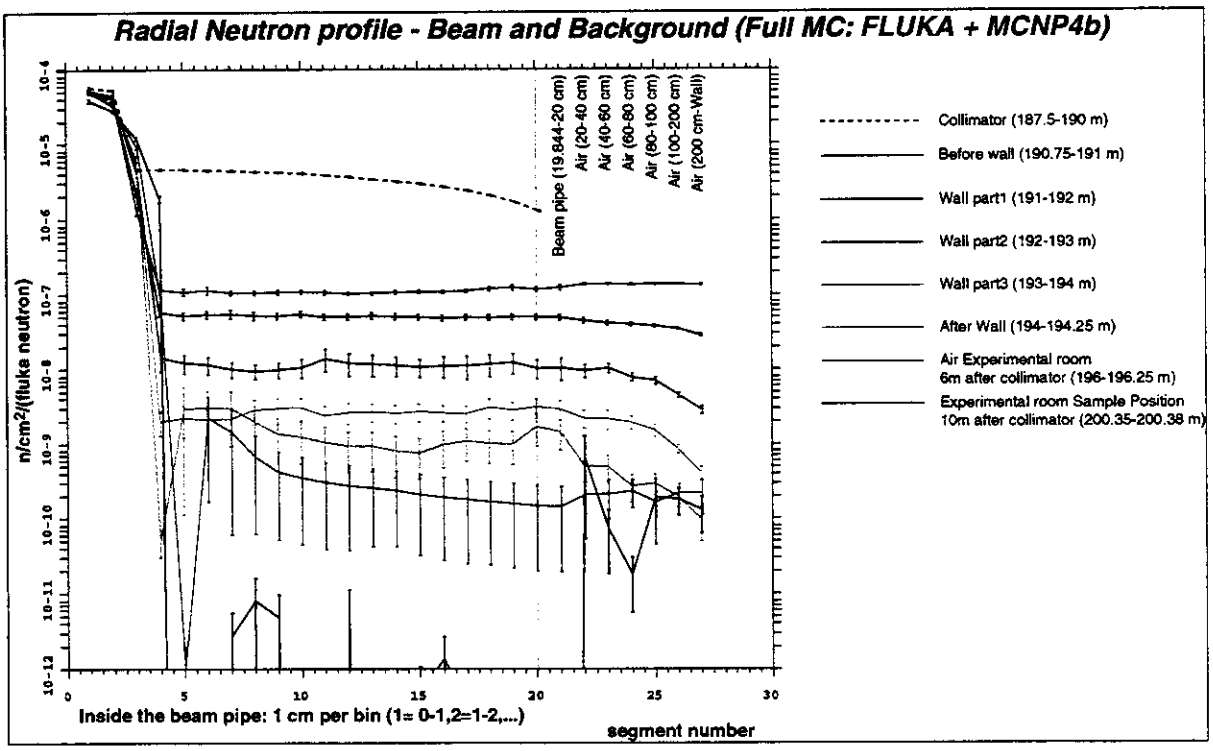

Figure 12.1: Spatial distributions of the neutron fluence, showing the main beam, halo and background at different positions, including the detector or experimental hall. Normalization should be taken as arbitrary.

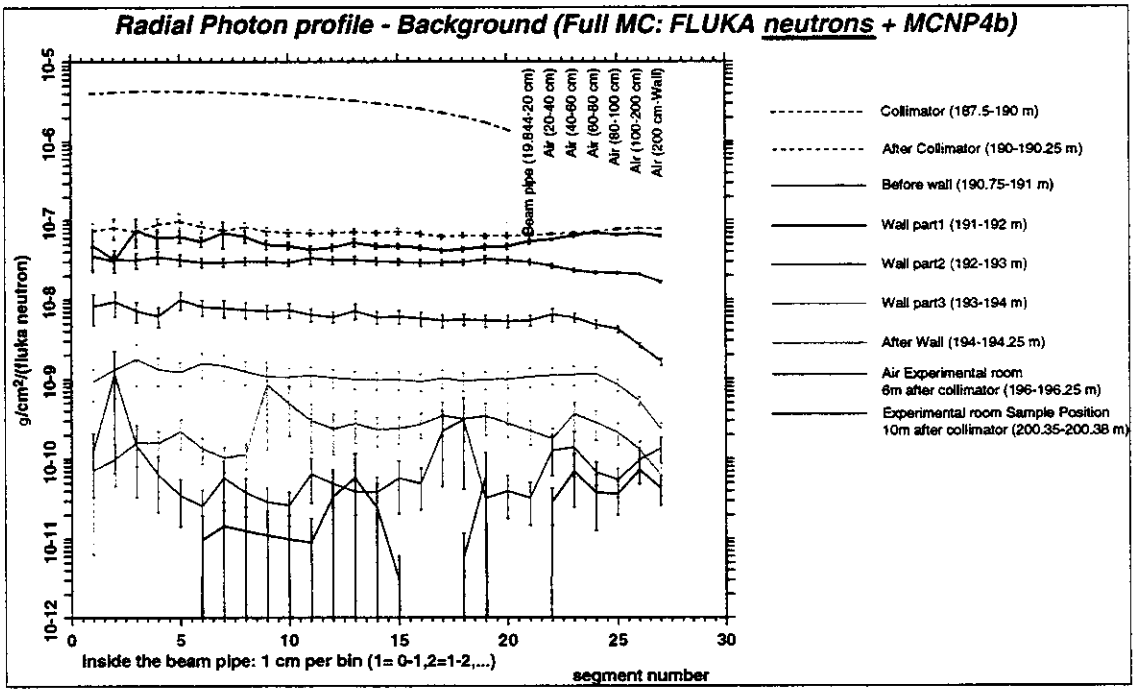

Figure 12.2: Spatial distributions of the photon fluence, showing the photon background at different positions, including the detector or experimental hall. Normalization should be taken as arbitrary but the same than in Fig. 12.1.

in the detector. First results on prompt photons from the lead target, water and water tank are given in Chapter 10. Next, the secondary particles produced after the interactions of the charged particles (produced in the spallation target) with the

tunnel materials. Third, the background produced by the neutrons arriving at the end of the beam pipe. In order to minimize this background, a specially designed beam dump will have to be built several meters after the sample. All these three sources of background are being investigated.

13. COMMISSIONING OF THE FACILITY

13.1 GENERAL REMARKS

The actual planning foresees that the installation of the TOF facility is finished in April 2000, where the tube will end between 160 – 180 m. However at this date, neither the collimator nor the experimental area 200 m away from the target will be ready, mainly because all the simulation work is not yet actually finished.

While these two last items still need to be constructed, they should not encroach upon the commissioning actions. Therefore, it seems reasonable that the first measurements could be done at a distance of ≈ 180 m downstream from the target. This position, placed presumably after the collimator and the height of the beam line with respect to the ground, is such to allow disposing experimental devices.

Commissioning of TOF should prove that the installation is able to provide neutron beams with characteristics close to those specified in the design phase. For this purpose, a number of actions appear as mandatory.

a) First of all, the neutrons are produced by lead spallation by the 20 GeV protons delivered by the PS. Therefore, the intensity and energy of the proton beam must be known with accuracy of the order of 1%. Moreover, the position of the proton beam may slightly influence the neutron yield, with the consequence that information on position should be permanently monitored. To comply with these requirements, one can use the existing intensity transformers and the capacitive pick up in an electrostatic q-pole. The DAQ system should be able to accommodate this information in a synchronous mode. PS will provide a fast signal synchronous with the proton pulse that can be used as a time reference (trigger signal).

b) Secondly, one should be able to measure the characteristics of the produced neutron beam: intensity (or flux in neutrons/cm^2/pulse), spectral function (flux of neutrons in a definite energy bin) and spatial distribution (beam profile). This imposes constraints on the choice of detectors and their handling: they must have enough small dimensions to allow for the determination of the beam profile by using an adequate scanning device.

c) Thirdly, one needs to have knowledge about the background conditions. The background can be defined in different ways. Of interest in the commissioning phase are the following:
   - the presence of a gamma background at the end of the beam line;
   - the background of charged particles at the same place and the background of neutrons, gammas and charged particles outside the beam line.

If the same detectors can be used for neutrons, as stated in the previous point, special detectors will be needed for evaluating the gamma and charged particle background. Background measurements at other distances around the beam line could equally be needed.

All measurements will be done first of all in air and an existing scanning device (range on x and y: about 1 m) will be used to which the detectors will be attached. The intention at the beginning is to use the detectors proposed below and to make more precise measurements at a later date, certainly for the neutron flux and spectrum, with larger and more sophisticated detectors. This would need to be discussed and decided within the TOF collaboration.

13.2 DETECTORS

13.2.1 Neutron detectors

The neutrons produced by the spallation source are expected to span a wide energy range, from 10^{-2} eV to several hundreds of MeV. There is not a unique physical phenomenon capable of ensuring their detection with reasonable efficiency over this whole range. Therefore, the detection of neutrons is based on different physical processes according to their energy domain. In this situation, care should be taken to ensure an overlap between the regions measured in each case.

For *thermal and epithermal neutrons*, Bicron proposes a detector, the BC702 based on a plastic that includes definite amounts of ^{6}Li (95% enrichment) and ZnS (Ag). The lithium has an interaction cross-section for neutrons that decreases with energy until about 1 barn for 10 keV neutrons. From the interaction, an alpha particle and a triton will emerge with energies of 2.1 and 2.7 MeV respectively. These particles in turn, induce scintillation in ZnS that could be detected with a PM tube. The energy needed to create a photon in ZnS is 27 eV and the scintillation efficiency is about 9%. The plastic is shaped like a disk with an active area of 3.8 cm^2 (one inch external diameter) and a thickness of 6.35 mm. The lithium content is 11 mg/cm^2 and the decay time for the scintillation is 200 ns with a maximum of the emission spectrum at 461 nm. Taking into account the estimated flux and spectral function of the neutron beam at D = 160 m, the expected number of reactions that will lead a signal for DAQ is of the order of 8000/pulse spread over a time interval ranging from 100 μs to 100 ms.

For *fast neutrons*, Bicron proposes another detector the BC720: a clear hydrogenous plastic with a ZnS (Ag) phosphor embedded in it. The detector has the form of a disk with an external diameter of one inch and a thickness of 15.9 mm. The proton recoiling after the interaction with the neutron will induce a scintillation in the phosphor if its energy suffices for that. The scintillation is subsequently detected with a PM tube. The estimated reaction rate is about 8000 reactions (leading to a signal for DAQ) per proton pulse if the energy domain of neutrons is taken in-between 10 keV and 20 MeV. The energy domain of the above detectors slightly overlaps, ensuring measurements of the entire spectral function.

Finally, one should mention that, according to the specifications, both the above detectors have a low sensitivity for gamma rays.

13.2.2 Gamma detector

There are several sources of gamma rays with different characteristics. The gamma rays produced by the spallation source are emitted essentially in the forward direction in a very narrow cone and have a spectral function that spans a wide energy domain (from a few keV up to hundreds of MeV). Because of the angle of 10° in-between the directions of the proton and the neutron beams, the gamma background at the end of TOF tube is drastically reduced. Due to the fact that all gamma rays arrive at the detector at the same time (gamma flash), an individual detection is impossible; all one can measure is a global effect (gamma calorimeter).

Convoluting the presumed spectral function with the efficiency of the detector as a function of energy and comparing it with the global effect above, one may conjecture the correctness of the initial hypothesis. The thermalization of spallation neutrons by the water in which the lead target is immersed, gives rise to a second gamma flash, arriving about 100 μs after the prompt one and much broader (FWHM = 200 μs). The 2.2 MeV ray dominates its energy spectrum. Finally, the activation of the target during the exploitation and the induced activity in the tube and vault walls will produce a gamma background uncorrelated with the proton beam. A simple and adequate detector in this case will be a NaI (Tl) cylindrical crystal coupled to a PM tube. The dimensions of the crystal could be 2.5 cm in height and 2.5 cm in diameter. Different lead shields placed in front of the detector could serve both for selecting ever higher gamma energies and for estimating the non-forward contribution.

13.2.3 Charged particle detector

The expected flux of charged particles comprises forwardly emitted electrons, muons, pions, kaons and protons of various energies (see Fig. 4.5a). They should be swept out from the beam line by a magnet placed at 140 m downstream from the target (and described above) if their momentum is lower than 10 GeV/c. However, due to the hard component of the spectral function, one may still have some charged particles at 160 m where the commissioning tests will be done. Their energy will be very high and they can be considered as minimum ionizing particles. In this case, the detection is routinely done by using thin (300 microns) silicon detectors in which such a particle will deposit typically 100 keV. These particles are relativistic and will arrive at the detector at almost the same time, therefore giving a cumulated effect like the gamma flash. Measurements at various intensities of the proton beam will be performed. This detection is practically insensitive to gamma rays and neutrons.

14. SCHEDULE

The schedule of the remaining work to finalize the TOF facility up to 180 m tube length including all shieldings is shown in Fig. 14.1. The installation of detectors and final validation of the neutron beam with precise measurements of the spectrum and the resolution will follow after the installation of the collimator.

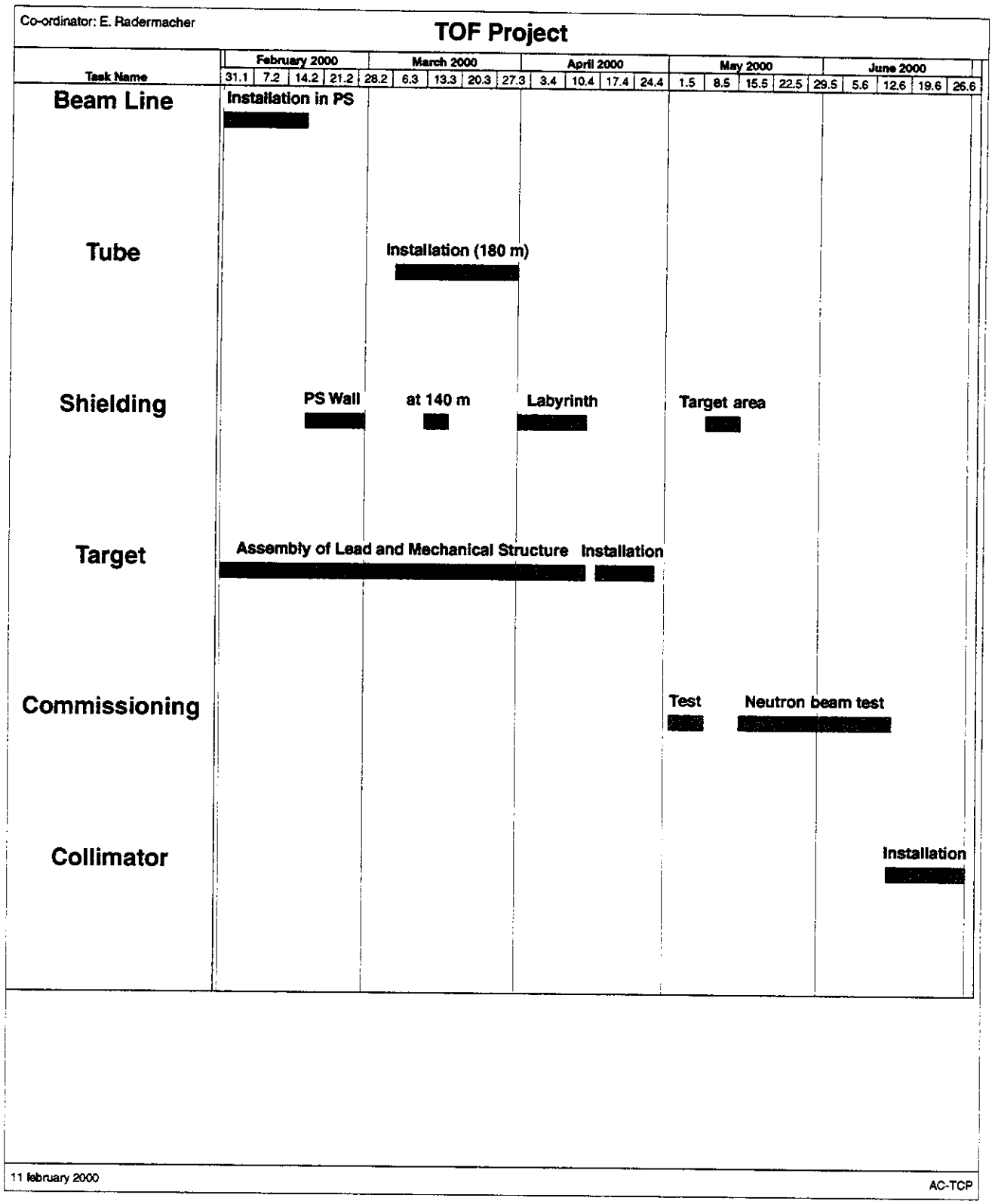

Figure 14.1: Schedule.

15. REFERENCES

[1] Data from the following nuclear data libraries have been compared:
JENDL-3.2, OECD NEA Data bank (1996);
JEF-2.2, OECD NEA Data bank (1996);
ENDF/B-VI, OECD NEA Data bank (1996);
BROND-2, OECD NEA Data bank (1996).
See also J. Cobo et al., 'Notes on the Study of the Most Reliable Neutron Cross Section Data', CERN/AT/95-035 (ET).

[2] C. Rubbia et al., 'A Realistic Plutonium Elimination Scheme with Fast Energy Amplifiers and Thorium-Plutonium Fuel', CERN/AT/95-53 (ET); C. Rubbia et al., 'Fast Neutron Incineration in the Energy Amplifier as Alternative to Geological Storage: the Case of Spain', CERN/LHC/97-01 (EET).

[3] C. Rubbia, J-A. Rubio, S. Buono, F. Carminati, N. Fiétier, J. Galvez, C. Gelès, Y. Kadi, R. Klapisch, P. Mandrillon, J.-P. Revol and Ch. Roche, 'Conceptual Design of a fast Neutron Operated High Power Energy Amplifier', CERN/AT/95-44 (ET); see also C. Rubbia, 'A High Gain Energy Amplifier Operated with fast Neutrons', AIP Conference Proceedings 346, International Conference on Accelerator-Driven Transmutation Technologies and Applications, Las Vegas, 1994.

[4] Carlo Rubbia, 'Resonance Enhanced Neutron Captures for Element Activation and Waste Transmutation', CERN/LHC/97-04 (EET).

[5] For the thermal neutron capture cross section of ^{90}Sr, the Atomic data and Nuclear data Tables, Vol. 29, Number 2, Sept. 1983, give a capture cross section of 0.9 barns, while M.A. Lone et al, NIM A332 (1993) 232-238 find 9.7 ± 0.7 mb. There is essentially no data at other energies.

[6] S. Andriamonje et al., TARC Proposal, 'Experimental Study of the Phenomenology of Spallation Neutrons in a Large Lead Block', CERN/SPSLC 95-17, SPSLC/P291, 5th May, 1995.
H. Arnould et al., 'Experimental Verification of Neutron Phenomenology in Lead and Transmutation by Adiabatic Resonance Crossing in Accelerator Driven Systems', submitted to Phys. Letters B.

[7] C. Rubbia et al., 'A high Resolution Spallation driven Facility at the CERN-PS to measure Neutron Cross Sections in the Interval from 1 eV to 250 MeV', CERN/LHC/98-02 (EET), Geneva, May 30, 1998.

[8] C. Rubbia et al., 'A high Resolution Spallation driven Facility at the CERN-PS to measure Neutron Cross Sections in the Interval from 1 eV to 250 MeV: *a relative Performance Assessment*', CERN/LHC/98-02 (EET)-Add. 1, Geneva, June 15, 1998.

[9] Proposal for a Neutron Time Of Flight Facility, CERN/SPSC 99-8, SPSC/P 310, 17 March 1999.

[10] S. Andriamonje et al., 'Feasibility Study of a Neutron TOF Facility at the CERN-PS, CERN/PS 98-065 (CA), Geneva, 5 November 1998.

[11] M. Giovannozzi, Alternative Layout of the Transfer Line for the Time-Of-Flight Neutron Facility at CERN-PS, CERN/PS/CA/Note 99-17, 1999.

[12] M. Giovannozzi, New Transfer Line in the TT2 Tunnel for the Time-Of-Flight Neutron Facility at CERN-PS, CERN/PS/CA/Note 98-23, 1998.

[13] G. Arduini, M. Giovannozzi, K. Hanke, J-Y. Hémery, M. Martini, MAD and Beam Optics description of the TT2/TT10 transfer lines. Part I: optics without emittance exchange insertion, CERN/PS/CA/Note 98-14, 1998.

[14] H. Grote, F. C. Iselin, The MAD program – User's Reference Manual, CERN/SL/AP 90-13, 1990.

[15] M. Giovannozzi, M. Sassowsky, Sweeping Magnet for the Time Of Flight Facility at the CERN PS, CERN/PS/CA/Note 99-12, 1999.

[16] B. Langeseth, G. Pluym, B. de Raad, Magnetic Measurements on the Bending Magnets of the Beam Transport System of the CERN PS, PS Int. (EA)60-14, 1960.

[17] H. Arnould et al., Neutron-Driven Nuclear Transmutation by Adiabatic Resonance Crossing, CERN-SL-99-036 EET, also as final report to the European Commission, Contract No F141-CT96-0009, EUR 19117 EN, ISBN 92-828-7759-0.

[18] A. Fontaine, H. Schönbacher, M. Tavlet, Compilation of radiation damage test data, CERN 98-01, 1998.

[19] A. Fasso et al., in *'Intermediate Energy Nuclear Data: Models and Codes'*, Proceedings of a Specialists Meeting, Issy les Moulineaux (France) 30 May – 1-June 1994, p.271, published by OECD, 1994 and references therein.

[20] M. Höfert et al., 'The prediction of radiation levels from induced radioactivity discussion of an internal dump facility in the PS;, DI/HP/185 Health Physics Group, 27 January 1975.

[21] V. Vlachoudis, 'Results on the Beam Quality, Halo and Neutron Background from MC Simulation', Proceeding of the 3rd TOF Collaboration Meeting, CERN, Geneva, 5 May 1999.

[22] A.V. Sannikov, E.N. Savitskaya, 'Ambient Dose and Ambient Dose Equivalent Conversion Factors for High-Energy neutrons' CERN/TIS-RP/93-14 (1993)

[23] R.H. Thomas, R.G Stevenson, 'Radiological Safety Aspects of the Operation of Proton Accelerators', Technical Report Series nº 283, IAEA, Vienna 1988.

[24] D. Cano-Ott et al. Parameterization of the neutron source at the n_TOF and its influence on the collimation system. DFN/TR-03/II-00. CIEMAT (2000).

[25] D. Cano-Ott et al. Proposal for a two-step cylindrical collimation system for the nTOF facility. DFN/TR-04/II-00. CIEMAT (2000).

[26] M. Heil et al., Geant simulations of shielding and collimators for n-TOF. FZK contribution to the 2nd MC meeting of the n_TOF collaboration. CERN, 28 February 2000.

[27] N. Colonna, GEANT Simulation of the "common geometry", neutron and photon background studies. INFN contribution to the 2nd MC meeting of the n_TOF collaboration. CERN, 28 February 2000.

[28] D. Cano-Ott et al., FLUKA/MCNP Simulation of the "common geometry", neutron and photon background studies. CIEMAT contribution to the 2nd MC meeting of the n-TOF collaboration. CERN, 28 February 2000.

[29] A. Tzima et al., FLUKA Simulation of an alternative geometry, neutron and photon background studies. CERN (Greek group+CIEMAT) contribution to the 2nd MC meeting of the n_TOF collaboration. CERN, 28 February 2000.

[30] V. Vlachoudis, Particle distribution entering the vacuum tube from a $80 \times 80 \times 60$ cm^3 lead target. CERN contribution to the 2nd MC meeting of the n_TOF collaboration. CERN, 28 February 2000.

[31] D. Cano-Ott et al., Analysis of the neutron source at the entrance to the vacuum pipe, from the data produced by the CERN EET group. CIEMAT contribution to the 2nd MC meeting of the n-TOF collaboration. CERN, 28 February 2000.